Controlling Arrhythmias Using Optogenetic Actuators in Computational Simulations

Alexander Richard Ochs

A dissertation
submitted in partial fulfillment of the
requirements for the degree of

Doctor of Philosophy

University of Washington
2023

Reading Committee:
Patrick M. Boyle, Chair
Claudia Moreno
Andre Berndt

Program Authorized to Offer Degree:
Department of Bioengineering
University of Washington

Abstract

Controlling Arrhythmias Using Optogenetic Actuators in Computational Simulations

Alexander R. Ochs

Chair of the Supervisory Committee:
Patrick M. Boyle
Department of Bioengineering

This dissertation discusses the application of light-induced stimulation (optogenetics) in computational models of heart cells (cardiomyocytes), cardiac tissues, and heart chambers to control arrhythmia development. Chapter 1 presents an overview of cardiac anatomy, relevant physiology, and cardiac electrophysiology computational models. Chapter 2 provides a basic explanation of optogenetic actuators (opsins), covering past applications (both experimental and computational) in cardiac tissue at various scales. Chapter 3 examines the efficacy of expressing an anion-conducting opsin (GtACR1) to terminate atrial and ventricular arrhythmias in 3D patient-derived models. Additionally, a 2-state photocurrent model for GtACR1 is introduced. Chapter 4 studies the use of subthreshold optogenetic stimulation to up- and down-regulate early afterdepolarization propensity (cell-scale) and related premature ventricular complexes (organ-scale) in patient models. Chapter 5 evaluates the use of optogenetic stimulation to modulate spontaneous beating in pluripotent stem cell-derived cardiomyocytes (cell-scale) and graft-to-host excitation in 2D, histology-derived tissue models (tissue-scale). The work presented here demonstrates how optogenetic stimulation can be used to control the initiation and suppression of arrhythmias in computational models across a variety of arrhythmia-prone conditions.

Table of Contents

List of Figures

List of Tables

Acknowledgements

The advancement of science is dependent on the community of teachers, colleagues, and advisors who make growth possible. Consequently, there are many people that I need to thank for helping me through my doctoral journey as well as building me up to this point.

I would first like to thank my family for the opportunity to pursue this doctorate, particularly my mother Dr. Sheri-Colberg Ochs. Her joy for teaching and willingness to explain human physiology to me when I was a child was a strong driving force for my eventual pursuit of biomedical engineering. My family supported me financially, logistically, and personally to pursue bachelors, masters, and now doctorate degrees. My mom and I have called to catch up weekly since I left for undergrad in 2012, and weekly gaming sessions with my brothers over the past couple years have provided me with some much needed stress relief.

I would also like to thank my advisor, Dr. Patrick M. Boyle, whom without this work would not have been possible. Pat's passion for research, knowledge in both electrophysiology and the openCARP software package, and vast array of perl scripts defined my scientific training in the CardSS lab. I particularly appreciate his patience for my unending stream of questions over the years. He also facilitated my biggest contribution to science to this day: the implementation of colorblind-friendly viridis color palettes into openCARP visualization software, which I see used frequently in other groups' papers. Anyone who works with Pat can clearly see how he would rather be coding and conducting experiments rather than performing stuffy professor duties, and I'm excited for the lab's exciting future publications over the coming decades.

I also strongly credit my peer Ph.D. students in the CardSS lab, Savannah Bifulco and Chelsea Gibbs, for their invaluable assistance to my work. I wish to thank them both for always providing engaged feedback, taking the time to explain their new science to me, and for navigating the turbulent pandemic times with me. Certain experiments and figures may not have happened

without their curious questions and ideas. Their companionship and support was a large part of what made research in the CardSS lab fun and engaging.

To all of my friends on both coasts, of whom there are too many to name: thank you for the support, coffee/tea catchups, video calls, and adventures in Seattle and beyond. It was a joy to always have friends to game with, snowshoe in the Cascades with, and hangout and/or commiserate with. These people provided much needed validation, sanity checks, and reframing in the sometimes zany world of academia. You are all wonderful, and beloved confidants.

A large part of my non-research footprint at UW was sourced from the BioE community, who from day 1 was extremely welcoming, friendly, and curious. Our department's culture was a strong motivator for me to get involved with running events and managing event finances over 4 years, and I appreciate finally finding a home with joy for the biotechnology space. In the past year, I also wish to commend the younger graduate students for demonstrating enthusiasm and perspective as I continued emotionally "aging out" of grad school.

Plenty of non-humans have also been instrumental to my mental health and routine. I wish to thank the Lofi Girl hip hop music stream (available on Youtube and Spotify) and ChillHop Music's annual end-of-year lofi mixes (2018-2022) for providing a reliable rhythm to calm down and focus with. Additionally, big thanks to Miro Tea (in Ballard, Seattle) for positively facilitating the vast majority of writing for this thesis.

Since the majority of my PhD was done from home, I would especially like to thank my two cats, the stoic Lady Gray and excitable Gemini, for keeping me company. Both of them would take turns being excellent lap cats, providing sleepy picture opportunities, and reminding me that life doesn't have to always be so serious (lying upside down). Their warm fur and purrs helped me get through the low points of graduate school, especially when coupled with a pandemic.

Finally, I would like to thank my partner (and soon to be Dr.) Tammi van Neel for her unending support and love throughout my doctorate. Tammi was one of the very important people who helped me stabilize my PhD during some crisis moments, and has always been above-and-beyond supportive of me through my struggles. I'm extremely excited to see what the future holds together for us.

Dedication

I dedicate this dissertation to my mother, Dr. Sheri Colberg-Ochs, who bred a love for physiology through her explanations of diabetes.

Preface

Like breathing air, the heartbeat is an autonomic bodily process that, if stopped for more than a few minutes, usually results in our untimely demise. Most do not often think of the heart consciously, and in human society we evoke it as a metaphor for emotional or relationship turmoil far more often than to effuse its physical benefits to our continued existence. Yet day after day, the heart keeps beating, and we keep living. This organ has a tremendous range to adjust its beating rate and contractile force, alternating between peak cardiac output (such as during a long-distance running event) and tepid blood flow levels (such as during meditation or sleep). It can also stop unexpectedly, known as cardiac arrest or cardiac sudden death. Although centuries of research have helped us better understand how precisely the heart works, we often cannot ascribe precisely why or how specific individuals develop abnormal heart rhythms. The cost is serious: hundreds of millions worldwide experience substantial morbidity and mortality as a result of disrupted cardiac rhythm (1, 2).

State-of-the-art research using actual human hearts is often directly tied to unsuccessful heart transplants (3-5) or cadaver hearts donated to science (6), which are often sourced from older and sicker individuals. For ethical reasons, transplants are always attempted first using individuals on organ recipient waitlists and scientific studies are only conducted when there are no other alternatives. Because there is inherently limited human cardiac tissue data available, proxies for human hearts are needed for consistent heart studies. Hundreds of studies using the sacrificed mammalian hearts of mice, rats, rabbits, guinea pigs, cats, dogs, pigs, and non-human primates have been pivotal for expanding our knowledge about the heart and its diseases, but their findings have not always been applicable to humans (7). Advances in genomics, computing, and statistics have improved our understanding and prediction of certain conditions' associative causes of cardiac death. Frequently, we have theories (backed up by varying degrees of evidence) on how those conditions lead to cardiac damage and death. But more tools and means

of studying and understanding pathologies of the heart are necessary to continue advancing our knowledge and subsequent treatments to improve human health.

Decades of work have established robust, biophysically detailed, and experimentally validated computational cardiac electrophysiology models (8-13). Computational models are a good tool for examining poorly understood topics and probing areas that are too difficult or risky for initial experimental research. Our lab and my research exist because we believe that computational models can help inform clinical and scientific understanding of the heart and related electrophysiological phenomena. We stand on the shoulders of giants because of the incredible work that previous scientists conducted (14-16) without the technological advantages we have today. To the readers of this dissertation, I hope I can help explain what has been established to date in my niche subdomain of cardiac optogenetics, posit about what the near future might hold for this area, and ultimately convince you of the value of our work.

Chapter 1 | Cardiac Electrophysiology Background

1.1 Cardiac anatomy and circulation

The heart is an encapsulated, hollow mass of muscle responsible for regularly contracting and relaxing to circulate blood throughout the human body. There are four primary chambers: the left atrium (LA), right atrium (RA), left ventricle (LV), and right ventricle (RV). The RV is primarily responsible for pushing oxygen-poor blood towards the lungs for oxygenation (pulmonary circulation) and the LV is primarily responsible for ejecting oxygen-rich blood to the rest of the body (systemic circulation) (17). The atria are lower pressure, thinner walled chambers that function more as reservoirs of blood for their corresponding ventricles (i.e., RA → RV and LA → LV) than as important pumps.

To briefly summarize blood flow during a typical heartbeat (**Fig. 1.1**): during relaxation (diastole), oxygen-poor blood enters into the RA from the superior and inferior vena cava. At the same time, oxygen-rich blood fills into the LA from pulmonary veins, which connect to lungs. During the start of systole (contraction), both atria contract and this contraction pushes the blood into their corresponding ventricles (i.e., from RA to RV and LA to LV). The tricuspid and mitral valves close afterwards to prevent backflow into the atria. After a brief pause, the ventricles contract: the RV contraction pushes oxygen-poor blood through the pulmonary artery towards the lungs, where oxygenation occurs. The LV contracts simultaneously, pushing oxygen-rich blood through the aorta outward to the rest of the body. After systole ends, diastole begins again: the pulmonic and aortic valves close and blood begins to pool once again within the RA and LA.

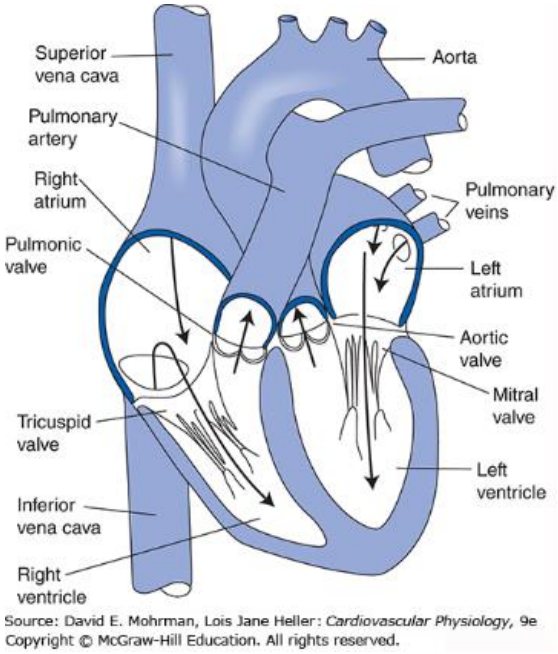

Figure 1.1*: Pathway of blood flow through the heart. Reproduced with permission from Mohrman DE & Heller LJ, Cardiovascular Physiology, 9th edition, 2018.*

Cardiomyocytes are long, striated, multi-nucleated, cardiac-specific muscle cells (myocytes) responsible for contraction of the heart. These cells are electrically excitable and connected to one another, allowing propagation of electrical activity necessary for heartbeats. Cardiomyocytes are also physically connected in series form cardiac muscle fibers, which contract together to generate force. In the heart as an organ, cardiac fibers are organized in a circular helical fashion, facilitating the critical push of blood out towards the rest of the body (18). The total volume of blood pumped by the heart per minute is called cardiac output. Of the four chambers, the LV is responsible for the vast majority of cardiac output. Consequently, damage or impairment of LV function can lead to some of the most serious and prevalent heart conditions.

One of the common LV damaging conditions is called myocardial infarction (commonly known as a heart attack), occurring when a clot severely reduces or occludes blood flow in the heart vasculature thereby depriving oxygen supply to highly aerobic heart tissue. Although myocardial infarctions are not the primary focus of my dissertation, understanding the condition

is extremely important for explaining its arrhythmia risks and chronic remodeling. Deeper reviews on the topic can be found elsewhere (2).

The severity of an MI is affected by the clot's size and location, with immediate symptoms varying between being asymptomatic, having chest pain, or undergoing sudden cardiac death (SCD) (19). In the days to weeks following an MI, all-cause mortality risk is greatly elevated due to ventricular arrhythmia risk. For those who survive this period, the acute post-trauma response (i.e., dead and damaged cardiac tissue) compacts into infarct scar and ischemic border zone (BZ) tissue during the remodeling process over weeks to months (20). Infarct scar is mechanical stiffer and electrically impaired, as compared to normal myocardium, and can contribute to the formation of potentially lethal ventricular arrhythmias (21). BZ tissue is electrically remodeled to have slower conduction, and has been also associated with ventricular arrhythmias (22, 23). Furthermore, the damage caused by the MI can lead to excessive myofibroblast deposition of extracellular matrix proteins (called fibrosis), also leading to stiffer myocardial walls (24).

If cardiac output drops enough as a result of this reduced mechanical compliance, the heart will compensate by upregulating contraction force, which in itself can cause wall thickening and reduced cardiac output. A metric measuring cardiac output is called left ventricle ejection fraction (LVEF). If the heart ever fails to pump enough blood to the rest of the body necessary for life, as measured by LVEF, this condition is called heart failure (HF) and is associated with previous MI (2).

1.2 Cardiac conduction system

Within the cardiomyocyte, specialized protein aggregate structures in the membrane called gap junctions allow for electrical impulse propagation between cells. Gap junctions are composed of proteins called connexins (Cx). In the heart, Cx43 is most frequently expressed, but Cx30.2, Cx37, Cx40, and Cx45 are also present (25). Cx proteins tend to be located at the ends of cardiomyocytes, which facilitates a preferential direction of conduction longitudinal to a given

cardiomyocyte's length rather than laterally from cell-to-cell (where gap junctions are sparse) (17). The relationship of electrical activity to contraction in myocytes is referred to as excitation-contraction coupling (26). To summarize the molecular mechanism in extremely broad strokes: the change in membrane potential caused by excitation results in intracellular Ca^{2+} release from the sarcoplasmic reticulum (ryanodine receptors). Free intracellular Ca^{2+} binds to troponin-C, which leads to actin filaments sliding against myosin heads (contraction), and is eventually followed by an unbinding of Ca^{2+} and a restoration of the initial cardiomyocyte length (relaxation) (17).

There is a beautifully complex diversity of cell types within the heart, spanning a range of genotypes and phenotypes that are still not well understood (27, 28). The most abundant cell type is the cardiac fibroblast, which are responsible for producing connective tissue. The second most abundant cell type and the largest cell type by volume is the cardiomyocyte, a muscle cell which causes the contraction necessary for a regular heartbeat. Other cardiac cell types include specialized conduction system cells (such as Purkinje fibers), immune cells (such as lymphocytes and macrophages), neurons, adult stem cells, smooth muscle cells, endothelial cells, and mesothelial cells. However, this dissertation will elaborate primarily about cardiomyocytes and conduction system cells; a far more complete summary of different heart cells and their roles can be found elsewhere (29).

The electrophysiological properties of various heart cells often also vary as a function of location within each heart chamber and its myocardial walls (**Fig. 1.2**). Some specific cardiomyocyte subtypes include atrial cardiomyocytes, ventricular cardiomyocytes, pacemaker cells, and cardiac Purkinje cells (30). Furthermore, within the myocardial wall the innermost surface (endocardium), outermost surface (epicardium), and the interior wall (midmyocardium) layers have been found to have different action potential AP characteristics, facilitating a dispersion of repolarization across a cross-section of the myocardial wall. Groups of electrically

distinct calls called “M cells” within the midmyocardium that may play a role in those repolarization differences (5). However, there has been disagreement and controversy about M cells’ functional significance *in vivo* (31). Other unresolved controversies include whether cardiomyocytes electrically couple to cardiac fibroblasts (32, 33) and whether cardiomyocytes electrically couple to post-MI scar (34).

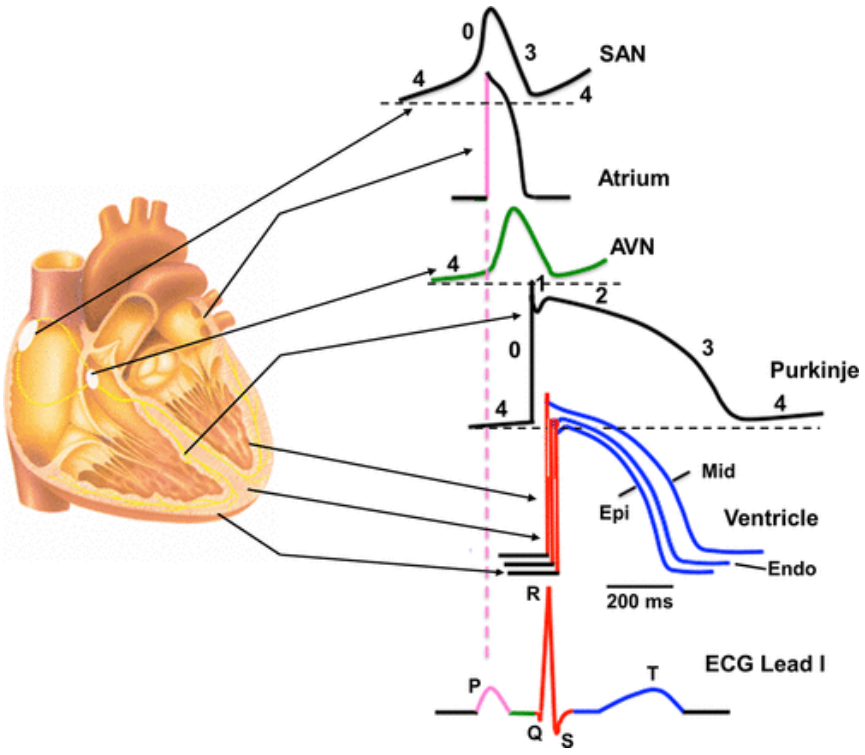

Figure 1.2*: Regional differences in cardiac action potential configurations. Schematic cross section of the heart depicting the corresponding action potential configuration from different regions of the heart indicated by arrows. Color-coded sections on the action potentials refer to the corresponding sections on the schematic electrocardiogram (ECG). AVN, atrioventricular node; Endo, endocardial; Epi, epicardial; Mid, midmyocardial; SAN, sinoatrial node. Reproduced with permission from Varró A et al., Physiol Rev, 2021; 101: 1083–1176.*

Conduction throughout the heart is facilitated by the cardiac conduction system (**Fig. 1.3**). This specialized tissue is nestled in the myocardial walls, conducts faster than normal myocardium, and helps coordinate the precisely timed contraction of each chamber for systemic blood flow. To summarize the role of electrical excitation in a typical sinus beat (**Fig. 1.3**): initiation from pacemaker cells in the sinoatrial (SA) node occurs in the RA. The resulting electrical wavefront propagates throughout the RA and LA, with both contracting fairly quickly and uniformly

with each other). The excitation wave continues propagating, but slows down significantly as it enters into a specialized conduction structure called the bundle of His, which is both part of the atrioventricular (AV) node and of a broader conduction system called the His-Purkinje system (35). There is a small delay as a result of this slowing of conduction, which allows the atria to fully contract and push blood into ventricles. When the excitation propagation exits the bundle of His, there are specialized Purkinje fibers lining the LV and RV myocardial walls that allow for electrical activation of both ventricles in an extraordinarily fast fashion. The electrical impulse conducts through the septal wall (separating the LV and RV chambers) then throughout the LV and RV near simultaneously. This allows for both ventricles to contract in unison, which is critical particularly for the LV to push oxygenated blood out to the rest of the body. After the sinus beat has completed, and a relatively long period of repolarization occurs prior to the next heartbeat.

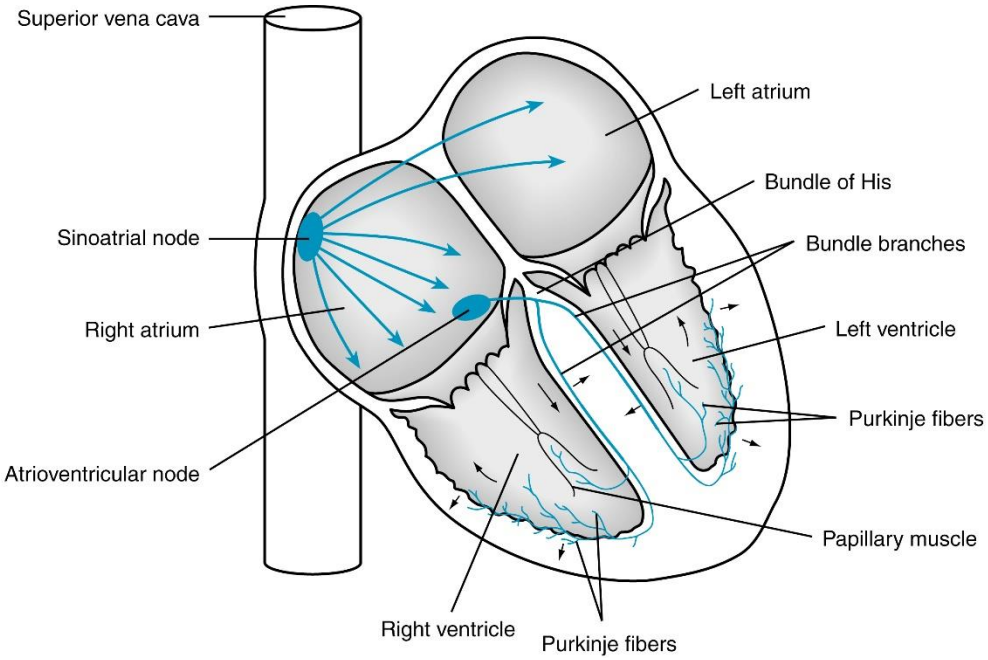

Figure 1.3*: Schematic representation of the conduction system of the heart. Reproduced with permission from Pappano, A.J.W., Withrow Gil, Cardiovascular physiology. 11th ed. 2019, Philadelphia, PA: Elsevier.*

When considering heart conduction and propagation, the concept of electrotonic coupling is also important to consider (36). Given that myocytes are electrically coupled via gap junctions

in healthy tissue, successful propagation is not only dependent on the excitation of a single cell but also the excitation of the surrounding tissue. This can be explained using the analogies of "source" (depolarizing current) and "sink" (the tissue that is absorbing said current). In the typical isolated cardiomyocyte, cell excitation is achieved using some fixed amount of source current; in a well-coupled tissue, the locally applied source spreads throughout the system of interconnected cells. Propagation within a tissue requires two steps: 1) each cell reaching its activation threshold and initiating an action potential, and 2) the cell providing excess current to its neighboring cells (electrotonic conduction) (37). When the source current is insufficient and conduction block occurs, this can be viewed through the lens of source-sink mismatch: the source is mismatched to the sink that is being excited. This can be resolved either by increasing the source or decreasing the sink. In diseased conditions (such as during heart failure, fibrosis deposition, or MI scar), source-sink mismatch often occurs, which can lead to conduction block and arrhythmia development (38).

1.3 Ionic currents of cardiac action potentials

The bi-lipid layer of a cardiomyocyte cellular membrane has millions of proteins embedded within its surface that are essential for biological functioning. Some of these proteins form pores that can passively allow ion flow across membranes, called ion channels. Ion channels are fundamental to cellular membrane excitation. The transport of charged particles across the cellular membrane is an electrical current (by definition), and by Ohm's law also directly causes change of the membrane voltage potential (V_m). This rapid change in V_m is called an action potential (AP). In cardiomyocytes, this is characterized by an initial depolarization then gradual repolarization to resting membrane potential; the time to fulfill this cycle is called AP duration (APD). The AP propagates between electrically coupled cells to achieve a specific biological function (such as contraction in cardiomyocytes). In a tissue of many coupled cardiomyocytes, this propagating change in V_m manifests as an electrical impulse (also known as excitation

wavefront). Across an entire heart, an excitation wavefront can lead to a sinus heartbeat, as discussed in previously (section 1.2).

The AP trace was first recorded by Alan Hodgkin and Andrew Huxley in 1939, during studies on nerve conduction using giant squid axons (39, 40). During their studies, a fine capillary electrode was inserted into the squid axon and upon excitation an AP was observed. Nearly a decade later, they discovered that they could use capillary electrodes and a current generator to iteratively measure the change in voltage in response to current changes, now known as a current clamp (41). This allowed for the study of voltage sensitivity (inactivation) and kinetics of ion channels in neurons, and eventually also in cardiomyocytes. More will be discussed about Hodgkin and Huxley's mathematical AP model later (see section 1.5).

The characterization and study of cardiac ion channel physiology is a robust field with over a century of detailed study (42). For the purposes of this dissertation, I will focus on providing a robust introduction to the important ions and ionic currents necessary for understanding the cardiac AP.

The primary ions that are responsible for a cardiomyocyte AP are Na^+, K^+, and Ca^{2+}. It is also worth noting that chloride ions (Cl^-) are also trafficked and can affect the cardiac AP, but are frequently inactive and are activated by agonists or physical stress (43, 44). These ion channels are voltage-gated (or voltage-dependent), meaning that their function changes based on the cellular V_m. Gating refers to pores opening and closing, which directly affects their current flow. Once a channel opens (activation), ions are conducted. However, there are two forms of closure: deactivation (which can be re-activated) and inactivation (which cannot be re-activated until the channel has transitioned from inactivated to deactivated states). Channel inactivation is foundational to the concept of refractoriness in cardiac tissue (see section 1.4) and helps prevent premature re-excitations (45). These ion channels are also selectively permeable, meaning that the ions transported are physically restricted to specific charge and size properties.

The balance of both charge and chemical concentrations seek equilibrium between the extracellular (outside the cell) and intracellular (inside the cell) spaces. These two distinct qualities have competing gradients that form electrochemical gradient, which determines the direction and magnitude of ion transport during an AP. This equilibrium can be quantified using the Nernst equation (**Equation 1.1**). This equation establishes the membrane potential where current flow is zero for a given ion (i.e., where the current direction reverses), called reversal potential (E_{rev}) or Nernst potential.

$$E_{ion} = \frac{-61}{z} log_{10}(\frac{[Ion]_i}{[Ion]_o})$$

Equation 1.1*: Nernst equation, where $[Ion]_i$ is intracellular concentration, $[Ion]_o$ is extracellular concentration, and z is the valence of the given ion.*

Representative intracellular and extracellular concentrations of cardiomyocyte concentrations of Na^+, K^+, and Ca^{2+} ions are shown in **Table 1.1**. Recovery from ionic imbalances following an AP is facilitated using active transport against the electrochemical gradient. This is accomplished through proteins called ion pumps (also known as ion transporters) using ATP as energy. Examples of these transporters include the sodium-potassium pump and the sodium-calcium exchanger.

Table 1.1*: Intracellular and Extracellular Ion Concentrations and Equilibrium Potentials in Cardiac Muscle Cells. Directly sourced from Pappano, A.J.W., Withrow Gil, Cardiovascular physiology. 11th ed. 2019, which had modified the table from Ten Eick, R. E., Baumgarten, C. M., & Singer, D. H. (1981). Ventricular dysrhythmias: Membrane bias, or, of currents, channels, gates, and cables. Progress in Cardiovascular Diseases, 24,157-188.*

Ion	Extracellular Concentration (mM)	Intracellular Concentration (mM)	Reversal Potential (mV)
Na^+	145	10	71
K^+	4	135	–94
Ca^{2+}	2	0.0001	132

The typical cardiomyocyte AP has five phases: the initial AP upstroke (phase 0), brief repolarization (phase 1), plateau phase (phase 2), repolarization (phase 3), and resting V_m (phase 4). Different ionic currents predominantly drive and compete within these phases, as

demonstrated using a human ventricular cardiomyocyte in **Figure 1.4**. However, different subtypes of excitable cardiac cells (such as atrial, ventricular myocytes) have different expression levels of various ion channels, resulting in different AP morphologies and electrophysiological properties. Precise characterization of these currents, their respective ion channels, and unmentioned subcurrents are described in detail elsewhere (42, 45, 46). The most important ionic currents forming the typical ventricular myocyte cardiac action potential will be discussed briefly.

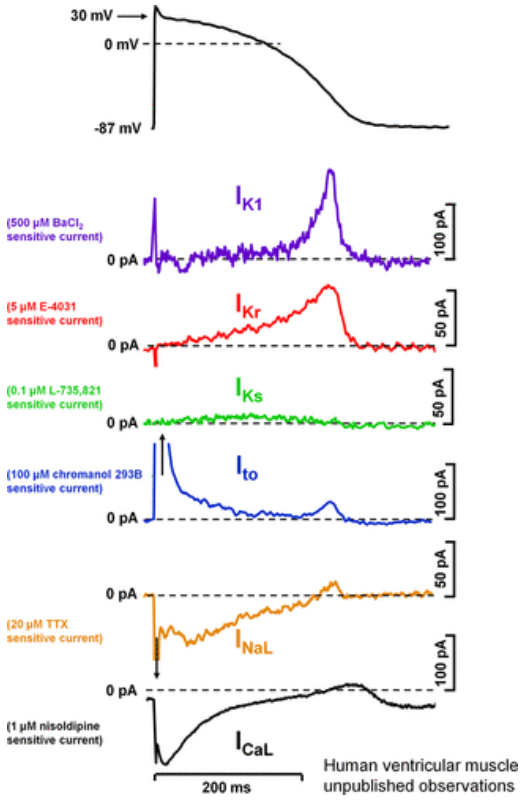

Figure 1.4*: Action potential and underlying ionic currents recorded from human ventricular myocytes with the patch-clamp technique applying human ventricular action potential as command pulses at 1 Hz stimulation frequency, in the absence of any sympathetic effects. Inward rectifier potassium current (IK1), rapid (IKr) and slow (IKs) components of delayed rectifier potassium current, transient outward current (Ito), and L-type calcium current (ICa,L) were measured as difference current following application of selective channel inhibitors. INaL, late sodium current. Unpublished data from our laboratory at the Department of Pharmacology and Pharmacotherapy, University of Szeged. Reproduced with permission from Varró A et al., Physiol Rev, 2021; 101: 1083–1176.*

The sodium current (I_{Na}) is characterized by an initial sodium influx, which is primarily responsible for the AP upstroke (phase 0). The fast component of I_{Na} is inactivated within a few

milliseconds after AP upstroke, but some current persists during the plateau phase, termed as late I_{Na} current, slow I_{Na} current, or the 'Na^+ - window current' (47). This late I_{Na} current opposes repolarization by potassium currents during the plateau and repolarization currents. I_{Na} inactivation recovers at quite negative V_m values (< –80 mV) near the typical cardiomyocyte resting membrane potentials, but can recovery from inactivation within tens of milliseconds (46). I_{Na} is likely the largest contributor cellular excitability, given the necessity of I_{Na} to initiate the AP. Sodium channel mutations in cardiomyocytes can result in cardiac arrest in fetuses and infants, in part due to the critical role of I_{Na} in cardiomyocyte excitability (48).

The net potassium current (I_K) is primarily repolarizing current, with multiple components acting at different timings: the transient outward current (I_{to}), the rapid delayed rectifier outward potassium current (I_{Kr}), the slow delayed rectifier outward potassium current (I_{Ks}), and the inward rectifier potassium current (I_{K1}). Each potassium current component will be described briefly.

I_{to} is a rapidly activating and inactivating current (at V_m > –30 mV) associated with phases 0 and 1 (42). Together with I_{Na}, I_{to} is important for AP upstroke and rapid repolarization (creating the AP "notch") while having little impact on APD.

I_{Kr} channels open after the plateau phase (values ≤ 0 mV) and is generally considered to be one of the most important currents affecting phase 3 repolarization. This is partially due to its slow deactivation during repolarization.

I_{Ks} is a relatively small current that activates slowly (500-1000 ms) during the plateau phase and inactivates rapidly at more negative V_m. However, I_{Ks} plays a larger role in repolarization when opposing APD lengthening, especially when other repolarizing currents (e.g., I_{Kr}) are downregulated (49).

I_{K1} conducting channels open rapidly as V_m values decrease during repolarization, and this inward rectification forms a negative feedback loop as V_m approaches resting membrane

potential (46). It is one of the most important currents in the maintenance of resting V_m phase 4, along with contributing to phase 3 repolarization with I_{Kr}.

Moving on to Ca^{2+} currents, the L-type calcium current (I_{CaL}) is primarily responsible for persistent inward depolarizing currents during phase 2 plateau and phase 3 repolarization. The precise impact and gating of I_{CaL} is complicated and poorly understood (50). This is in part because the inactivation of the current is dependent on intracellular [Ca^{2+}] and modulated by many cellular processes and molecules. Broadly speaking, I_{CaL} current is initially a repolarizing current during AP upstroke, then later it acts as a primarily depolarizing current that opposes phase 3 repolarization. Furthermore, intracellular Ca^{2+} is tightly controlled at resting V_m. Initial Ca^{2+} release can trigger the release of more calcium from the Sarcoendoplasmic Reticulum Calcium ATPase (SERCA) within the mitochondria, a positive feedback phenomenon known as calcium-induced calcium release (CICR). CICR demonstrates how Ca^{2+} acts as both a trafficked ion during cardiac APs as well as a signaling molecule. Disease conditions related to leaky or poorly controlled Ca^{2+} can be highly consequential for arrhythmia development, in particular in the formation of delayed afterdepolarizations (51, 52) and premature beats (53).

To provide a sense of scale for the relative contributions to total membrane current for each of these constituents, Table 1.2 shows the maximum conductance values from an adult ventricular cardiomyocyte ionic model published by O'Hara et al. (12). Please note that current conductances are not universally identical and will vary between different AP models.

Table 1.2*: Maximum conductance values of ionic currents in the O'Hara and Rudy (ORd) ionic model. Directly sourced from supplemental information values listed in (12).*

Ionic Current names	Symbol	Maximum conductance (mS/µF)
Early component of sodium current	$G_{Na,early}$	75
Late component of sodium current	$G_{Na,late}$	0.0075
Transient outward potassium current	G_{to}	0.02
Rapid delayed rectifier potassium current	G_{Kr}	0.046
Slow delayed rectifier potassium current	G_{Ks}	0.0034
Inward rectifier potassium current	G_{K1}	0.1908

Sodium/Calcium exchange current	G_{NaCa}	0.0008
Background potassium current	G_{Kb}	0.003
Sarcolemmal calcium pump	G_{pCa}	0.0005

1.4 Arrhythmias

Arrhythmias are irregular heart rhythms that deviate from typical sinus activation. These disorders frequently result from other genetic (i.e., mutations that increase arrhythmia risk) or acquired (i.e., heart damage and remodeling such as MI, HF, or fibrosis) causes (1, 54). The degree of severity can vary wildly, between relatively benign premature ectopic (extra) beats in the atria or ventricles, up to imminently life-threatening arrhythmias such as ventricular tachycardias (VT) or ventricular fibrillation (VFib). There is such a large variability in appearances (e.g., bradycardia and different types of tachycardia), location (atrial, ventricular, or both), and underlying diseases (e.g., previous heart damage, heart failure, gene mutations) that it is commonly agreed that there is no single mechanism of arrhythmia development (42). More thorough reviews of arrhythmias and their mechanisms can be found elsewhere (42, 54, 55). This dissertation will cover the basics of arrhythmia mechanisms, then highlight the most common arrhythmias' pathology and treatment.

The three primary mechanisms of arrhythmias are: 1) reentry, 2) triggered activity, and 3) enhanced automaticity (54). Reentry, or reentrant arrhythmia, is the re-excitation of tissue prior to the next sinus beat. The concept of reentry was first posited in the early 20th century (15, 56) and has been supported by many subsequent studies, including modern electroanatomical mapping data in humans (57, 58). Reentry is the dominant arrhythmia mechanism observed clinically (55), but this can partially attributed to differences in occurrence: it can be rare to observe triggered activity directly and conditions involving enhanced automaticity are also relatively uncommon.

To provide a framework for considering this phenomenon: if an electrical stimulus (of sufficient current strength) is applied to a well-coupled cardiac tissue, the stimulus will be

conducted and propagated across the tissue as an excitation wavefront. This wavefront moves at a certain speed (conduction velocity) and can fail to propagate (conduction block, possibly due to source-sink mismatch). In areas that the wavefront has recently passed, the recently depolarized tissue is refractory (i.e., is not electrically excitable) for a fixed amount of time, called effective refractory period (ERP). The period of time for tissue that can be re-excited (prior to the next sinus beat) is referred to as the excitable gap (59) or vulnerable window for reentry (60). As mentioned earlier, refractoriness occurs due to recovery of inactivated Na^+ channels (occurring at more negative membrane voltages) necessary for the initial action potential upstroke. Electrophysiological conditions associated with a shortened refractory period and/or a prolonged conduction velocity are more prone to reentrant arrhythmias (54).

There are two types of reentry: anatomical reentry and functional reentry (55). Anatomical reentry occurs when a reentrant (re-occurring) excitation wavefront repeatedly travels around the boundary of an anatomical obstacle to conduction (such as post-MI infarct scar). A classic example of anatomic reentry is shown in Figure 1.5A: an excitation wave in a fixed, ring-like path, localized to an anatomic (non-conducting) obstacle, with an excitable gap (shown in white) existing between the leading wavefront edge (shown in red) and its refractory tail (shown in green). A spiral wave is an example of 2D reentry: circulating wavefronts that conduct into the excitable gap repeatedly (**Figure 1.5B-C**).

On the other hand, functional reentry is a reentrant wavefront that is occurs without a specific anatomical obstacle. Rather, the arrhythmia is maintained by the wavefront "chasing" its own refractory tail, by constantly propagating into the excitable gap. The functional reentry example visualized in (**Figure 1.5D-F**) can also referred to as a rotor, which some individuals describe to interchangeably with spiral waves (55, 61). This terminology is inconsistent across authors; the clearest explanation is while rotors are only associated with functional reentry, spiral waves can be either functional and anatomic reentry.

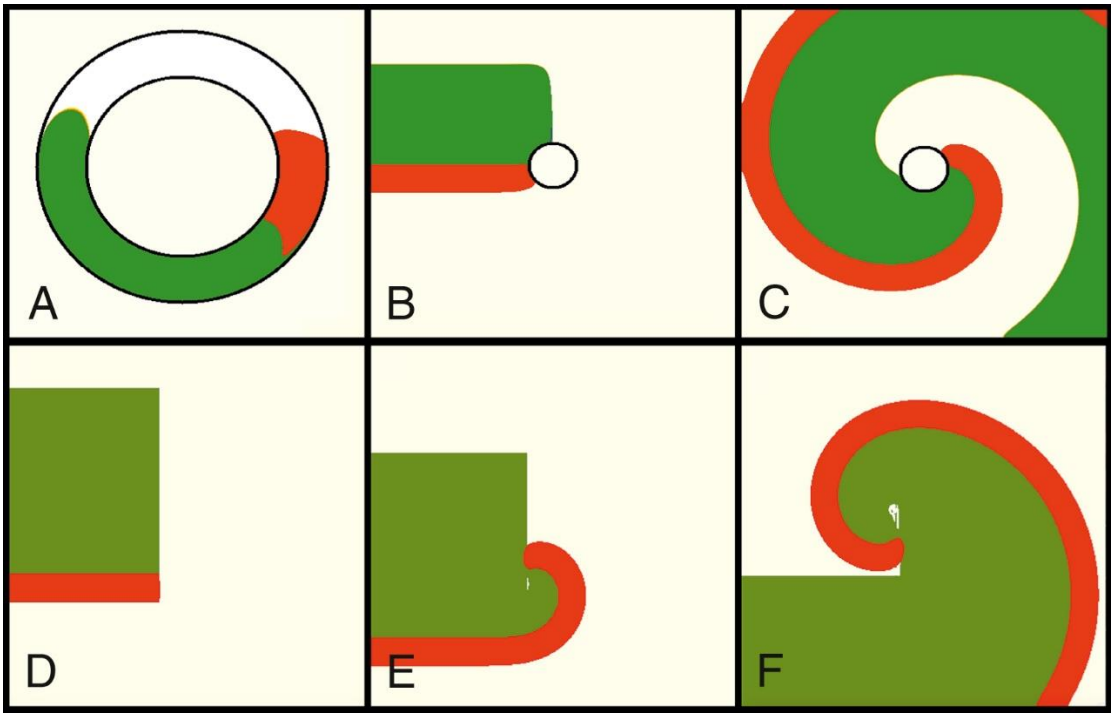

Figure 1.5*: Examples of reentry mechanisms. (**A**) One-dimensional anatomic reentry. (**B–C**) formation of a spiral wave rotating around an obstacle. (**D–F**) formation of a rotor. Red denotes the leading edge of an excitation wavefront; green denotes recently depolarized tissue; white denotes the excitable gap; and beige denotes repolarized tissue. Reproduced with permission from Chapter 33 ("Theory of Rotors and Arrhythmias" by Alexander V. Panfilov and Hans Dierckx) in "Zipes and Jalife's cardiac electrophysiology: from cell to bedside" (by José Jalife and William G. Stevenson, 2022).*

Spatially heterogeneous differences in electrophysiological properties strongly affect the occurrence of reentrant arrhythmias. This can result from conditions such as atrial fibrillation, which has been established to structurally remodel the affected chambers (1), or MIs forming fibrotic regions called border zone (BZ) tissue, in addition to infarct scar (62). Excellent reviews on cardiac fibrosis and its relationship to arrhythmias have been written elsewhere (24, 63). Briefly, environmental stress causes cardiac fibroblasts to differentiate into myofibroblasts, which deposit collagen (extreacellular matrix proteins). The excessive buildup of collagen is known as fibrosis, which can be categorized by different textures such as interstitial, compact, diffuse, and patchy fibrosis (24). Regardless of pattern, fibrosis has altered electrophysiological properties characterized by slowed conduction velocity and susceptibility to unidirectional conduction block. This increased spatial heterogeneity is strongly associated with increased risk of arrhythmia

formation. It is possible for reentrant arrhythmias to occur without structural remodeling, due to conduction block near non-conductive pulmonary veins and chamber valves (64). However, this is significantly rarer than in individuals with structural remodeling.

Arrhythmias can also result from triggered activity. Triggered activity is characterized by spontaneous depolarizations preceding the next sinus beat (54). At the organ-scale, this can manifest as a premature or ectopic beat, either in the ventricles (premature ventricular complex; PVC) or the atria (premature atrial complex). Ectopic beats are not inherently dangerous, and PVCs have been observed in a majority of individuals during long-term ambulatory monitoring (65) However, increased PVC occurrence has also been associated with increased mortality in post-MI patients (66-68). The arrhythmia theory of “trigger and substrate” is partially attributable: increased ectopic beats correspond to more “trigger” opportunities, and the presence of heterogeneous substrate (such as scar and BZ formation following an MI) can together result in arrhythmia occurrence (24).

Ectopic beats are believed to be caused by to afterdepolarization events, which are grouped into early afterdepolarizations (EADs) and delayed afterdepolarizations (DADs). Both are myocyte-level events described by voltage fluctuations that result in a new AP; EADs occur during phase 2 or 3 repolarization in the cardiac AP, whereas DADs occur after full repolarization (phase 4). However, the mechanisms of EADs versus DADs are rather distinct.

EADs are associated with conditions of prolonged APD and reduced repolarization reserve (RRR), such as in genetic mutation long QT syndrome (LQTS) and in the presence of APD-prolonging drugs (69). Heart failure is also associated with EAD occurrence (70). Precise linking of cell-scale EADs to tissue- and organ-scale triggered activity has remained poorly understood (49, 69), since EADs would have to synchronize across different cells to have enough source to trigger a premature beat (71).

In comparison, DADs are caused by Ca^{2+} leak from the ryanodine receptors (RyRs) within the sarcoplasmic reticulum and are associated with conditions of intracellular Ca^{2+} overload (72). For instance, this has been established in the ischemic BZ tissue proximal to MI-induced scar (22, 23). Similarly to EADs, how exactly DADs (cell-scale events) can manifest into PVCs is not well understood (73).

In 1989, a randomized clinical trial (RCT) called the Cardiac Arrhythmia Suppression Trial (CAST) tested the hypothesis that reducing PVC occurrence could improve mortality in post-MI patients. However, the trial was halted prematurely after two of the three drug arms (flecainide and encainide) were shown to increase mortality and nonfatal cardiac arrests as compared to placebo, despite decreased PVC occurrence (74). The enrollment protocol was modified to instead patients more likely to experience serious arrhythmias and resumed as a second RCT (called CAST II) using just one of the drug arms (moricizine). CAST II was halted after the first 14-day period after preliminary data showed increased mortality and nonfatal cardiac arrest with moricizine as compared to placebo (75). Recent trials have continued to seek methods of reducing PVC occurrence in post-MI individuals (65), but significant caution has been exercised in treating PVCs since the outcomes from CAST and CAST II.

Finally, enhanced automaticity can be a mechanism of arrhythmia development. Automaticity is intrinsically present in the heart, such as in pacemaker cells in the SA node (that typically initiates sinus beats) (61). Enhanced automaticity is the initiation of poorly timed impulses by of these already automaticity predisposed cells, as well as cardiac cells from other sources (such as ectopic pacemaker cells) (55). For instance, if the SA node is damaged, other “latent” pacemakers (such as the AV node or Purkinje system) take over the role of maintaining intrinsic beating rate (61). Pacemaker tissue has also been found throughout the RA, rather than only in the SA node (76). Dysfunction of these automaticity-prone cell types, such as through genetic

mutations, reduction of external [K^+], and β-adrenergic agonists can result in ectopic pacemakers competing with the intrinsic pacemaker (61).

To transition to discussing the most common arrhythmia types, this dissertation will focus solely on atrial fibrillation (AFib) and ventricular tachycardia. Interestingly, the development of an atrial arrhythmia does not necessitate the development of a ventricular arrhythmia and vice versa. This is due to attributes of the His-Purkinje system conduction that acts as a signal filter and can prevent the abnormal conduction from propagating between the atria and ventricles.

Clinically, AFib is the most common heart arrhythmia and its incidence has been increasing in recent decades. AFib is primarily associated with an increased risk of ischemic stroke, and the first-line clinical response is to put the individual on blood thinners in an attempt to mitigate this risk (1). Although the rapid atrial contractions disrupt proper blood pooling in the atria before movement into the ventricles, this is not life-threatening because the atria can still partially fill without coordinated sinus contractions. AFib can occur asymptomatically, leading to a lack of proper treatment in part of the population.

The two primary treatments for AFib are anti-arrhythmic drugs (AADs) and catheter ablation procedures. AADs are not tolerated well by all patients, and can have decreasing effects over time. Catheter ablations are relatively non-invasive, frequently entering through the femoral artery and snaking up to the heart, where either localized heat (radiofrequency ablation) or localized cold temperatures (cryoballoon ablation) damages the surface of the heart. By rendering selected areas non-conductive, ablation procedures have been proven to reduce AFib occurrence but the 5-year survival rate from AFib nears 50% (1). A significant amount of research has been invested in recent decades into improving catheter ablation efficacy in the clinic (77).

Although atrial arrhythmias are more prevalent than ventricular arrhythmias, the difference in severity and immediate mortality risk is notable. VT can progress to VFib, which can result in

cardiac arrest (where the heart stops beating) and sudden cardiac death within minutes. Because contraction of the LV is responsible for a majority of blood flow, insufficient blood filling of the chamber results in a disruption of blood perfusion throughout the body. If this persists for more than a few minutes, irreversible damage occurs to major organs, such as the brain, heart, and lungs. All arrhythmias have a chance to terminate on their own, for reasons we do not fully understand. However, upwards of >90% of individuals who experience an out-of-hospital VFib for the first time die within 1 month; survival rates in individuals with short delay-to-defibrillation increased had survival rates of ≈50% but survival dropped rapidly with longer delays (78).

For those who have VT or VFib occur, shock therapy is the primary life-saving treatment, whether in the form of an automatic cardioverter defibrillator (AED) or implantable cardioverter defibrillator (ICD). Although AED access in public spaces has increased in recent decades in the US, most of the world lives without nearby access of an AED and thus mortality risk remains high in those who experience VT or VFib (79). ICDs are a valuable tool for preventing SCD, but must be proactively implanted into the patient (80). If an individual has strong risk factors for SCD (such as previous heart damage, or certain genetic mutations), then ICD implantation is frequently the first-line treatment. ICDs are frequently favored by clinicians and patients because of the security the implanted device provides. However, there are documented reductions of quality of life associated with ICD implantations, including psychological stress following inappropriate or appropriate shocks, damage to the heart by ICD shocks (81, 82). The second treatment option for VT/VFib risk are AADs, but these are poorly tolerated in most individuals and have significant side effects including heart failure (81). The third treatment option is a catheter ablation procedure, which decreases VT risk but is not always dependable (e.g., 50-75% freedom from VT at 6-12 months) (83). Proactively identifying those who are at risk for VT and VFib is an ongoing area of active research (84).

1.5 Cardiac action potential models

One of the most famous mathematical models in history was a series of papers by Hodgkin and Huxley in 1952 (14, 85-88). Their articles modeled the AP of a giant squid axon. When the pair were evaluating the voltage-dependent kinetics of various ion channels, the measured results differed markedly from expectations. However, Huxley proposed a series of gating variables to describe ion transport and gating: n^4 (to describe K^+ channels), and m^3 and h (to describe Na^+ channels) (40). A "leak" current (no gating variable) was also included to account for the remaining difference between predicted versus observed currents in the nerve. The ionic current summation was published as **Equation 1.2**:

$$I = C_M \frac{dV}{dt} + g_K n^4 (V - V_K) + g_{Na} m^3 h (V - V_{Na}) + g_1 (V - V_1)$$

Equation 1.2: Hodgkin-Huxley equation. Describes the action potential of a giant squid axon in terms of K^+, Na^+, and leak current, where C_m is membrane capacitance, V is membrane potential, V_{ion} is the reversal potential of each current (K^+, Na^+, and leak), g is conductance of the different currents, and n, m, and h are gating variables.

This computational model has been shown to be surprisingly accurate, partially because the giant squid axon has a relatively simple nervous mechanism (89). However, the Hodgkin-Huxley model proved to be pivotal to generations of electrophysiologists.

The first cardiac action potential model was published in 1962 by Denis Noble, which modified the Hodgkin-Huxley formulation to model cardiac Purkinje and pacemaker cells (10). Even though APDs differ enormously between neurons and cardiomyocytes (in humans: ≈1 ms in neurons vs. ≈300 ms in cardiomyocytes) potassium current changes, such as considering "two types" of K^+ channels (I_{K1} and I_{K2}) describing both inward and outward currents, recapitulated this discrepancy. Descriptions about the changes in modeled ionic currents provided insights into ion trafficking that were not experimentally observable at the time.

The original Hodgkin-Huxley formulations modeled the transport of ions as if there were a singular channel for each ion. In the present day, our knowledge of mammalian cardiomyocyte

ion channel physiology and genes encoding channel subunits has expanded greatly (42). We now know that there can be over a dozen genes encoding ion channels to transport a given ion, such as K^+ (42). We better appreciate now that excitable cell APs are species-dependent (54), cell-type dependent (29), location-dependent (5), and phenotype/genotype-dependent (90, 91) in ways that cause significant variability between individuals (92). More recently published human action potential models have expanded the number of modifiable ionic currents from three (Na^+, K^+, and leak current) to ≥15 in some recent models (12).

Later work published in the 1970s to 1990s established cardiomyocyte AP models of increasing complexity. This included advances such as the expanded ionic current formulations for Purkinje fibers (93), first mammalian ventricular AP model (94), considerations of intra- and extracellular ionic concentrations (95), inclusion of Ca^{2+} formulations (8, 9), adjustments to study APs during HF (96), the first human-specific atrial AP model (97), and the first human-specific ventricular AP model (13, 98). Current state-of-the-art AP models have significantly improved Ca^{2+} formulations (11, 12), have accurately recapitulated drug effects on certain ionic currents (99), and frequently consider data from multiple datasets (100). The heart has become one of the most computationally modeled organs (101, 102), because of the advancement of these biophysically-detailed, experimentally-validated cardiac action potential models and the insights into disease conditions (35, 98, 103-107) that these models have provided.

1.6 Image-derived computational cardiac models

In the past decade, an advancement in computational cardiac modeling has been the formulation of image-based, patient-specific heart models. These models were derived from patient cardiac images, typically either MRI or CT scans, by segmentation of the heart wall from the blood pool (108). A contrast agent (such as late gadolinium enhancement) is also administered, since areas of cardiac remodeling (such as fibrosis in the atria (109) or infarct scar and ischemic border zone tissue in the ventricles (110)) do not clear the contrast agent as quickly

as healthy myocardium. The remodeled tissue regions are also segmented and combined with the chamber wall data to form an 3D finite element (FE) model (111).

As described earlier (section 1.2), the organization of myofibrils into myocardial fibers creates a preferential conduction along the fiber orientation. Patient-specific modeling of myocardial fiber orientation has been difficult to achieve due to difficulties imaging cardiac fibers *in vivo* (112). However, both atlas-based (113) or rules-based (114) estimations have been shown to reasonably match *ex vivo* human fiber data, and have been incorporated into multiple FE heart model studies since then (108, 110, 111, 115, 116).

Once patient-derived FE models have been created, action potential models can be applied to model the continuum that comprises a tissue. Changes to the electrophysiological parameters based on experimental data (117-119) can be made to reflect the remodeled regions, such as infarct scar and border zone tissue in MI patients (115). Conductivity values for the respective regions (whether healthy or remodeled tissue) are adjusted to reflect experimental measurements for the corresponding tissues (115). It is worth noting that these modeling frameworks do not directly model Cx proteins and changes thereof during of diseased states. Instead, conductivity values are matched to conduction velocities observed experimentally. This approach homogenizes what is understood to be a complicated and spatially heterogeneous population of Cx proteins (25).

Examples of the full segmentation pipeline for atrial (120) and ventricular (111) models can be found elsewhere. Beyond studies examining experimental and theoretical concepts, patient-derived FE modeling have also begun to be evaluated for impact in clinical care. Recent studies published by Natalia Trayanova's group at Johns Hopkins have demonstrated that FE modeling can better inform individualized catheter ablation treatments when treating AFib (121) and post-MI VTs (122). Further work is needed to evaluate the therapeutic benefit of computationally guided FE models on catheter ablation techniques.

1.7 References

1. Boyle, P.M., J.C. Del Alamo, and N. Akoum, *Fibrosis, atrial fibrillation and stroke: clinical updates and emerging mechanistic models.* Heart, **2021**. 107(2): p. 99-105.

2. Waks, J.W. and A.E. Buxton, *Risk Stratification for Sudden Cardiac Death After Myocardial Infarction.* Annu Rev Med, **2018**. 69: p. 147-164.

3. Fedorov, V.V., et al., *Optical mapping of the isolated coronary-perfused human sinus node.* J Am Coll Cardiol, **2010**. 56(17): p. 1386-94.

4. Lou, Q., et al., *Transmural heterogeneity and remodeling of ventricular excitation-contraction coupling in human heart failure.* Circulation, **2011**. 123(17): p. 1881-90.

5. Glukhov, A.V., et al., *Transmural dispersion of repolarization in failing and nonfailing human ventricle.* Circ Res, **2010**. 106(5): p. 981-91.

6. Sanchez-Quintana, D., et al., *Anatomical Basis for the Cardiac Interventional Electrophysiologist.* Biomed Res Int, **2015**. 2015: p. 547364.

7. Milani-Nejad, N. and P.M. Janssen, *Small and large animal models in cardiac contraction research: advantages and disadvantages.* Pharmacol Ther, **2014**. 141(3): p. 235-49.

8. Luo, C.H. and Y. Rudy, *A dynamic model of the cardiac ventricular action potential. I. Simulations of ionic currents and concentration changes.* Circ Res, **1994**. 74(6): p. 1071-96.

9. Luo, C.H. and Y. Rudy, *A dynamic model of the cardiac ventricular action potential. II. Afterdepolarizations, triggered activity, and potentiation.* Circ Res, **1994**. 74(6): p. 1097-113.

10. Noble, D., *A modification of the Hodgkin--Huxley equations applicable to Purkinje fibre action and pace-maker potentials.* J Physiol, **1962**. 160(2): p. 317-52.

11. Grandi, E., F.S. Pasqualini, and D.M. Bers, *A novel computational model of the human ventricular action potential and Ca transient.* J Mol Cell Cardiol, **2010**. 48(1): p. 112-21.

12. O'Hara, T., et al., *Simulation of the undiseased human cardiac ventricular action potential: model formulation and experimental validation.* PLoS Comput Biol, **2011**. 7(5): p. e1002061.

13. ten Tusscher, K.H. and A.V. Panfilov, *Alternans and spiral breakup in a human ventricular tissue model.* Am J Physiol Heart Circ Physiol, **2006**. 291(3): p. H1088-100.

14. Hodgkin, A.L. and A.F. Huxley, *A quantitative description of membrane current and its application to conduction and excitation in nerve.* J Physiol, **1952**. 117(4): p. 500-44.

15. Mines, G.R., *On dynamic equilibrium in the heart.* J Physiol, **1913**. 46(4-5): p. 349-83.

16. Durrer, D., et al., *Total excitation of the isolated human heart.* Circulation, **1970**. 41(6): p. 899-912.

17. Pappano, A.J.W., Withrow Gil, *Cardiovascular physiology*. 11th ed. **2019**, Philadelphia, PA: Elsevier.

18. Nishitani, S., et al., *Development of Helical Myofiber Tracts in the Human Fetal Heart: Analysis of Myocardial Fiber Formation in the Left Ventricle From the Late Human Embryonic Period Using Diffusion Tensor Magnetic Resonance Imaging.* J Am Heart Assoc, **2020**. 9(19): p. e016422.

19. Boateng, S. and T. Sanborn, *Acute myocardial infarction.* Dis Mon, **2013**. 59(3): p. 83-96.

20. Dries, E., et al., *Altered adrenergic response in myocytes bordering a chronic myocardial infarction underlies in vivo triggered activity and repolarization instability.* J Physiol, **2020**. 598(14): p. 2875-2895.

21. Johnson, D.M. and G. Antoons, *Arrhythmogenic Mechanisms in Heart Failure: Linking β-Adrenergic Stimulation, Stretch, and Calcium.* Front Physiol, **2018**. 9: p. 1453.

22. Amoni, M., et al., *Discrete sites of frequent premature ventricular complexes cluster within the infarct border zone and coincide with high frequency of delayed afterdepolarizations under adrenergic stimulation.* Heart Rhythm, **2021**. 18(11): p. 1976-1987.

23. Campos, F.O., et al., *Subthreshold delayed afterdepolarizations provide an important arrhythmogenic substrate in the border zone of infarcted hearts.* Heart Rhythm, **2023**. 20(2): p. 299-306.

24. Nguyen, T.P., Z. Qu, and J.N. Weiss, *Cardiac fibrosis and arrhythmogenesis: the road to repair is paved with perils.* J Mol Cell Cardiol, **2014**. 70: p. 83-91.

25. Hesketh, G.G., J.E. Van Eyk, and G.F. Tomaselli, *Mechanisms of gap junction traffic in health and disease.* J Cardiovasc Pharmacol, **2009**. 54(4): p. 263-72.

26. Bers, D.M., *Cardiac excitation-contraction coupling.* Nature, **2002**. 415(6868): p. 198-205.

27. Grandi, E., et al., *Diversity of cells and signals in the cardiovascular system.* J Physiol, **2023**.

28. Tucker, N.R., et al., *Transcriptional and Cellular Diversity of the Human Heart.* Circulation, **2020**. 142(5): p. 466-482.

29. Litvinukova, M., et al., *Cells of the adult human heart.* Nature, **2020**. 588(7838): p. 466-472.

30. Ideker, R.E., W. Kong, and S. Pogwizd, *Purkinje fibers and arrhythmias.* Pacing Clin Electrophysiol, **2009**. 32(3): p. 283-5.

31. Nattel, S., C. Antzelevitch, and D. Noble, *Resolving the M-cell debate: why and how.* Heart Rhythm, **2011**. 8(8): p. 1293-5.

32. Hulsmans, M., et al., *Macrophages Facilitate Electrical Conduction in the Heart.* Cell, **2017**. 169(3): p. 510-522 e20.

33. Kohl, P., et al., *Electrical coupling of fibroblasts and myocytes: relevance for cardiac propagation.* J Electrocardiol, **2005**. 38(4 Suppl): p. 45-50.

34. Quinn, T.A., et al., *Electrotonic coupling of excitable and nonexcitable cells in the heart revealed by optogenetics.* Proc Natl Acad Sci U S A, **2016**. 113(51): p. 14852-14857.

35. Vigmond, E.J. and B.D. Stuyvers, *Modeling our understanding of the His-Purkinje system.* Prog Biophys Mol Biol, **2016**. 120(1-3): p. 179-88.

36. Rudy, Y., *Electrotonic cell-cell interactions in cardiac tissue: effects on action potential propagation and repolarization.* Ann N Y Acad Sci, **2005**. 1047: p. 308-13.

37. Spector, P., *Principles of cardiac electric propagation and their implications for re-entrant arrhythmias.* Circ Arrhythm Electrophysiol, **2013**. 6(3): p. 655-61.

38. Ciaccio, E.J., et al., *Source-Sink Mismatch Causing Functional Conduction Block in Re-Entrant Ventricular Tachycardia.* JACC Clin Electrophysiol, **2018**. 4(1): p. 1-16.

39. Hodgkin, A., Huxley, A, *Action Potentials Recorded from Inside a Nerve Fibre.* Nature, **1939**. 144: p. 710-711.

40. Schwiening, C.J., *A brief historical perspective: Hodgkin and Huxley.* J Physiol, **2012**. 590(11): p. 2571-5.

41. Hodgkin, A.L., A.F. Huxley, and B. Katz, *Measurement of current-voltage relations in the membrane of the giant axon of Loligo.* J Physiol, **1952**. 116(4): p. 424-48.

42. Varro, A., et al., *Cardiac transmembrane ion channels and action potentials: cellular physiology and arrhythmogenic behavior.* Physiol Rev, **2021**. 101(3): p. 1083-1176.

43. Hiraoka, M., et al., *Role of cardiac chloride currents in changes in action potential characteristics and arrhythmias.* Cardiovasc Res, **1998**. 40(1): p. 23-33.

44. Adkins, G.B. and M.J. Curtis, *Potential role of cardiac chloride channels and transporters as novel therapeutic targets.* Pharmacol Ther, **2015**. 145: p. 67-75.

45. Grant, A.O., *Cardiac ion channels.* Circ Arrhythm Electrophysiol, **2009**. 2(2): p. 185-94.

46. Varró, A. and I. Baczkó, *Cardiac ventricular repolarization reserve: a principle for understanding drug-related proarrhythmic risk.* Br J Pharmacol, **2011**. 164(1): p. 14-36.

47. Attwell, D., et al., *The steady state TTX-sensitive ("window") sodium current in cardiac Purkinje fibres.* Pflugers Arch, **1979**. 379(2): p. 137-42.

48. Benson, D.W., et al., *Congenital sick sinus syndrome caused by recessive mutations in the cardiac sodium channel gene (SCN5A).* J Clin Invest, **2003**. 112(7): p. 1019-28.

49. Qu, Z., et al., *Early afterdepolarizations in cardiac myocytes: beyond reduced repolarization reserve.* Cardiovasc Res, **2013**. 99(1): p. 6-15.

50. Agrawal, A., et al., *Models of the cardiac L-type calcium current: A quantitative review.* WIREs Mech Dis, **2023**. 15(1): p. e1581.

51. Lo, A.C.Y., et al., *Afterdepolarizations and abnormal calcium handling in atrial myocytes with modulated SERCA uptake: a sensitivity analysis of calcium handling channels.* Philos Trans A Math Phys Eng Sci, **2020**. 378(2173): p. 20190557.

52. Song, Z., et al., *Calcium-voltage coupling in the genesis of early and delayed afterdepolarizations in cardiac myocytes.* Biophys J, **2015**. 108(8): p. 1908-21.

53. Campos, F.O., et al., *Stochastic spontaneous calcium release events trigger premature ventricular complexes by overcoming electrotonic load.* Cardiovasc Res, **2015**. 107(1): p. 175-83.

54. Blackwell, D.J., J. Schmeckpeper, and B.C. Knollmann, *Animal Models to Study Cardiac Arrhythmias.* Circ Res, **2022**. 130(12): p. 1926-1964.

55. Tse, G., *Mechanisms of cardiac arrhythmias.* J Arrhythm, **2016**. 32(2): p. 75-81.

56. Guevara, M.R., et al., *George Ralph Mines (1886-1914): the dawn of cardiac nonlinear dynamics.* J Physiol, **2016**. 594(9): p. 2361-71.

57. Mechulan, A., et al., *An improved window of interest for electroanatomical mapping of atrial tachycardia.* J Interv Card Electrophysiol, **2022**. 63(1): p. 29-37.

58. Tung, R., *Substrate Mapping in Ventricular Arrhythmias.* Card Electrophysiol Clin, **2019**. 11(4): p. 657-663.

59. Peters, N.S., et al., *Characteristics of the temporal and spatial excitable gap in anisotropic reentrant circuits causing sustained ventricular tachycardia.* Circ Res, **1998**. 82(2): p. 279-93.

60. Shaw, R.M. and Y. Rudy, *The vulnerable window for unidirectional block in cardiac tissue: characterization and dependence on membrane excitability and intercellular coupling.* J Cardiovasc Electrophysiol, **1995**. 6(2): p. 115-31.

61. Antzelevitch, C. and A. Burashnikov, *Overview of Basic Mechanisms of Cardiac Arrhythmia.* Card Electrophysiol Clin, **2011**. 3(1): p. 23-45.

62. Arbustini, E., C.M. Kramer, and J. Narula, *Arrhythmogenic Potential of Border Zone After Myocardial Infarction: Scar Is More Than Just a Healed Wound.* JACC Cardiovasc Imaging, **2018**. 11(4): p. 573-576.

63. de Jong, S., et al., *Fibrosis and cardiac arrhythmias.* J Cardiovasc Pharmacol, **2011**. 57(6): p. 630-8.

64. Mahida, S., et al., *Science Linking Pulmonary Veins and Atrial Fibrillation.* Arrhythm Electrophysiol Rev, **2015**. 4(1): p. 40-3.

65. Marcus, G.M., *Evaluation and Management of Premature Ventricular Complexes.* Circulation, **2020**. 141(17): p. 1404-1418.

66. Bigger, J.T., Jr., et al., *The relationships among ventricular arrhythmias, left ventricular dysfunction, and mortality in the 2 years after myocardial infarction.* Circulation, **1984**. 69(2): p. 250-8.

67. Mukharji, J., et al., *Risk factors for sudden death after acute myocardial infarction: two-year follow-up.* Am J Cardiol, **1984**. 54(1): p. 31-6.

68. Moss, A.J., et al., *Ventricular ectopic beats and their relation to sudden and nonsudden cardiac death after myocardial infarction.* Circulation, **1979**. 60(5): p. 998-1003.

69. Weiss, J.N., et al., *Early afterdepolarizations and cardiac arrhythmias.* Heart Rhythm, **2010**. 7(12): p. 1891-9.

70. Maruyama, M., et al., *Genesis of phase 3 early afterdepolarizations and triggered activity in acquired long-QT syndrome.* Circ Arrhythm Electrophysiol, **2011**. 4(1): p. 103-11.

71. Xie, Y., et al., *So little source, so much sink: requirements for afterdepolarizations to propagate in tissue.* Biophys J, **2010**. 99(5): p. 1408-15.

72. Wit, A.L., *Afterdepolarizations and triggered activity as a mechanism for clinical arrhythmias.* Pacing Clin Electrophysiol, **2018**.

73. Liu, M.B., et al., *Delayed afterdepolarizations generate both triggers and a vulnerable substrate promoting reentry in cardiac tissue.* Heart Rhythm, **2015**. 12(10): p. 2115-24.

74. Cardiac Arrhythmia Suppression Trial, I., *Preliminary report: effect of encainide and flecainide on mortality in a randomized trial of arrhythmia suppression after myocardial infarction.* N Engl J Med, **1989**. 321(6): p. 406-12.

75. Cardiac Arrhythmia Suppression Trial, I.I.I., *Effect of the antiarrhythmic agent moricizine on survival after myocardial infarction.* N Engl J Med, **1992**. 327(4): p. 227-33.

76. Monfredi, O., et al., *The anatomy and physiology of the sinoatrial node--a contemporary review.* Pacing Clin Electrophysiol, **2010**. 33(11): p. 1392-406.

77. Krummen, D.E., et al., *Mechanisms of human atrial fibrillation initiation: clinical and computational studies of repolarization restitution and activation latency.* Circ Arrhythm Electrophysiol, **2012**. 5(6): p. 1149-59.

78. Holmberg, M., S. Holmberg, and J. Herlitz, *Incidence, duration and survival of ventricular fibrillation in out-of-hospital cardiac arrest patients in sweden.* Resuscitation, **2000**. 44(1): p. 7-17.

79. Mao, R.D. and M.E. Ong, *Public access defibrillation: improving accessibility and outcomes.* Br Med Bull, **2016**. 118(1): p. 25-32.

80. Moss, A.J., et al., *Prophylactic implantation of a defibrillator in patients with myocardial infarction and reduced ejection fraction.* The New England journal of medicine, **2002**. 346(12): p. 877-883.

81. Poole, J.E., et al., *Prognostic importance of defibrillator shocks in patients with heart failure.* The New England journal of medicine, **2008**. 359(10): p. 1009-1017.

82. Pedersen, S.S., et al., *Risk of chronic anxiety in implantable defibrillator patients: a multi-center study.* International journal of cardiology, **2011**. 147(3): p. 420-423.

83. Tung, R., N.G. Boyle, and K. Shivkumar, *Catheter ablation of ventricular tachycardia.* Circulation, **2010**. 122(3): p. e389-91.

84. Vergara, P., et al., *Predictive Score for Identifying Survival and Recurrence Risk Profiles in Patients Undergoing Ventricular Tachycardia Ablation: The I-VT Score.* Circ Arrhythm Electrophysiol, **2018**. 11(12): p. e006730.

85. Hodgkin, A.L. and A.F. Huxley, *The dual effect of membrane potential on sodium conductance in the giant axon of Loligo.* J Physiol, **1952**. 116(4): p. 497-506.

86. Hodgkin, A.L. and A.F. Huxley, *The components of membrane conductance in the giant axon of Loligo.* J Physiol, **1952**. 116(4): p. 473-96.

87. Hodgkin, A.L. and A.F. Huxley, *Currents carried by sodium and potassium ions through the membrane of the giant axon of Loligo.* J Physiol, **1952**. 116(4): p. 449-72.

88. Hodgkin, A.L. and A.F. Huxley, *Propagation of electrical signals along giant nerve fibers.* Proc R Soc Lond B Biol Sci, **1952**. 140(899): p. 177-83.

89. Noble, D., *Modeling the heart.* Physiology (Bethesda), **2004**. 19: p. 191-7.

90. Moss, A.J., et al., *Clinical aspects of type-1 long-QT syndrome by location, coding type, and biophysical function of mutations involving the KCNQ1 gene.* Circulation, **2007**. 115(19): p. 2481-9.

91. Modell, S.M. and M.H. Lehmann, *The long QT syndrome family of cardiac ion channelopathies: a HuGE review.* Genet Med, **2006**. 8(3): p. 143-55.

92. Varshneya, M., X. Mei, and E.A. Sobie, *Prediction of arrhythmia susceptibility through mathematical modeling and machine learning.* Proc Natl Acad Sci U S A, **2021**. 118(37).

93. McAllister, R.E., D. Noble, and R.W. Tsien, *Reconstruction of the electrical activity of cardiac Purkinje fibres.* J Physiol, **1975**. 251(1): p. 1-59.

94. Beeler, G.W. and H. Reuter, *Reconstruction of the action potential of ventricular myocardial fibres.* J Physiol, **1977**. 268(1): p. 177-210.

95. DiFrancesco, D. and D. Noble, *A model of cardiac electrical activity incorporating ionic pumps and concentration changes.* Philos Trans R Soc Lond B Biol Sci, **1985**. 307(1133): p. 353-98.

96. Priebe, L. and D.J. Beuckelmann, *Simulation study of cellular electric properties in heart failure.* Circ Res, **1998**. 82(11): p. 1206-23.

97. Courtemanche, M., R.J. Ramirez, and S. Nattel, *Ionic mechanisms underlying human atrial action potential properties: insights from a mathematical model.* Am J Physiol, **1998**. 275(1): p. H301-21.

98. ten Tusscher, K.H., et al., *A model for human ventricular tissue.* Am J Physiol Heart Circ Physiol, **2004**. 286(4): p. H1573-89.

99. Tomek, J., et al., *Development, calibration, and validation of a novel human ventricular myocyte model in health, disease, and drug block.* Elife, **2019**. 8.

100. Kernik, D.C., et al., *A computational model of induced pluripotent stem-cell derived cardiomyocytes incorporating experimental variability from multiple data sources.* J Physiol, **2019**. 597(17): p. 4533-4564.

101. Noble, D., *Modeling the heart--from genes to cells to the whole organ.* Science, **2002**. 295(5560): p. 1678-82.

102. Henriquez, C.S., *A brief history of tissue models for cardiac electrophysiology.* IEEE Trans Biomed Eng, **2014**. 61(5): p. 1457-65.

103. Vandersickel, N., et al., *A study of early afterdepolarizations in a model for human ventricular tissue.* PLoS One, **2014**. 9(1): p. e84595.

104. Huang, X., Z. Song, and Z. Qu, *Determinants of early afterdepolarization properties in ventricular myocyte models.* PLoS Comput Biol, **2018**. 14(11): p. e1006382.

105. Barrio, R., et al., *Dynamical analysis of early afterdepolarization patterns in a biophysically detailed cardiac model.* Chaos, **2021**. 31(7): p. 073137.

106. Moreno, J.D., et al., *A computational model to predict the effects of class I anti-arrhythmic drugs on ventricular rhythms.* Sci Transl Med, **2011**. 3(98): p. 98ra83.

107. Morotti, S., et al., *A novel computational model of mouse myocyte electrophysiology to assess the synergy between Na+ loading and CaMKII.* J Physiol, **2014**. 592(6): p. 1181-97.

108. Prakosa, A., et al., *Methodology for image-based reconstruction of ventricular geometry for patient-specific modeling of cardiac electrophysiology.* Prog Biophys Mol Biol, **2014**. 115(2-3): p. 226-34.

109. Oakes, R.S., et al., *Detection and quantification of left atrial structural remodeling with delayed-enhancement magnetic resonance imaging in patients with atrial fibrillation.* Circulation, **2009**. 119(13): p. 1758-67.

110. Ukwatta, E., et al., *Image-based reconstruction of three-dimensional myocardial infarct geometry for patient-specific modeling of cardiac electrophysiology.* Med Phys, **2015**. 42(8): p. 4579-90.

111. Arevalo, H.J., et al., *Arrhythmia risk stratification of patients after myocardial infarction using personalized heart models.* Nat Commun, **2016**. 7: p. 11437.

112. Watson, S.R., J.D. Dormer, and B. Fei, *Imaging technologies for cardiac fiber and heart failure: a review.* Heart Fail Rev, **2018**. 23(2): p. 273-289.

113. Vadakkumpadan, F., et al., *Image-based estimation of ventricular fiber orientations for personalized modeling of cardiac electrophysiology.* IEEE Trans Med Imaging, **2012**. 31(5): p. 1051-60.
114. Bayer, J.D., et al., *A novel rule-based algorithm for assigning myocardial fiber orientation to computational heart models.* Ann Biomed Eng, **2012**. 40(10): p. 2243-54.
115. Ochs, A.R., et al., *Optogenetic Stimulation Using Anion Channelrhodopsin (GtACR1) Facilitates Termination of Reentrant Arrhythmias With Low Light Energy Requirements: A Computational Study.* Front Physiol, **2021**. 12: p. 718622.
116. Karathanos, T.V., et al., *Opsin spectral sensitivity determines the effectiveness of optogenetic termination of ventricular fibrillation in the human heart: a simulation study.* J Physiol, **2016**. 594(23): p. 6879-6891.
117. Ashikaga, H., et al., *Feasibility of image-based simulation to estimate ablation target in human ventricular arrhythmia.* Heart Rhythm, **2013**. 10(8): p. 1109-16.
118. Deng, D., et al., *Accuracy of prediction of infarct-related arrhythmic circuits from image-based models reconstructed from low and high resolution MRI.* Front Physiol, **2015**. 6: p. 282.
119. Maguire, C.T., et al., *Implications of ventricular arrhythmia vulnerability during murine electrophysiology studies.* Physiol Genomics, **2003**. 15(1): p. 84-91.
120. Zahid, S., et al., *Patient-derived models link re-entrant driver localization in atrial fibrillation to fibrosis spatial pattern.* Cardiovasc Res, **2016**. 110(3): p. 443-54.
121. Boyle, P.M., et al., *Computationally guided personalized targeted ablation of persistent atrial fibrillation.* Nat Biomed Eng, **2019**. 3(11): p. 870-879.
122. Jelvehgaran, P., et al., *Computational Re-Entry Vulnerability Index Mapping to Guide Ablation in Patients With Postmyocardial Infarction Ventricular Tachycardia.* JACC Clin Electrophysiol, **2023**. 9(3): p. 301-310.

Chapter 2 | Optogenetics Background

2.1 Brief Overview about Optogenetics

Optogenetics is the genetic transduction of non-mammalian, light-sensitive ion pumps and channels (opsins) into mammalian cells. There are two main classes of opsins: optogenetic actuators (which facilitate current flow across the membrane in response to light) and optogenetic sensors (which emit light in response to intracellular changes). For the purposes of this dissertation, only optogenetic actuators will be covered; applications of optogenetic sensors can be found elsewhere (1, 2).

The foundational science of optogenetics was built upon the study of rhodopsins. Rhodopsins are light-activated ion-trafficking pumps trafficking primarily protons (H^+) that were found in algae and single-cell organisms. The group of Peter Hegemann discovered the channelrhodopsin in 2002: a light-sensitive ion channel derived from algae (3). This finding intrigued a neuroscientist at Stanford named Karl Deisseroth, who communicated with Dr. Hegemann about the discovery. In 2005, Deisseroth's group successfully expressed the algal protein Channelrhodopsin-2 (ChR2) in mouse neuronal cells and used blue light to trigger action potentials (4). Previously, neuroscientists were limited to electrical or pharmacological stimulation methods, which had low spatial specificity or long time scales of action (minutes to hours), respectively. However, ChR2 could be selectively expressed in a particular brain structure (through the use of cell-specific promoters) thereby allowing for selective stimulation without activating other areas. Furthermore, the speed of excitation (≈ms), lack of negative basal interference on neuronal function, and rapid opsin channel recovery after light removal all provided significant advantages over previous tools. This technique was eventually coined as optogenetics (5). In the nearly two decades since this seminal paper, this technology has received an enormous amount of attention and study, primarily because of its critical importance to the

neuroscience field. This has provided a diverse toolbox to those interested in controlling excitable cell electrical activity.

The expression of optogenetic actuators in cardiomyocytes was first achieved in 2010, by different groups expressing ChR2 in zebrafish hearts (6) and transgenic mice (7). A variety of cardiac applications were later explored using optogenetic stimulation: termination of ventricular (8-10) and atrial (11, 12) arrhythmias, pacing (7, 13), control of spiral waves (14-17), control of G-coupled protein signaling (18, 19), the probing of specific cardiac adjacent cell types (20, 21), and the creation of all-optical measurement assays (20, 22-24). These studies have been instrumental to establishing cardiac optogenetics as a valuable experimental tool.

2.2 A Brief Survey of Relevant Opsins and their Characteristics

In the ~15-20 years since optogenetics was founded, there are now hundreds of discovered opsins and characterized variants (25, 26) and opsin discovery remains an area of active research (27, 28). In some cases, genetic engineering has designed, created, and expressed created man-made opsins (29, 30). A number of different characteristics define this breadth of opsins: ion selectivity (or lack thereof); E_{rev} (often directly related to the ions trafficked); responsive wavelength range; unitary channel conductance; and the photocurrent kinetics (e.g., speed of current onset, speed of current inactivation after light cessation, and speed of inactivated channel recovery following light exposure).

Of these properties, attention towards opsin wavelength has often been focused on red-shifted and red wavelength opsins (31). This is because the majority of opsins respond primarily to blue light (32), which has lower tissue penetration (see section 2.4). The other important characteristic has been the E_{rev} for a given opsin. Most channelrhodopsins have tended to have E_{rev} at positive enough voltages to have depolarizing effects in human excitable cells (such as neurons and cardiomyocytes). In comparison, opsins with repolarizing or hyperpolarizing E_{rev} in these cells have been primarily limited to ion pumps that move a single ion per photon, such as

archrhodopsin (Arch) or Halorhodopsin (33). Discoveries of anion channelrhodopsins and channelrhodopsins with more negative E_{rev} have been much welcomed because of the previous dearth of inhibition optogenetic tools with higher photocurrents (relative to ion pumps) (34).

To briefly discuss some of the most important opsins that are used in this dissertation, one should look no further than channelrhodopsin-2 (ChR2). ChR2 is the most characterized and applied opsin to date (35). It has been established as a cation-unspecific conducting opsin with rapid on-rate, moderate channel closing rate, and high sensitization (36). Since its first expression in neurons in 2005 (4), there have been many dozens of characterized variants. However, early discovered H134R variant had higher photocurrents but slower kinetics than the original ChR2 and is frequently used in optogenetics experiments to this day (37).

The discovery of *Guillardia theta* anion-conducting channelrhodopsins (ACRs) in 2015 established channelrhodopsins with up to 12-fold higher photocurrents (albeit with 3-fold higher expression) than the proton pump Arch (38). These GtACRs were characterized as trafficking primarily Cl^- ions (38, 39). Anion channelrhodopsin-1 (GtACR1) in particular had a higher photocurrent than anion channelrhodopsin-2 (GtACR2), and a slightly more red-shifted maximum wavelength response (515 nm “green” light, rather than ~480 nm blue light range). A later study established a family of red-shifted ACRs, although their stationary photocurrents were notably lower than GtACR1 (40).

When GtACR1 was first expressed in cardiomyocytes in 2016, the opsin was initially published as having hyperpolarizing effects in primary neonatal rat cardiomyocytes (E_{rev} = –90 mV, (39)). However, a later study demonstrated that this was inaccurate, by using GtACR1 to *trigger* action potentials in zebrafish cardiomyocytes (41). This would not have been possible in a truly hyperpolarizing opsin. The study characterized GtACR1 of –43 to –51 mV at moderate and high internal [Cl^-] in zebrafish cardiomyocytes (Fig. S1C, (41)). With hindsight, it appears that in the original GtACR1 study, the pipette (extracellular solution) [Cl^-] in the main text body were non-

physiologic for typical cardiomyocytes. When pipette [Cl^-] was varied (Fig. S1, (39)), the GtACR1 E_{rev} shifted closer to –40 mV. Although this was disappointing, studies by our group and others (41, 42) have demonstrated the repolarizing benefits of GtACR1, even while the opsin reverses its current and has depolarizing effects at V_m above –40 mV.

Significant advances in repolarizing and hyperpolarizing channelrhodopsin discovery have been published in the past year: naturally-occurring, potassium-conducting channelrhodopsins. Two opsins have been identified: *Hyphochytrium catenoides* kalium rhodopsins (HcKCRs) (28, 43) and *Wobblia* inhibitory channelrhopsin (WiChRs) (28). Potassium-conducting channelrhodopsins have been long sought after, due to how potassium conduction is strongly repolarizing and trafficked through more normal physiological means than chloride ions. This is also significant in part because there has long been concerns about Cl- concentrations in cardiomyocytes and recovery following continued stimulation of ACRs. The HcKCR opsins expressed in two studies have demonstrated a relatively strong photocurrents and relatively negative E_{rev}, although those E_{rev} values appeared to shift over time with constant illumination (HcKCR1: E_{rev} ≈–63 mV initially → ≈–55 mV after 1000 ms illumination (27)). In comparison, the opsin WiChR appears to have a hyperpolarizing reversal potential (E_{rev} ≈–90 mV in both ND7/23 mouse neuroblastoma cells and induced pluripotent stem cell-derived cardiomyocytes) and fast on kinetics (28). However, one of the primary limitations of WiChR (from this dataset) is the extremely long off kinetics of the channel. These were so extended that a 5 ms pulse of light in mouse neurons (using 2-photon microscopy) prevented APs paced at 2 Hz for >400 ms afterwards (Fig. S13A, (28)). Depending on the intended experiment (in both neurons and cardiomyocytes), having such an extremely long inhibitory effect may limit its broad application.

To contrast the magnitude of optogenetic currents against the ionic currents (**Table 1.2**), **Table 1.3** shows the maximum conductance values for the different opsins used in this dissertation. For rationale and citations for each value, please refer to the Methods sections for

each chapter. ChR2 is used in Chapters 3-5, GtACR1 is used in Chapters 3-5, and Wobblia inhibitory channelrhodopsin is used only in Chapter 5.

Table 2.1*: Maximum conductance values of opsins used throughout this dissertation.*

Opsin names	Symbol	Maximum conductance (mS/μF)
(Chapter 3) Channelrhodopsin-2	G_{ChR2}	0.11
(Chapters 4 & 5) Channelrhodopsin-2	G_{ChR2}	0.17
Guillardia theta anion channelrhodopsin	G_{GtACR1}	1.4
Wobblia inhibitory channelrhodopsin	G_{WiChR}	1.4

2.3 Opsin gene delivery and expression

One of the fundamental aspects of optogenetics is the *heterologous* expression of opsins, meaning that the protein is expressed in cells that do not normally have that protein. An important litmus test for opsin expression is whether the expressed protein significantly alters the "native" electrical behavior of the cell. This matters because although most opsins have not established damaging effects on the cell membrane, the presence of current flow without light stimulation (termed "dark currents") would be dangerous or disruptive to the cell being studied. Expression of opsins in specific cell types can also be variable or difficult (44).

Two primary expression methods exist: the viral transduction of the opsin (44, 45), or the transgenic expression of the opsin into a particular animal line (frequently mice or rats) (46). Both methods will be talked about briefly and specifically in the context of cardiac optogenetics.

Traditionally, lentiviruses, adenoviruses (AVs), and adeno-associated viruses (AAVs) have all been used. Broadly, the opsin is conjugated to viruses, then delivered through a variety of methods, such as portal vein delivery (45) or "gene painting" by delivering the solution using an open chest setup (12). Most of these studies have been conducted in small animal models (e.g., mice or rats). Several studies have shown that AVs have had relatively low long-term expression (~days to weeks) (44). In comparison, AAV transduction in cardiomyocytes have

found that transfection can persist for long periods of time (e.g. studies testing up to 1 year following transfection) (12).

2.4 Attenuation of light, and Methods of Light Delivery

A difficult problem for cardiac optogenetics is the application of this visible light to the transfected tissue. Initial cardiac optogenetics studies that were performed using *in vitro* cardiomyocyte monolayers (14, 47, 48) and *ex vivo* Langendorff-perfused mouse hearts (7, 8). Because the light was *not* obstructed in any meaningful way from reaching the opsin-expressing tissue, there would be no reduction of the applied irradiance (i.e., no light attenuation). When the first *in vivo* cardiac optogenetics studies were performed (10, 12), the experimental setup used an open-chest surgery to bypass the problem of skin, ribcage bones, and other fibrous tissue from absorbing the applied light.

Two primary attenuation problems can occur when light passes through mammalian tissue: photons can be scattered or absorbed. As stated earlier (section 1.2), the majority of opsins respond to the blue wavelength light, which unfortunately have high attenuation by cardiac tissue. A study evaluating the optical properties of porcine heart tissue using visible light (49) demonstrated that visible light in the approximately 470-630 nm (by eye: blue to red-orange) range was significantly absorbed and moderately scattered by the myocardial tissue. This maximal absorption peaked at 560 nm (by eye: yellow-green). In comparison, visible light in the 630-700 nm (by eye: red-orange to dark red) range and near infrared light in the 700-900 nm range had relatively very little absorption and less scattering than 470-630 nm.

LV wall thicknesses can vary significantly between individuals, partially influenced by age, gender, ethnicity, and physical fitness status (50, 51). Previous modeling studies (8, 10) have consistently found that the attenuation of light by heart tissue is one of the primary problems of whole-heart illumination. Furthermore, the degree of light-elicited current varies as a function of myocardial depth in these experiments, creating a heterogeneous optogenetic effect.

For similar reasons, cardiac optogenetic stimulation only affecting small regions could be pro-arrhythmogenic. It has been previously established that local heterogeneity in repolarization capacity can act as a substrate that initiates and perpetuates arrhythmias (52). To this date, selective light patterning of cardiac tissue *in vivo* remains relatively unexplored. However, for *in vitro* applications this heterogeneity is less consequential, and can even be used to creatively control arrhythmias. A beautiful study by Burton et al. previously demonstrated the use of spatially timed and patterned light on a cardiac monolayer to control the chirality of a spiral wave arrhythmia (14), and work by Crocini et al. demonstrated how spatially controlled light ("triple barrier") could terminate arrhythmias without illuminating the entire substrate (48).

Finally, there has been an explosion of novel illumination device publications in the past several years that have not been harnessed yet by experimentalists. These include tightly spatially controlled light illumination of a mouse heart with simultaneous electrical mapping (53), self-adaptive strain sensors with feedback loop for cardiac optogenetic stimulation (54), and leadless, battery-free pacemakers and optogenetic stimulation devices (55-57). Although these devices have only been explored in rodent models to date, it could eventually facilitate the possibility of whole-organ illumination in future experiments, with simultaneously greater optogenetic control and electrical measurements than ever previously possible.

2.5 References

1. Entcheva, E. and M.W. Kay, *Cardiac optogenetics: a decade of enlightenment.* Nat Rev Cardiol, **2020**.

2. Rost, B.R., et al., *Optogenetic Tools for Subcellular Applications in Neuroscience.* Neuron, **2017**. 96(3): p. 572-603.

3. Nagel, G., et al., *Channelrhodopsin-1: a light-gated proton channel in green algae.* Science, **2002**. 296(5577): p. 2395-8.

4. Boyden, E.S., et al., *Millisecond-timescale, genetically targeted optical control of neural activity.* Nature neuroscience, **2005**. 8(9): p. 1263-1268.

5. Deisseroth, K., et al., *Next-generation optical technologies for illuminating genetically targeted brain circuits.* J Neurosci, **2006**. 26(41): p. 10380-6.

6. Arrenberg, A.B., et al., *Optogenetic control of cardiac function.* Science, **2010**. 330(6006): p. 971-4.

7. Bruegmann, T., et al., *Optogenetic control of heart muscle in vitro and in vivo.* Nature methods, **2010**. 7(11): p. 897-900.

8. Bruegmann, T., et al., *Optogenetic defibrillation terminates ventricular arrhythmia in mouse hearts and human simulations.* J Clin Invest, **2016**. 126(10): p. 3894-3904.

9. Rao, P., et al., *Near-infrared light driven tissue-penetrating cardiac optogenetics via upconversion nanoparticles in vivo.* Biomed Opt Express, **2020**. 11(3): p. 1401-1416.

10. Nyns, E.C.A., et al., *Optical ventricular cardioversion by local optogenetic targeting and LED implantation in a cardiomyopathic rat model.* Cardiovasc Res, **2021**.

11. Bruegmann, T., et al., *Optogenetic termination of atrial fibrillation in mice.* Cardiovasc Res, **2018**. 114(5): p. 713-723.

12. Nyns, E.C.A., et al., *An automated hybrid bioelectronic system for autogenous restoration of sinus rhythm in atrial fibrillation.* Science translational medicine, **2019**. 11(481): p. eaau6447.

13. Nussinovitch, U., R. Shinnawi, and L. Gepstein, *Modulation of cardiac tissue electrophysiological properties with light-sensitive proteins.* Cardiovascular research, **2014**. 102(1): p. 176-187.

14. Burton, R.A., et al., *Optical control of excitation waves in cardiac tissue.* Nat Photonics, **2015**. 9(12): p. 813-816.

15. Hussaini, S., et al., *Drift and termination of spiral waves in optogenetically modified cardiac tissue at sub-threshold illumination.* Elife, **2021**. 10.

16. Majumder, R., et al., *Pulsed low-energy stimulation initiates electric turbulence in cardiac tissue.* PLoS Comput Biol, **2021**. 17(10): p. e1009476.

17. Li, T.C., et al., *Control of the chirality of spiral waves and recreation of spatial excitation patterns through optogenetics.* Phys Rev E, **2022**. 105(1-1): p. 014214.

18. Beiert, T., T. Bruegmann, and P. Sasse, *Optogenetic activation of Gq signalling modulates pacemaker activity of cardiomyocytes.* Cardiovasc Res, **2014**. 102(3): p. 507-16.

19. Makowka, P., et al., *Optogenetic stimulation of G(s)-signaling in the heart with high spatio-temporal precision.* Nature communications, **2019**. 10(1): p. 1281-1281.

20. Boyle, P.M., et al., *OptoGap is an optogenetics-enabled assay for quantification of cell-cell coupling in multicellular cardiac tissue.* Sci Rep, **2021**. 11(1): p. 9310.

21. Zaglia, T., et al., *Optogenetic determination of the myocardial requirements for extrasystoles by cell type-specific targeting of ChannelRhodopsin-2.* Proceedings of the National Academy of Sciences of the United States of America, **2015**. 112(32): p. E4495-E4504.

22. Ambrosi, C.M., et al., *Cardiac applications of optogenetics.* Progress in biophysics and molecular biology, **2014**. 115(2-3): p. 294-304.

23. Klimas, A., et al., *OptoDyCE as an automated system for high-throughput all-optical dynamic cardiac electrophysiology.* Nat Commun, **2016**. 7: p. 11542.

24. Mullenbroich, M.C., et al., *Novel Optics-Based Approaches for Cardiac Electrophysiology: A Review.* Front Physiol, **2021**. 12: p. 769586.

25. Fenno, L., O. Yizhar, and K. Deisseroth, *The development and application of optogenetics.* Annu Rev Neurosci, **2011**. 34: p. 389-412.

26. Joshi, J., M. Rubart, and W. Zhu, *Optogenetics: Background, Methodological Advances and Potential Applications for Cardiovascular Research and Medicine.* Front Bioeng Biotechnol, **2019**. 7: p. 466.

27. Govorunova, E.G., et al., *Kalium channelrhodopsins are natural light-gated potassium channels that mediate optogenetic inhibition.* Nat Neurosci, **2022**. 25(7): p. 967-974.

28. Vierock, J., et al., *WiChR, a highly potassium selective channelrhodopsin for low-light one- and two-photon inhibition of excitable cells.* Sci Adv, **2022**: p. eadd7729.

29. Berndt, A., et al., *Structure-guided transformation of channelrhodopsin into a light-activated chloride channel.* Science, **2014**. 344(6182): p. 420-4.

30. Berndt, A., et al., *Structural foundations of optogenetics: Determinants of channelrhodopsin ion selectivity.* Proc Natl Acad Sci U S A, **2016**. 113(4): p. 822-9.

31. Lehtinen, K., M.S. Nokia, and H. Takala, *Red Light Optogenetics in Neuroscience.* Front Cell Neurosci, **2021**. 15: p. 778900.

32. Losi, A., K.H. Gardner, and A. Moglich, *Blue-Light Receptors for Optogenetics.* Chem Rev, **2018**. 118(21): p. 10659-10709.

33. Kandori, H., *Ion-pumping microbial rhodopsins.* Front Mol Biosci, **2015**. 2: p. 52.

34. Govorunova, E.G., O.A. Sineshchekov, and J.L. Spudich, *Emerging Diversity of Channelrhodopsins and Their Structure-Function Relationships.* Front Cell Neurosci, **2021**. 15: p. 800313.

35. Lin, J.Y., *A user's guide to channelrhodopsin variants: features, limitations and future developments.* Exp Physiol, **2011**. 96(1): p. 19-25.

36. Nagel, G., et al., *Light activation of channelrhodopsin-2 in excitable cells of Caenorhabditis elegans triggers rapid behavioral responses.* Curr Biol, **2005**. 15(24): p. 2279-84.

37. Lin, J.Y., et al., *Characterization of engineered channelrhodopsin variants with improved properties and kinetics.* Biophys J, **2009**. 96(5): p. 1803-14.

38. Govorunova, E.G., et al., *Natural light-gated anion channels: A family of microbial rhodopsins for advanced optogenetics.* Science, **2015**. 349(6248): p. 647-50.

39. Govorunova, E.G., et al., *Anion channelrhodopsins for inhibitory cardiac optogenetics.* Sci Rep, **2016**. 6: p. 33530.

40. Govorunova, E.G., et al., *RubyACRs, nonalgal anion channelrhodopsins with highly red-shifted absorption.* Proc Natl Acad Sci U S A, **2020**. 117(37): p. 22833-22840.

41. Kopton, R.A., et al., *Cardiac Electrophysiological Effects of Light-Activated Chloride Channels.* Front Physiol, **2018**. 9: p. 1806.

42. Ochs, A.R., et al., *Optogenetic Stimulation Using Anion Channelrhodopsin (GtACR1) Facilitates Termination of Reentrant Arrhythmias With Low Light Energy Requirements: A Computational Study.* Front Physiol, **2021**. 12: p. 718622.

43. Gruber, A., et al., *Optogenetic Control of Human Induced Pluripotent Stem Cell-Derived Cardiac Tissue Models.* J Am Heart Assoc, **2022**. 11(4): p. e021615.

44. Ambrosi, C.M., et al., *Optogenetics-enabled assessment of viral gene and cell therapy for restoration of cardiac excitability.* Sci Rep, **2015**. 5: p. 17350.

45. Vogt, C.C., et al., *Systemic gene transfer enables optogenetic pacing of mouse hearts.* Cardiovasc Res, **2015**. 106(2): p. 338-43.

46. Ting, J.T. and G. Feng, *Development of transgenic animals for optogenetic manipulation of mammalian nervous system function: progress and prospects for behavioral neuroscience.* Behav Brain Res, **2013**. 255: p. 3-18.

47. Bingen, B.O., et al., *Light-induced termination of spiral wave arrhythmias by optogenetic engineering of atrial cardiomyocytes.* Cardiovasc Res, **2014**. 104(1): p. 194-205.

48. Crocini, C., et al., *Optogenetics design of mechanistically-based stimulation patterns for cardiac defibrillation.* Scientific reports, **2016**. 6: p. 35628-35628.

49. Swartling, J., et al., *Changes in tissue optical properties due to radio-frequency ablation of myocardium.* Med Biol Eng Comput, **2003**. 41(4): p. 403-9.

50. Lee, P.T., et al., *Left ventricular wall thickness and the presence of asymmetric hypertrophy in healthy young army recruits: data from the LARGE heart study.* Circ Cardiovasc Imaging, **2013**. 6(2): p. 262-7.

51. Kawel, N., et al., *Trabeculated (noncompacted) and compact myocardium in adults: the multi-ethnic study of atherosclerosis.* Circ Cardiovasc Imaging, **2012**. 5(3): p. 357-66.

52. Glukhov, A.V., et al., *Transmural dispersion of repolarization in failing and nonfailing human ventricle.* Circ Res, **2010**. 106(5): p. 981-91.
53. Rieger, M., et al., *Enabling comprehensive optogenetic studies of mouse hearts by simultaneous opto-electrical panoramic mapping and stimulation.* Nat Commun, **2021**. 12(1): p. 5804.
54. Hong, W., et al., *Self-adaptive cardiac optogenetics device based on negative stretching-resistive strain sensor.* Sci Adv, **2021**. 7(48): p. eabj4273.
55. Ausra, J., et al., *Wireless, fully implantable cardiac stimulation and recording with on-device computation for closed-loop pacing and defibrillation.* Sci Adv, **2022**. 8(43): p. eabq7469.
56. Choi, Y.S., et al., *A transient, closed-loop network of wireless, body-integrated devices for autonomous electrotherapy.* Science, **2022**. 376(6596): p. 1006-1012.
57. Choi, Y.S., et al., *Fully implantable and bioresorbable cardiac pacemakers without leads or batteries.* Nat Biotechnol, **2021**. 39(10): p. 1228-1238.

Chapter 3│*Optogenetic Stimulation Using Anion Channelrhodopsin (GtACR1) Facilitates Termination of Reentrant Arrhythmias With Low Light Energy Requirements: A Computational Study*

Reproduced in part from Ochs A.R., Karathanos T.V.*, Trayanova N.A., and Boyle P.M. "Optogenetic Stimulation Using Anion Channelrhodopsin (GtACR1) Facilitates Termination of Reentrant Arrhythmias With Low Light Energy Requirements: A Computational Study." Front Physiol 2021. (* denotes co-first authors)*

3.1 Introduction

Cardiac optogenetics is an emerging field that stems from work involving genetic transduction of light-sensitive ion channels into mammalian neurons (1, 2). The use of light for current induction in cardiac tissue with precise spatial and temporal precision has led to *in vivo* studies describing selective excitation of specific cell populations (3, 4), control of spiral waves (5, 6), and cardiac pace-making (7-10) or arrhythmia termination in animal models (11-14). *In vitro* applications of optogenetics have yielded all-optical methods for contactless, high-throughput measurement of electrophysiological properties like action potential duration and inter-cellular electric coupling at different spatial scales (15, 16). Lastly, *in silico* tools have been created to elucidate mechanisms and test feasibility of optogenetic approaches in larger hearts without the use of preclinical animal models (17-21).

An appealing, long-term translational application of cardiac optogenetics is selectively exciting the heart to terminate arrhythmia. Current standard-of-care treatments for individuals at risk of sudden cardiac death include implantable cardioverter defibrillators (ICDs) and anti-arrhythmic drugs (22-24). While ICDs reduce mortality by eliciting high-energy electrical shocks to defibrillate lethal arrhythmias such as ventricular fibrillation, electrotherapy is also associated with increased mortality, chronic anxiety, and post-traumatic stress disorder (23, 25). For individuals with atrial arrhythmias, cardioversion treatments are effective but limited by the in-patient nature of the procedure and the need for anesthesia (26). Optogenetic defibrillation has the potential to circumvent these drawbacks, but prior modeling studies (11, 17, 27, 28) suggest

that it would be very difficult to accomplish with current tools, like the channelrhodopsin-2 (ChR2) H134R variant, due to light-attenuating properties of myocardium and high energy requirements.

A potential avenue for moving beyond these limitations is a recently discovered family of opsins called anion channelrhodopsins (ACRs), such as *Guillardia theta* anion channelrhodopsin-1 (GtACR1) (29). Originally derived from archaea, GtACR1 has desirable cardiac optogenetic characteristics including high single channel conductance, fast response kinetics, specificity in narrow wavelength ranges, and more negative reversal potential values than ChR2 (29-31). When excited by green illumination, GtACR1 conducts a flow of anions (e.g., Cl^-), eliciting outward current that accelerates repolarization (29-31). As such, a new ACR-based paradigm for arrhythmia termination would be distinct from approaches used in past optogenetic defibrillation studies, which have used light-based depolarization to disrupt arrhythmia reentry (17, 28).

Here, we conduct simulations in patient-derived, biophysically realistic computational models of the diseased atria and ventricles, reconstructed from human late gadolinium enhanced magnetic resonance imaging (LGE-MRI) scans, to investigate the feasibility of GtACR1-based optogenetic defibrillation. Specifically, we aim to determine if uniform endocardial illumination with green light can terminate reentrant arrhythmias in these models with suitable modifications to represent viral GtACR1 expression. Our analysis is designed to reveal (1) the illumination intensity sufficient for GtACR1 to terminate arrhythmia, (2) the mechanisms of defibrillation, and (3) the differences in efficacy between atrial and ventricular models. Simulations with different permutations are used to explore the robustness of light stimulus timing and magnitude. As a basis for comparison, we conduct parallel simulations in the same models expressing blue and red light-sensitive ChR2-H134R variants.

3.2 Methods

Computational modeling of diseased atrial and ventricles

We conducted computational simulations using six patient-specific finite element models (three atrial, three ventricular) reconstructed from LGE-MRI scans (**Fig. 3-1**). Atrial models were sourced from a cohort of patients with persistent atrial fibrillation (AFib) reconstructed for a prior modeling study (32); ventricular models came from a different simulation-based study of ischemic cardiomyopathy patients (33). The approach for simulation of cardiac electrophysiology in such models has been previously validated for their respective applications (34-36); detailed descriptions of atrial (32, 37) and ventricular (33) simulation methodologies can be found elsewhere (11, 28). Briefly, patient-specific geometry and spatial distribution of diseased tissue (fibrotic and non-fibrotic tissue in atrial models (38); normal, scar, and peri-infarct border zone (BZ) tissue in ventricular models (39)) were extracted from each patient's clinical MRI scan (**Fig. 3.1**). Realistic fiber orientations were introduced in each model, either via diffeomorphic transformation of an atlas geometry in the case of the atria (32, 40-42) or using a rules-based approach for the ventricles (43). Human atrial (44) and ventricular (45) myocyte membrane kinetics were represented using the formulations derived by Courtemanche et al. (44) and ten Tusscher et al. (45), respectively. The average element edge length used a 350 μm resolution, and temporal discretization used time steps of 25 μs. Electrical propagation in cardiac tissue was governed by the monodomain formulation (46, 47), and all simulations were conducted using the Cardiac Arrhythmia Research Package (CARP) software (46-48). Patient-derived data related to this article are not publicly available due to data privacy, but in an effort to expand data replicability, examples of ChR2, ChR2-RED, and GtACR1 optogenetic stimulation can be found at https://doi.org/10.6084/m9.figshare.14945412.

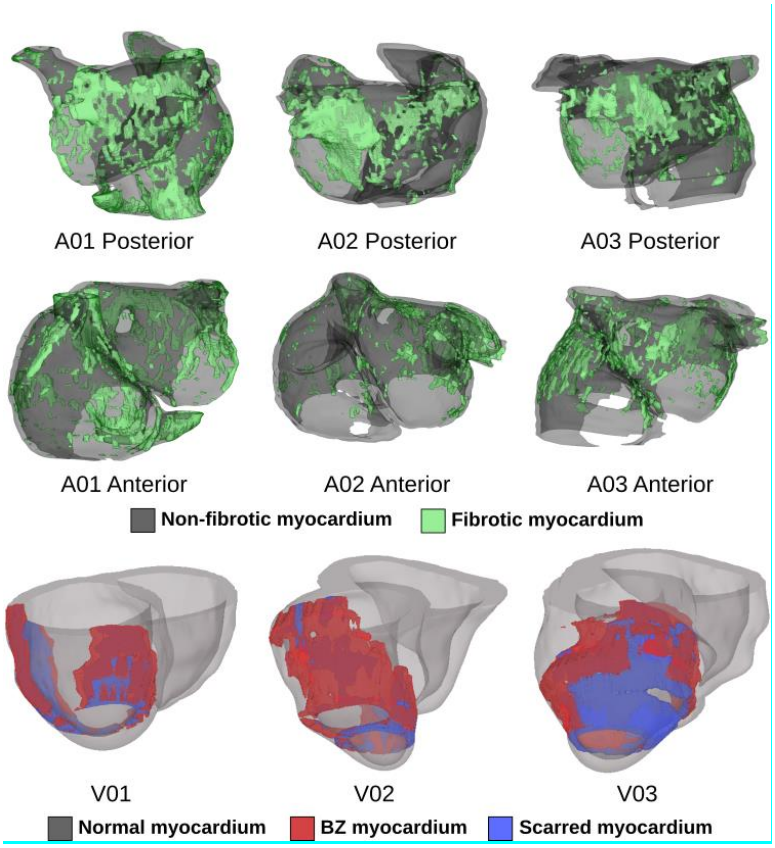

***Figure 3.1**: Patient-specific atrial (top two rows) and ventricular (bottom row) models reconstructed from LGE-MRI scans. Spatial distribution of diseased tissue is shown for all cases.*

Mathematical representation of light-induced current mediated by GtACR1

We formulated a model of GtACR1 photocurrent kinetics using patch clamp data from GtACR1-expressing neonatal rat ventricular cardiomyocytes as published by Govorunova et al. (30). Since previous works have suggested structural differences between ACRs and chloride-conducting channelrhodopsins (31), along with an absence of any reported dark- and light-adapted photocurrent branches in ACRs, we developed a two-state Markov chain model with a conducting ($P(O)$; light-activated/open) and non-conducting ($P(C)$; dark/closed) states:

$$P(O) + P(C) = 1 \tag{1}$$

$$\frac{dP(O)}{dt} = k_{OC} \tag{2}$$

$$\frac{dP(C)}{dt} = k_{CO} \tag{3}$$

$$k_{OC} = \frac{1}{\tau_{off}} \tag{4}$$

$$k_{CO} = \frac{1}{\tau_{on}} * \frac{5.878134701 + \ln(E_e + 0.0028)}{0.369864 - 0.1072 * \ln(E_e + 0.0028)} \tag{5}$$

where $P(O)$ is the open-state probability, $P(C)$ is the closed-state probability, k_{OC} is the open-to-closed transition rate, k_{CO} is the closed-to-open transition rate, τ_{off} is the inactivation time constant (119 ms), τ_{on} is the activation time constant (1110 ms), and E_e is the applied irradiance.

The open-to-closed transition rate (k_{OC}) was calibrated based on inactivation constant of GtACR1, and was fitted via the logarithmic relation of the opening rate to irradiance to ensure that the steady-state currents under illumination matched reported data (30). The closed-to-open transition rate (k_{CO}) equation varies as a function of irradiance (E_e); k_{CO} was derived by assuming equilibrium during the photocurrent plateau generated by steady state illumination, then fitting to the open probability $P(O)$ derived from experimental current traces. To derive maximal GtACR1 channel (g_{GtACR1}), we assumed a membrane capacitance of 100 pF, which is within the physiological range of previously reported NRVM single cell experiments (49). The GtACR1 photocurrent model was then characterized at different irradiances under voltage forcing conditions (**Fig. 3.2A-B**). When a holding potential of –80 mV was used, illumination elicited inward currents, with higher irradiance values leading to larger magnitudes (**Fig. 3.2A**). With a holding potential of 0 mV, the polarity of the induced photocurrents was reversed (**Fig. 3.2B**). Using a bisection approach, we found that the best value reconciling current values observed for these clamp levels with experimental data was g_{GtACR1} = 1.4 mS/cm^2. We also characterized the ChR2 photocurrent model for comparison to GtACR1 at holding potentials of –80 mV and 0 mV (**Fig. 3.2C**); GtACR1 currents were several-fold stronger than ChR2 at all irradiances when using –80 mV holding potential (**Fig. 3.2D**). A comparison of GtACR1 photocurrents from the 2-state model versus experimental currents is plotted in **Figure 3.3**.

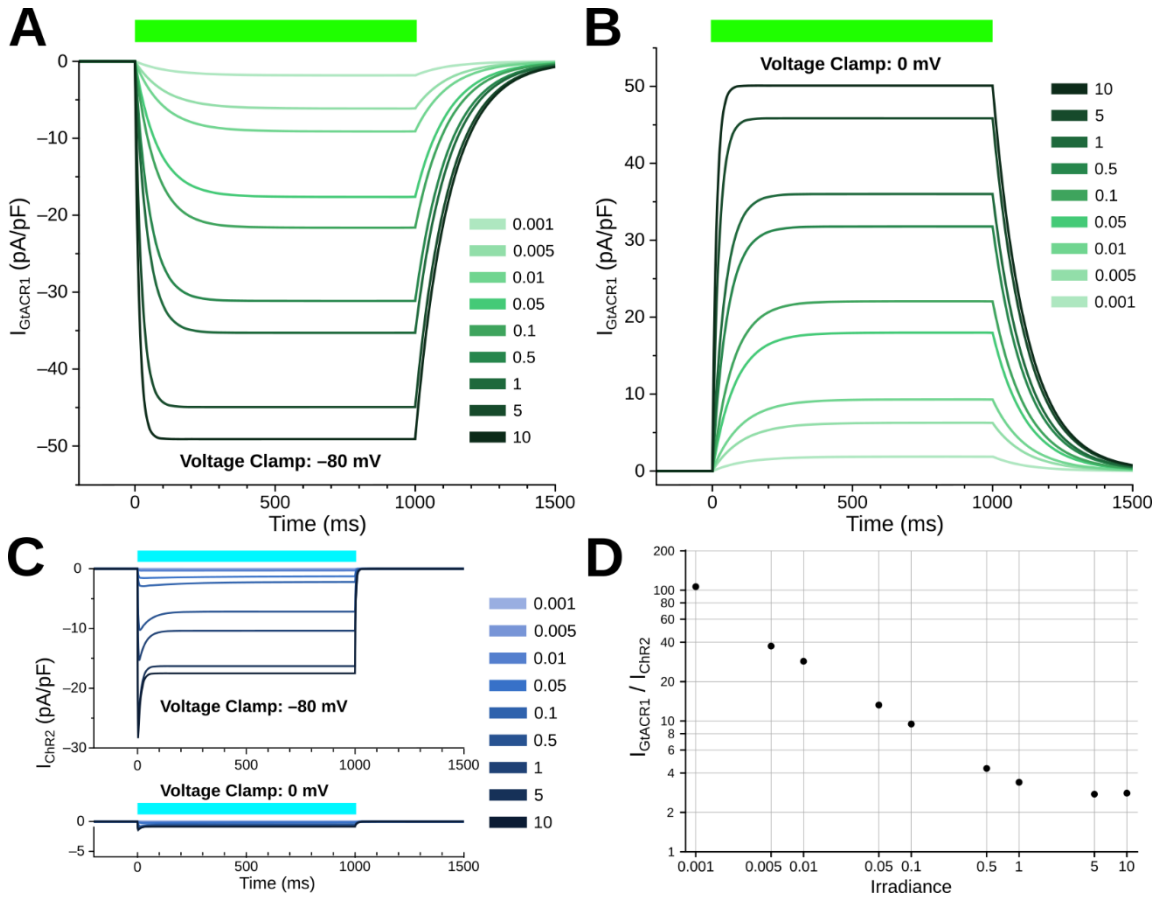

Figure 3.2: *Simulated GtACR1 and ChR2 currents in illumination voltage forcing experiments. **A-B**: Photocurrent conducted by GtACR1 generated in response to illumination with holding potentials of –80 (**A**) and 0 mV (**B**). **C**: Same as **A/B** but for ChR2. **D**: Comparison of steady-state I_{GtACR1} and I_{ChR2} values (plateau currents at t = 500 ms) for different irradiances under voltage forcing condition. In all panels, units of irradiance are mW/mm^2. Colored bars: intervals of illumination with green (515 nm; 1000 ms) or blue light (488 nm, 1000 ms).*

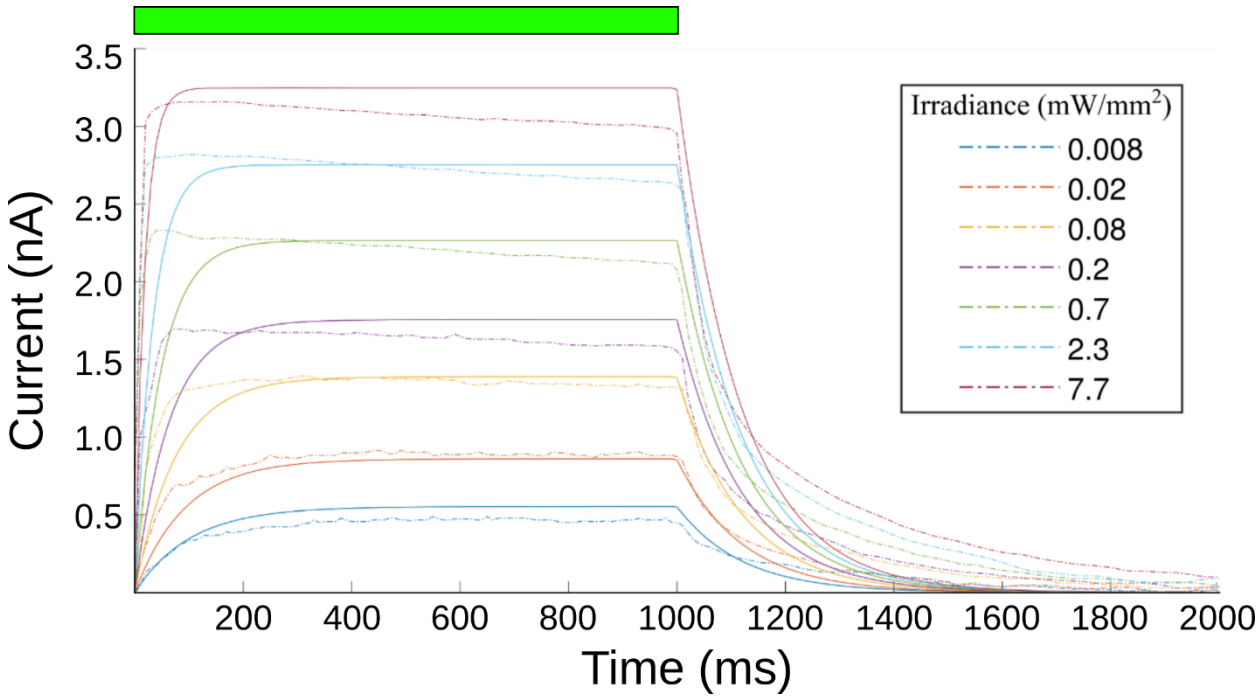

Figure 3.3: *Comparison of GtACR1 photocurrents in the 2-state model to experimental data. Illumination was applied for 1000 ms using 515 nm light, followed by 1000 ms of no illumination. Dashed lines are experimental $V_m(t)$ traces and solid lines are model-derived $V_m(t)$ traces across the various irradiances. Reproduced with permission from the dissertation of Thomas Karathanos (accessible at: http://jhir.library.jhu.edu/handle/1774.2/60956).*

Finally, the current density of the channel (I_{GtACR1}) was calculated using Ohm's law, adjusted for the channel open probability:

$$I_{GtACR1} = P(O) * g_{GtACR1} * (V - E_{GtACR1}) \quad (6)$$

where E_{GtACR1} is the GtACR1 reversal potential (–40 mV), which we based on prior reports for the reversal potential of chloride ions in cardiac cells under physiologic conditions (30, 50). Notably, the reported reversal potential for GtACR1 in experimental cardiomyocyte preparations was –90 mV (30); this discrepancy was likely a consequence of bath solution composition.

An implementation of our GtACR1 model compatible with the openCARP framework for cardiac electrophysiology simulations (http://opencarp.org), which is made freely available for non-commercial applications, is provided as supplementary material (see Appendix 1).

ChR2 model variants

The ChR2 photocycles were simulated using an model for ChR2-H134R (51), as in previous works (6, 11, 17, 28, 52). Briefly, the ChR2 was modelled as a 4-state Markov chain model with light-gated transitions between two closed (non-conducting) and two open states (permeable to cation flow). The ChR2 model conductance (g_{ChR2}) was originally calculated to be 0.4 mS/cm^2 based on experiments in HEK-293 cells (51), but photocurrents measured from patch clamped cells following viral gene delivery of ChR2 to mouse hearts suggest a lower value (10). Thus, we adjusted our model to fit ~2.2 pA/pF steady-state currents at 5 mW/mm^2 illumination (10), which resulted in a conductance of g_{ChR2} = 0.11 mS/cm^2. As in prior studies (11, 17, 28), we assumed ChR2 stimulation with 488 nm blue light. Since prior modeling studies showed higher defibrillation success rates with red light stimulation (11, 28), we also used a theoretical ChR2 model variant with red-shifted absorption (ChR2-RED). This model had the same properties as ChR2 (no modifications to light sensitivity or g_{ChR2}) but peak energy absorption wavelength was adjusted to 669 nm.

Simulation of opsin expression and light attenuation

To simulate optogenetic transduction of either the human atria or ventricles via viral gene delivery, we used our previously validated computational modeling framework (11, 53-55). Based on mouse experiments studying the effects of gene delivery and expression in cardiomyocytes (10, 11, 28), opsin expression (ChR2, ChR2-RED, or GtACR1) was incorporated into 58.2% of mesh nodes in a diffuse pattern (i.e., random selection with a uniform distribution), as described previously (55). To facilitate comparison of results across different experimental configurations, we only generated one 58.2% distribution per atrial/ventricular model (i.e., spatial patterns of opsin expression for different opsins were identical).

Light attenuation due to scattering and energy absorption in myocardial tissue was approximated using the steady-state photon diffusion equation (56, 57), as in previous modelling studies (11,

28, 55, 58-61). We defined the a parameter (values between 0 and 1) using the coefficient for light scattering μ_s', coefficient for light absorption μ_a, and the anisotropy factor g:

$$a = 1 - \frac{4}{5} \cdot \frac{\mu_s' + \mu_a}{\mu_s' \cdot (1 + g) + \mu_a} \tag{7}$$

We then defined the diffusion coefficient D using the formula (57):

$$D = \frac{1}{3(\mu_s' + \mu_a * a)} \tag{8}$$

We used experimentally-derived values found in the literature (58) for blue (μ_a = 0.52, D = 0.183) and red light (μ_a = 0.1, D = 0.34). For green light in cardiac tissue (μ_a = 0.7, μ_s' = 1.42 and g = 0.9 (62)) a was calculated to be 0.5, leading to a diffusion coefficient of D = 0.189. In effect, this means the penetration depth for green light is the shallowest of all the wavelengths used in the study ($\delta = \sqrt{D/\mu_a}$ = 519.6 μm vs. 593.2 μm and 1.844 mm for blue and red light, respectively).

We simulated uniform illumination of the left atrial (LA) endocardium in atrial models, and the left ventricular (LV) endocardium in ventricular models. Illumination was represented by defining a constant E_e value on the target surface, then modifying that value by an attenuation factor (derived by solving the photon diffusion equation) (17, 28, 58, 61) in the myocardial bulk. **Figure 3.4** shows the effects of light attenuation in atrial and ventricular models using the associated wavelengths of each opsin: blue light for ChR2 (488 nm), red light for ChR2-RED (669 nm), and green light for GtACR1 (515 nm).

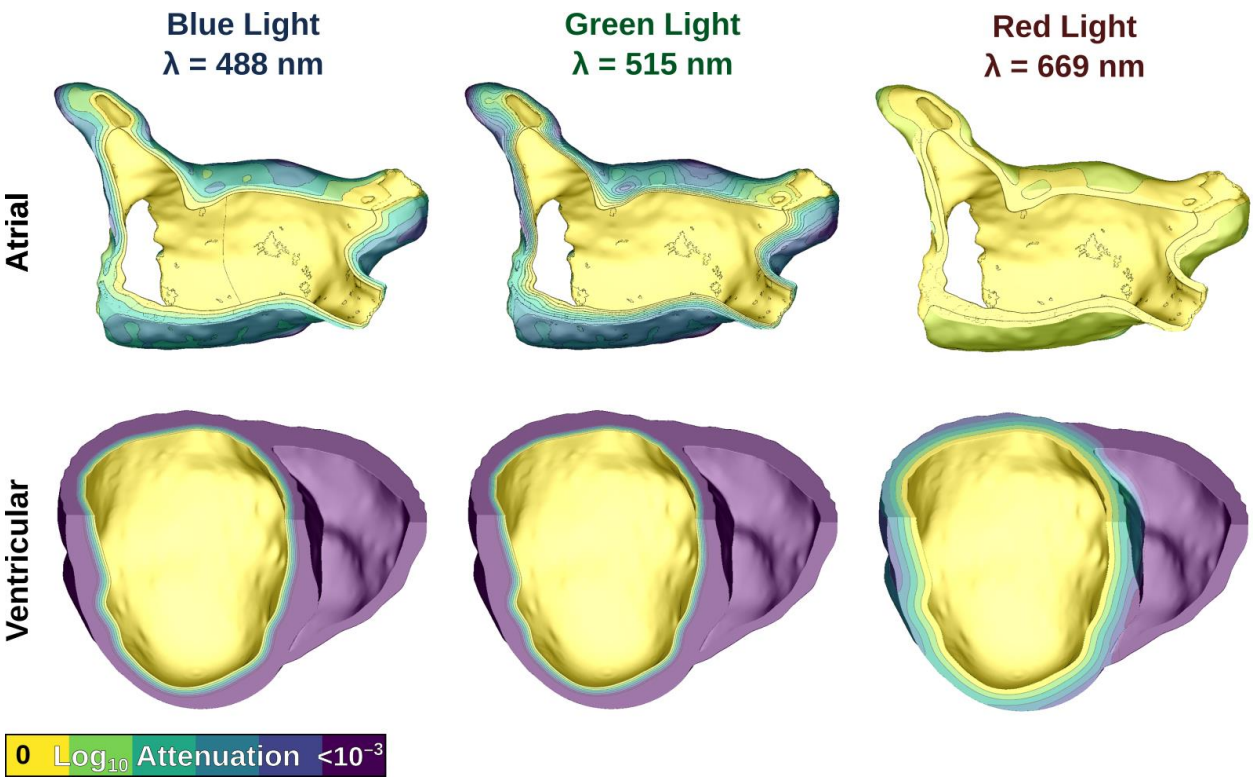

Figure 3.4: *Modeling illumination of atrial (top) and ventricular (bottom) models with light of different wavelengths. Attenuation color scale is shown on a log10 scale.*

Simulation protocol for arrhythmia induction and optogenetic defibrillation

Arrhythmias were induced by simulated rapid pacing in both atrial (32) and ventricular (33) models, as in prior studies (11, 17, 28, 32, 37). In atrial models, six electrical pulses of 5 ms duration were paced at coupling interval (CI) = 300 ms, decreasing in 20 ms decrements until CI = 200 ms (6 pulses), followed by six pulses at CI = 200 ms to induce AFib (12 pulses total). In ventricular models, eight pulses of 5 ms duration at CI = 600 ms were initially paced, followed by two pulses at reduced CIs of variable length to induce VT.

In atrial models, we simulated optogenetic defibrillation attempts with 1000 ms-long LA endocardial illumination pulses at E_e values varying from 0.001 to 1 mW/mm^2; these values are consistent with those used in prior experimental studies (14, 17, 27). In each model, we carried out separate simulation sets assuming expression of ChR2, ChR2-RED, and GtACR1. To span the re-entrant cycle, three light pulse onset times (+0, +70, +140 ms) were used for each E_e/opsin

condition. A similar, experimentally consistent (8, 11, 28) protocol was used in ventricular models, with the primary differences being E_e values (varying from 0.001 to 10 mW/mm^2), and light onset times (+0, +100, +200 ms) due to longer VT cycle length. In all cases, defibrillation was deemed successful if reentry terminated within 800 ms after the 1000 ms illumination pulse ended; this gave us an adequate timeframe to monitor for resumption of stable reentry (following failed attempts) or indirect successes (as described elsewhere (17)), wherein spontaneous termination occurs after the end of illumination due to light-induced destabilization.

3.3 Results

GtACR1 photocurrent model characterization

The GtACR1 photocurrent model and its response to light were evaluated in atrial (44) (**Fig. 3.5A**) and ventricular (45) (**Fig. 3.5B**) myocyte models. In both cell types, following an initial action potential evoked by electrical stimulation (first red star), subsequent light stimulation (green bar) resulted in an abrupt transient depolarization, after which the membrane voltage (V_m) was forced to the GtACR1 reversal potential (–40 mV). This light-induced forcing effect prevented the triggering of subsequent action potentials by electrical stimuli (second red star). After illumination ended, simulated cells repolarized to their resting potentials.

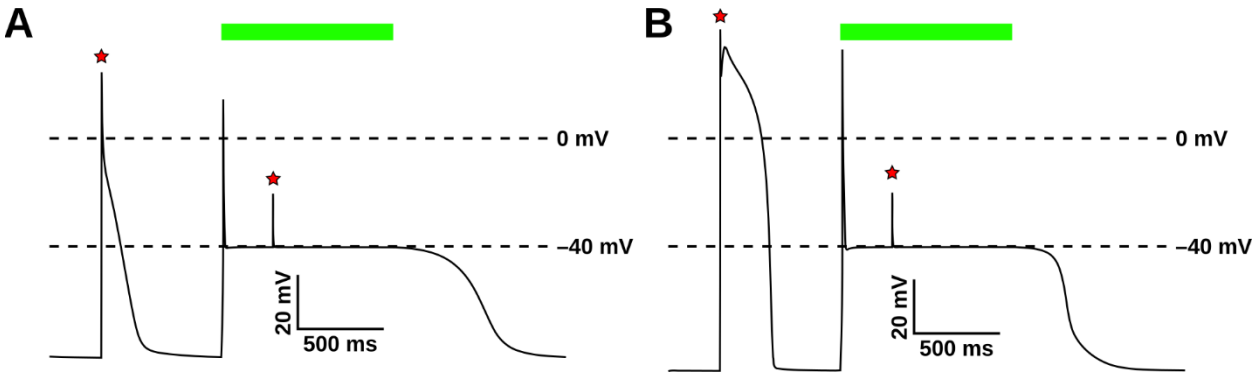

Figure 3.5: *Evaluation of GtACR1 currents upon illumination in single cell simulations. Light-elicited GtACR1 currents suppressed action potential formation in simulated atrial (**A**) or ventricular (**B**) myocyte models. Red stars show timing of electrical stimuli (30 pA/pF) and green bars represent the interval of illumination with green light (515 nm; 1.00 mW/mm^2; 1000 ms).*

Optogenetic defibrillation in atrial models

Here, we simulated optogenetic defibrillation attempts in three patient-specific atrial models using LA endocardial illumination at irradiances varying from 0.001 to 1 mW/mm^2. As summarized in **Table 3.1**, GtACR1-based termination was reliable (i.e., reentry activity terminated for all three light onset times tested) for light stimuli as weak as 0.005 mW/mm^2. Notably, this was 2-3 orders of magnitude lower than the weakest stimuli that reliably defibrillated models expressing ChR2-RED or ChR2 (0.1 and 0.5 mW/mm^2, respectively).

Table 3.1*: Defibrillation success rates for ChR2, ChR2-RED, or GtACR1-expressing atrial models for different irradiance values. "n/3" denotes that defibrillation was successful for n of the 3 light onset times tested (i.e., arrhythmia terminated within 800 ms of illumination ending).*

		Irradiance (mW/mm^2)						
		0.001	*0.005*	*0.01*	*0.05*	*0.1*	*0.5*	*1*
ChR2 (blue)	*A01*	0/3	0/3	0/3	0/3	0/3	3/3	3/3
	A02	0/3	0/3	0/3	0/3	0/3	3/3	3/3
	A03	0/3	0/3	0/3	0/3	2/3	3/3	3/3
ChR2-RED (red)	*A01*	0/3	0/3	0/3	2/3	3/3	3/3	2/3
	A02	0/3	0/3	0/3	0/3	3/3	3/3	3/3
	A03	0/3	0/3	0/3	2/3	3/3	3/3	3/3
GtACR1 (green)	*A01*	0/3	3/3	3/3	3/3	3/3	3/3	3/3
	A02	0/3	3/3	3/3	3/3	3/3	3/3	3/3
	A03	0/3	3/3	3/3	3/3	3/3	3/3	3/3

The effects of very weak (0.05 mW/mm^2) light stimuli in atrial models with expression of different opsins are illustrated in **Fig. 3.6**. In the absence of light stimulation (i.e., control case), reentry persisted; action potential timing and morphology were similar between epicardial and endocardial surfaces (**Fig. 3.6A**, right-most column). Attempted optogenetic defibrillation in the ChR2-expressing model did not disrupt reentrant activity transmurally (**Fig. 3.6B**); endocardial action potentials were blunted, but remained temporally synchronized with epicardial excitations, which were largely unaffected by optogenetic stimulation. Stimulation of ChR2-RED had a more prominent effect on the transmural spatiotemporal excitation sequence due to deeper penetration of red light (~3x exponential decay constant of blue light; **Fig. 3.6C**); some isolated instances of

conduction block were observed (e.g., double lines in 600 ms panel), but arrhythmia did not terminate. In contrast, illumination in the GtACR1-expressing atrial models imposed a voltage forcing effect throughout the LA (**Fig. 3.6D**, 600 ms), leading to rapid extinguishing of reentrant drivers. Notably, this light-induced forcing effect was non-uniform, with less depolarized plateau voltage at the epicardial surface (spatial gradient: 2.8 mV/mm) due to transmural light attenuation.

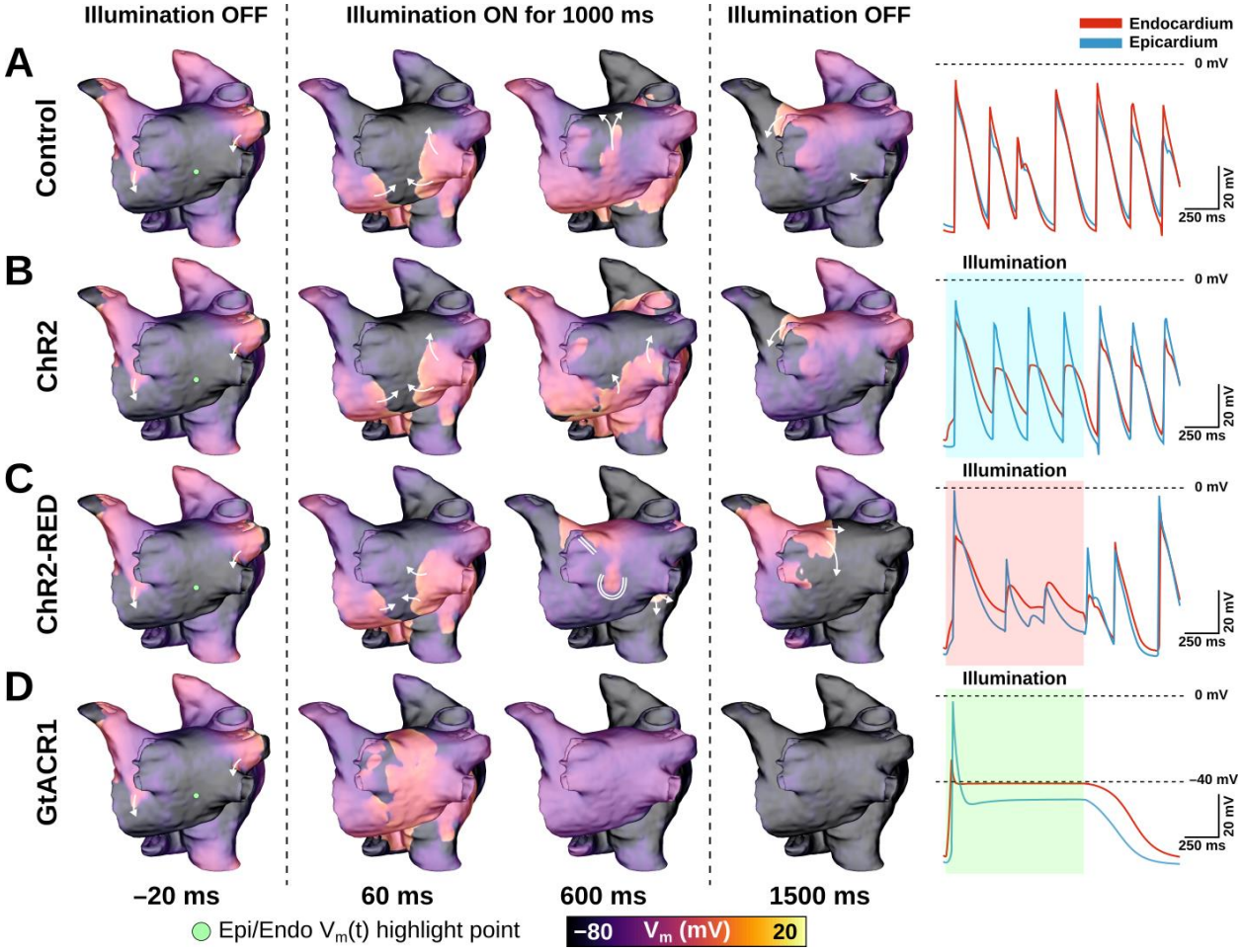

Figure 3.6: *LA defibrillation attempts with E_e = 0.05 mW/mm^2 in model A01 for all three opsins. The control case (**A**) is compared to endocardial illumination of ChR2- (**B**), ChR2-RED- (**C**), or GtACR1- (**D**) expressing models. Arrows indicate wavefront propagation directions. Double lines show sites of conduction block. Representative V_m(t) traces are shown from endocardial (red line) and epicardial (blue line) nodes at the same point on the LA posterior wall (green dot). All illumination begins at t = 0 ms and lasts 1000 ms.*

At extremely weak irradiances (i.e., 0.005 mW/mm^2) in GtACR1-expressing atria, light that reached the epicardium was too weak to induce optogenetic voltage forcing. Despite this,

defibrillation succeeded in all cases (9/9). To illustrate how this was possible, **Fig. 3.7** presents side-by-side activation maps for a GtACR1 defibrillation attempt (E_e = 0.005 mW/mm^2) and its corresponding control case. In the absence of light stimulus, a reentrant driver in the inferolateral LA propagates unabated (**Fig. 3.7A**); in contrast, GtACR1 activity elicited by weak illumination of the endocardium disrupted reentry and ultimately terminated the arrhythmia (**Fig. 3.7B**). Examination of transmural voltage traces in the latter case (**Fig. 3.7C**) showed that propagating wavefronts in sub-epicardial LA tissue created transient depolarizations from the forced level in the sub-endocardium, but arrhythmia extinguished ~100 ms after the end of illumination due to light-induced perturbation of excitation patterns near the arrhythmia driver.

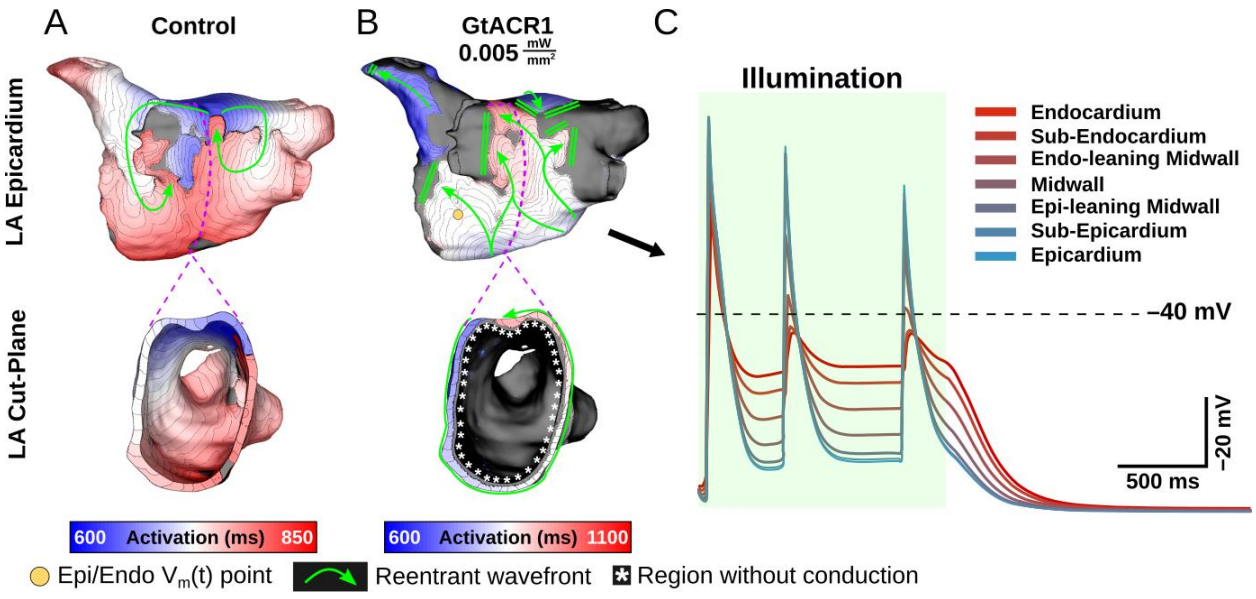

Figure 3.7: *<u>Defibrillation with very weak light stimuli succeeds in GtACR1-expressing models despite persistent sub-epicardial conduction</u>. **A-B**: Activation maps for no light control (**A**), and E_e = 0.005 mW/mm^2 stimulus applied to GtACR1-expressing model (**B**). Dashed lines (top) show cut plane locations for cross-sections (bottom). Arrows indicate wavefront propagation directions. Double lines show sites of conduction block. Asterisks highlight conduction block region on endocardium. **C**: V_m(t) traces for nodes spanning from LA endocardium to epicardium (golden dot) in the GtACR1 condition are provided. Illumination begins at t = 0 ms and lasts 1000 ms.*

Optogenetic defibrillation in ventricular models

Next, we simulated optogenetic defibrillation attempts in three patient-specific ventricular models using LV endocardial illumination at irradiances varying from 0.001 to 10 mW/mm^2. As

summarized in **Table 3.2**, GtACR1-based defibrillation was effective with light stimuli as weak as 0.005 mW/mm^2, which was 2-3 orders of magnitude weaker than for ChR2-RED or ChR2 (0.5 and 1 mW/mm^2, respectively). A representative example of VT termination (E_e = 0.5 mW/mm^2 in GtACR1-expressing model V01) is presented in **Fig. 3.8**. Without light stimulus, the arrhythmia is sustained (**Fig. 3.8A**) whereas illumination prevents conduction at the endocardial surface (**Fig. 3.8B**), resulting in successful GtACR1-mediated defibrillation via light-induced voltage forcing (**Fig. 3.8C**), like atrial models discussed in the prior section.

***Table 3.2**: Defibrillation success rates for ChR2, ChR2-RED, or GtACR1-expressing ventricular models for different irradiance values. "n/3" denotes that defibrillation was successful for n of the 3 light onset times tested (i.e., arrhythmia terminated within 800 ms of illumination ending).*

		Irradiance (mW/mm^2)								
		0.001	***0.005***	***0.01***	***0.05***	***0.1***	***0.5***	***1***	***5***	***10***
ChR2 (blue)	*V01*	0/3	0/3	0/3	0/3	0/3	1/3	3/3	3/3	3/3
	V02	0/3	0/3	0/3	0/3	0/3	0/3	0/3	0/3	0/3
	V03	0/3	0/3	0/3	0/3	0/3	0/3	2/3	2/3	2/3
ChR2-RED (red)	*V01*	0/3	0/3	0/3	0/3	0/3	3/3	3/3	2/3	3/3
	V02	0/3	0/3	0/3	0/3	0/3	0/3	0/3	1/3	1/3
	V03	0/3	0/3	0/3	0/3	0/3	3/3	3/3	2/3	2/3
GtACR1 (green)	*V01*	0/3	1/3	3/3	3/3	3/3	3/3	3/3	3/3	3/3
	V02	0/3	0/3	0/3	0/3	0/3	0/3	0/3	0/3	0/3
	V03	0/3	3/3	3/3	3/3	3/3	3/3	3/3	2/3	3/3

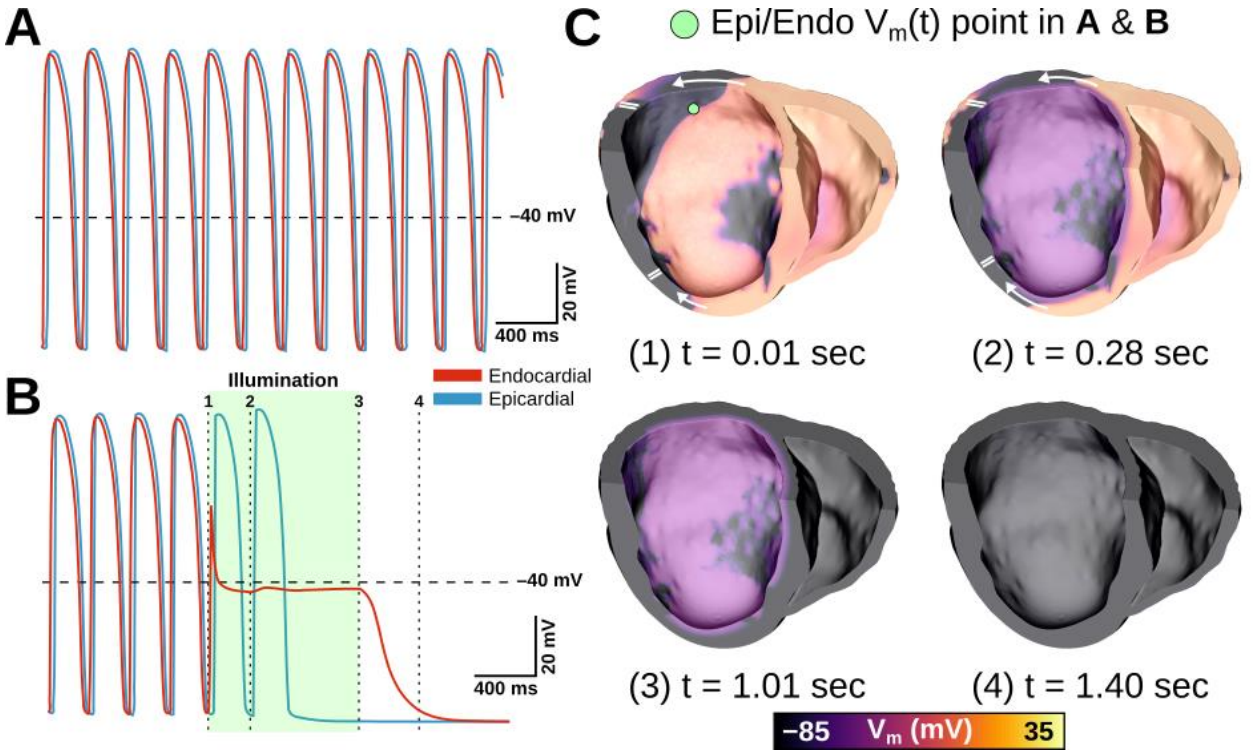

Figure 3.8: *Representative example of LV defibrillation attempt in GtACR1-expressing model V01 with E_e = 0.5 mW/mm^2. V_m(t) traces from the LV endocardial surface are provided for the control case (**A**) and GtACR1-expressing model (**B**). Cut plane V_m(t) snapshots of the GtACR1 case (**C**) show conduction block affecting wavefront propagating circumferentially in LV free wall, followed by eventual arrhythmia termination. Arrows indicate wavefront propagation directions. Double lines show sites of conduction block.*

One notable example of inconsistent defibrillation behavior between ventricular models was that defibrillation failed in V02 for nearly all stimuli, regardless of opsin, with success observed in only 2/33 simulations with ChR2-RED. The non-responsiveness of model V02 to optogenetic defibrillation is scrutinized in **Fig. 3.9**. In a representative GtACR1-expressing defibrillation failure (**Fig. 3.9A-B,** E_e = 1 mW/mm^2), endocardial excitation was suppressed by the optogenetic stimulus (endocardial trace) while the epicardium was unaffected (**Fig. 3.9A**). Due to light attenuation in the ventricular walls, the proportion of tissue directly depolarized by GtACR1 stimulation was smaller compared to atrial models, so reentrant wavefront conduction continued along a thin layer of epicardium (**Fig. 3.9B, inset**). This was made possible by the presence of a dense ring of scar and BZ near the LV apex (**Fig. 3.9C**), which created a protected region that was too far from the illuminated endocardium to be affected by the light stimulus and insulated

from indirect (electrotonic) effects in areas that *were* optogenetically depolarized. In cases where the reentrant wavefront was dislodged from that area, the arrhythmia driver then relocated to one of many other sites that were capable of sustaining a new spiral wave (**Fig. 3.9D**; GtACR1 expression, examples shown for E_e =5 and 10 mW/mm^2). In the small handful of V02 cases where light-based defibrillation did succeed, termination always occurred several hundred milliseconds after the end of illumination. The apparent mechanism (e.g., **Fig. 3.9E-F**) was that the dislodged reentrant wavefront serendipitously encountered tissue excited by propagation from another part of the ventricles, resulting in conduction block and subsequent termination.

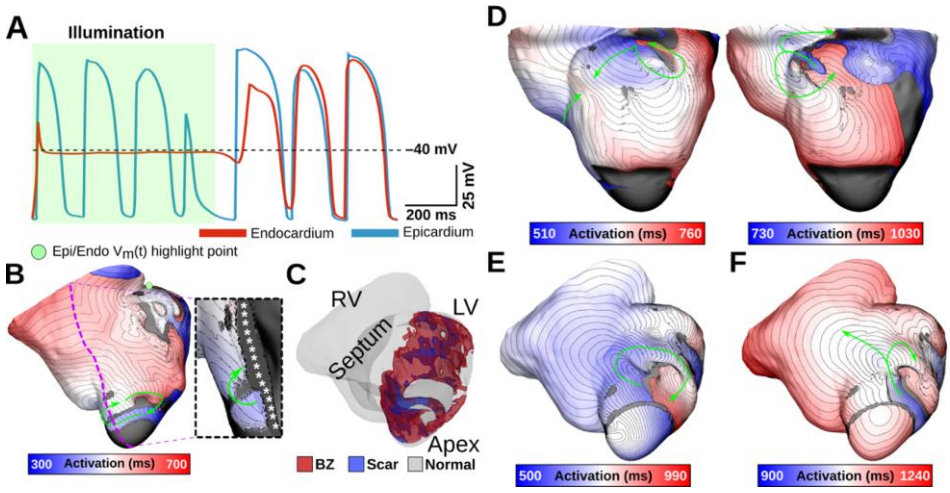

Figure 3.9: *Examining low optogenetic defibrillation success rates in V02. V_m(t) traces (**A**) and an activation map (**B**) showing an example of GtACR1-based defibrillation failure (E_e = 1 mW/mm^2). Excitation is silenced at the endocardium, but arrhythmia persists at the epicardium (inset) due to a protected VT circuit created by a particular geometry of BZ and scar (**C**). **D**: Representative examples to illustrate differences between destabilized reentrant circuits in GtACR1-expressing defibrillation failures (E_e = 5 mW/mm^2 and E_e = 10 mW/mm^2). **E-F**: Example of defibrillation success (ChR2-RED, E_e = 5 mW/mm^2) showing a normal cycle (**E**) and cycle with conduction block near LV apex (**F**) that leads to termination. Arrows indicate wavefront propagation.*

3.4 Discussion

In this study, we used computational models reconstructed from LGE-MRI scans of diseased human atrial and ventricles to assess the feasibility of reentrant arrhythmia termination via GtACR1-mediated optogenetic stimulation. To achieve this, we developed a 2-state photocurrent model for GtACR1 and evaluated it under realistic organ-scale conditions. In doing so, we showed

that GtACR1-mediated optogenetic defibrillation of the atria or ventricles is feasible and more efficacious than a ChR2-based approach, the limitations of which are well known from prior work. Our main findings are: (1) GtACR1-mediated voltage forcing to near the channel Cl^- reversal potential of –40 mV consistently terminated arrhythmia in most atrial and ventricular models (3/3 and 2/3, respectively); (2) the threshold irradiance for GtACR1-based atrial defibrillation was extremely low (E_e = 0.005 mW/mm^2) in all three cases, corresponding to a ~10-100x lower energy requirement than ChR2-based optogenetic therapy; and (3) the same very low E_e threshold was observed in two of three ventricular models.

Optogenetic stimulation is an appealing alternative to electric shocks for defibrillation or cardioversion due to its ability to affect V_m in the light-sensitized heart alone without triggering excitation and contraction of surrounding skeletal muscle (7, 28, 63-65). Nearly all past experimental and modeling studies exploring optogenetic defibrillation have used depolarizing opsins such as ChR2-H134R (9, 17, 28, 51, 59, 66), CatCh (67), and ReaChR (13). Opsins that hasten repolarization such as halorhodopsin Cl^- pumps (1) and bacteriorhodopsin proton pumps (e.g. Arch-3 and ArchT) (20, 68) have been used previously to silence action potentials in cardiomyocyte monolayers. However, these opsins can only transport a single ion per absorbed photon, resulting in relatively weak photocurrents (30). Consequently, when ventricular defibrillation via ArchT stimulation was attempted in Langendorff-perfused mouse hearts, termination success was much lower and more variable (~55%) (69) than a comparable study that used ChR2 instead (~97%) (11). Engineered ACRs (70, 71) also have limited photocurrent due to the intrinsic pore size of the channels (72). In contrast, natural-occurring ACRs (including GtACR1) from cryptophyte algae have higher photocurrents than previous alternatives by an order of magnitude (29, 30). As noted elsewhere (50), GtACR1 current depends on the chloride reversal potential (≈–40 mV in cardiomyocytes) and thus *depolarizes* cells at rest while *hastening early repolarization* in cells already undergoing excitation. This differs from the outright silencing

of action potentials seen in experimental preparations where the GtACR1 reversal potential was ≈–90 mV due to low [Cl^-] in the pipette (30). Nevertheless, our analysis shows that GtACR1-mediated optogenetic defibrillation in large mammalian hearts is theoretically feasible, with suppression of reentrant activity facilitated by forcing large tissue regions towards the reversal potential.

This GtACR1-mediated "optogenetic voltage forcing" mechanism is distinct from depolarization-based routes to termination, as described in prior studies. In the context of constant epicardial illumination of a ChR2-expressing model of infarcted ventricles, Bruegmann et al. (11) showed the defibrillation mechanism was steady state inactivation of fast Na^+ channels, resulting in reduced tissue excitability and conduction block; however, in contrast to the present work, the level of sustained depolarization observed in that study (≈–50 mV) was well below the effective ChR2 reversal potential (≈+10 mV) (51) due to offsetting effects from other ionic currents. In a different computational study, Karathanos et al. (28) simulated punctate illumination of the cardiac surfaces by multi-optrode grids in the fibrillating human ventricles under heart failure conditions. In that case, arrhythmia termination was facilitated by creation of new wavefronts by ChR2 stimulation, which eliminated excitable gaps.

Prior studies have identified poor transmural light penetration as a key limiting factor for optogenetic defibrillation of larger hearts, with deeper penetrating red light being highlighted as the most promising potential workaround (11, 28). Thus, it is notable that the present study predicts high success rates for optogenetic stimulation based on stimulation of GtACR1-expressing hearts with green light, which has inferior penetration depth compared to both blue and red light. This is a direct result of the lower irradiance threshold for evoking photocurrents in GtACR1 that are large enough to markedly change cardiomyocyte electrophysiology. For example, as shown in **Fig. 3.2C** using cells clamped to –80 mV, the same current (≈2 pA/pF) elicited by illumination of ChR2 at 0.5 mW/mm^2 can be achieved by stimulating GtACR1 at

0.001 mW/mm^2. Thus, for equally bright light stimuli, even though the penetration of green light across the myocardial wall is weaker, the dim illumination of distant regions with attenuated stimuli can produce photocurrents large enough to create a more pronounced electrophysiological effect compared to blue or red light. The recent discovery of red-shifted ACRs from non-algae sources (73) is also noteworthy in this context, although very slow on/off kinetics (>1 second time constants) make these unsuitable for cardiac applications. Nevertheless, the implication is that opsins even more promising than GtACR1 for optogenetic defibrillation may soon become available. One limitation of this work is that the modeled virus transfection assumed random dispersion of the channelrhodopsins which, despite the lack of data, is unlikely to be physiologically accurate.

Our computational findings complement a growing body of evidence from experimental work in animal models that light-based cardiac rhythm control is both feasible and efficacious. Initial proof-of-concept work involving optogenetic pacing of Langendorff-perfused transgenic mouse hearts (8) and optogenetic modulation of zebrafish heart rate *in vivo* (1) prompted speculation that light-based cardioversion and defibrillation might also be feasible (66). Subsequent studies demonstrated highly reliable approaches for optogenetic termination of ventricular arrhythmias in explanted mouse hearts expressing ChR2 (11) or ReaChR (13), or *in vivo* in open-chest preparations of rats following myocardial infarction (12). Proof of concept has also been shown for light-based defibrillation of atrial arrhythmias in open chest preparations *ex vivo* or *in vivo* (27), as well as closed-chest rat models involving automatic detection and termination (14). Prior computational modeling work has suggested that scaling these experiments in larger pre-clinical animal models with contemporary optogenetic tools would be difficult to justify due to constraints imposed by light attenuation in hearts with thicker walls (11, 28); the present work suggests that those studies can now be contemplated, thanks to the addition

of GtACR1 to the optogenetic armamentarium. However, additional studies may still be needed to verify GtACR1 channel conductance values *in vivo*.

A comparable avenue to expression of GtACR1 for anti-arrhythmic strategies could be the enhancement of inward rectifier potassium current I_{K1}. Moderate I_{K1} upregulation via the I_{K1} channel agonist zacopride has been previously shown to reduce triggered arrhythmias in acute ischemic animal models (74-77). Consequently, since long-term pharmacological use often has significant drawbacks, upregulation of IK1 ion channels could be transduced via AAVs. This is not dissimilar from posited opsin transfection, although the IK1 effects would be at least semi-permanent and would need extensive safety studies.Translation of the cardiac optogenetics for clinical applications remains an attractive goal due to the possibility of pain-free light-based defibrillation replacing electric shock therapy. The present study shows the most convincing evidence to date that arrhythmia in human atria or ventricles could, in theory, be terminated with extremely low-energy light stimuli. Nevertheless, two major hurdles to translation remain, and these parallel two major caveats that must be taken into consideration when interpreting our findings. First, long-term studies are needed to evaluate the safety and durability of opsin expression induced by viral gene delivery to light-sensitize the heart, which has not yet been studied in larger animals. In our study, we simulated distribution of opsin-expressing cells based on reported expression levels in mice one year after AAV9-ChR2 injection (58.2% in a diffuse spatial pattern) (10); a more recent study in rats with hearts light-sensitized by AAV-ChR2 showed defibrillation efficacy one year post-transfection (78). Although there are no known safety concerns for AAV-based transfection in humans (79, 80), it is not yet known if safe, long-term light-sensitization via ChR2, GtACR1, or any opsin is possible.

Second, even in the context of reduced light energy requirements facilitated by GtACR1, the delivery of sufficient optical energy to the intracardiac milieu in large mammalian hearts remains an unsolved problem. Here, we opted to simulate uniform endocardial illumination, rather

than light stimuli focused on specific areas (17) or delivered by a grid of point sources (28). We made this choice to facilitate comparison with prior experimental work in animal models, which has used uniform illumination of some kind (8, 11-14, 27); moreover, whole surface stimulation has been shown to result in lower energy requirements (81). Nevertheless, it would be challenging to use endocardial illumination *in vivo* due to concerns regarding hemodynamic stability. Although it might be possible to implant flexible and biocompatible LED strips (82, 83) along the endocardial surface, it remains unknown whether this type of device would be feasible in practice. An exciting possible alternative is the use of up-converting nanoparticles to facilitate local light release triggered by deeper-penetrating energy like near-infrared light, ultra-sound, and X-rays (59, 84-86). The first proof of concept for optogenetic pacing of rat hearts with this type of technology was recently shown (87), but more work will be needed to validate the approach and to determine the most suitable way of representing the relevant physics in our computational models. Finally, our approach to modeling illumination does not account for any inhomogeneities that might arise from uneven light delivery by an LED field or a flexible biocompatible fluorescent membrane (88); this simplification was deemed an acceptable tradeoff, since it allowed us to assay feasibility of optogenetic defibrillation in various atrial and ventricular models with distinct organ geometry and functional heterogeneity from disease-related remodeling in a straightforward way.

3.5 Conclusions

We have demonstrated the first computational proof-of-concept for optogenetic defibrillation via stimulation of GtACR1 in biophysically detailed models of diseased human hearts. In all atrial cases and two of three ventricular cases, arrhythmia termination via endocardial light delivery was effective using irradiances as low as 5 $\mu W/mm^2$. The defibrillation mechanism was identified as transmural optogenetic voltage forcing, which was possible because very dim light stimuli can produce large photocurrents in GtACR1-expressing myocytes, thereby mitigating the limitation imposed by light attenuation in cardiac tissue.

3.6 References

1. Arrenberg, A.B., et al., *Optogenetic control of cardiac function.* Science, **2010**. 330(6006): p. 971-4.

2. Boyden, E.S., et al., *Millisecond-timescale, genetically targeted optical control of neural activity.* Nat Neurosci, **2005**. 8(9): p. 1263-8.

3. Addis, R.C., et al., *Optimization of direct fibroblast reprogramming to cardiomyocytes using calcium activity as a functional measure of success.* J Mol Cell Cardiol, **2013**. 60: p. 97-106.

4. Jia, Z., et al., *Stimulating cardiac muscle by light: cardiac optogenetics by cell delivery.* Circ Arrhythm Electrophysiol, **2011**. 4(5): p. 753-60.

5. Burton, R.A., et al., *Optical control of excitation waves in cardiac tissue.* Nat Photonics, **2015**. 9(12): p. 813-816.

6. Hussaini, S., et al., *Drift and termination of spiral waves in optogenetically modified cardiac tissue at sub-threshold illumination.* Elife, **2021**. 10.

7. Ambrosi, C.M. and E. Entcheva, *Optogenetics' promise: pacing and cardioversion by light?* Future Cardiol, **2014**. 10(1): p. 1-4.

8. Bruegmann, T., et al., *Optogenetic control of heart muscle in vitro and in vivo.* Nat Methods, **2010**. 7(11): p. 897-900.

9. Nussinovitch, U. and L. Gepstein, *Optogenetics for in vivo cardiac pacing and resynchronization therapies.* Nat Biotechnol, **2015**. 33(7): p. 750-4.

10. Vogt, C.C., et al., *Systemic gene transfer enables optogenetic pacing of mouse hearts.* Cardiovasc Res, **2015**. 106(2): p. 338-43.

11. Bruegmann, T., et al., *Optogenetic defibrillation terminates ventricular arrhythmia in mouse hearts and human simulations.* J Clin Invest, **2016**. 126(10): p. 3894-3904.

12. Cheng, Y., et al., *Optogenetic approaches for termination of ventricular tachyarrhythmias after myocardial infarction in rats in vivo.* J Biophotonics, **2020**. 13(7): p. e202000003.

13. Nyns, E.C.A., et al., *Optogenetic termination of ventricular arrhythmias in the whole heart: towards biological cardiac rhythm management.* Eur Heart J, **2017**. 38(27): p. 2132-2136.

14. Nyns, E.C.A., et al., *An automated hybrid bioelectronic system for autogenous restoration of sinus rhythm in atrial fibrillation.* Sci Transl Med, **2019**. 11(481): p. eaau6447.

15. Boyle, P.M., et al., *OptoGap is an optogenetics-enabled assay for quantification of cell-cell coupling in multicellular cardiac tissue.* Sci Rep, **2021**. 11(1): p. 9310.

16. Klimas, A., et al., *OptoDyCE as an automated system for high-throughput all-optical dynamic cardiac electrophysiology.* Nat Commun, **2016**. 7: p. 11542.

17. Boyle, P.M., et al., *Termination of re-entrant atrial tachycardia via optogenetic stimulation with optimized spatial targeting: insights from computational models.* J Physiol, **2018**. 596(2): p. 181-196.

18. Crocini, C., et al., *Optogenetics design of mechanistically-based stimulation patterns for cardiac defibrillation.* Sci Rep, **2016**. 6: p. 35628.

19. Gepstein, L. and A. Gruber, *Optogenetic Neuromodulation of the Heart.* J Am Coll Cardiol, **2017**. 70(22): p. 2791-2794.

20. Nussinovitch, U., R. Shinnawi, and L. Gepstein, *Modulation of cardiac tissue electrophysiological properties with light-sensitive proteins.* Cardiovasc Res, **2014**. 102(1): p. 176-87.

21. Zaglia, T., et al., *Optogenetic determination of the myocardial requirements for extrasystoles by cell type-specific targeting of ChannelRhodopsin-2.* Proc Natl Acad Sci U S A, **2015**. 112(32): p. E4495-504.

22. Siebels, J. and K.H. Kuck, *Implantable cardioverter defibrillator compared with antiarrhythmic drug treatment in cardiac arrest survivors (the Cardiac Arrest Study Hamburg).* Am Heart J, **1994**. 127(4 Pt 2): p. 1139-44.

23. Poole, J.E., et al., *Prognostic importance of defibrillator shocks in patients with heart failure.* N Engl J Med, **2008**. 359(10): p. 1009-17.

24. Moss, A.J., et al., *Prophylactic implantation of a defibrillator in patients with myocardial infarction and reduced ejection fraction.* N Engl J Med, **2002**. 346(12): p. 877-83.

25. Pedersen, S.S., et al., *Risk of chronic anxiety in implantable defibrillator patients: a multi-center study.* Int J Cardiol, **2011**. 147(3): p. 420-3.

26. Sulke, N., et al., *Rhythm control and cardioversion.* Heart, **2007**. 93(1): p. 29-34.

27. Bruegmann, T., et al., *Optogenetic termination of atrial fibrillation in mice.* Cardiovasc Res, **2018**. 114(5): p. 713-723.

28. Karathanos, T.V., et al., *Opsin spectral sensitivity determines the effectiveness of optogenetic termination of ventricular fibrillation in the human heart: a simulation study.* J Physiol, **2016**. 594(23): p. 6879-6891.

29. Govorunova, E.G., et al., *Natural light-gated anion channels: A family of microbial rhodopsins for advanced optogenetics.* Science, **2015**. 349(6248): p. 647-50.

30. Govorunova, E.G., et al., *Anion channelrhodopsins for inhibitory cardiac optogenetics.* Sci Rep, **2016**. 6: p. 33530.

31. Govorunova, E.G., et al., *The Expanding Family of Natural Anion Channelrhodopsins Reveals Large Variations in Kinetics, Conductance, and Spectral Sensitivity.* Sci Rep, **2017**. 7: p. 43358.

32. Zahid, S., et al., *Patient-derived models link re-entrant driver localization in atrial fibrillation to fibrosis spatial pattern.* Cardiovasc Res, **2016**. 110(3): p. 443-54.

33. Arevalo, H.J., et al., *Arrhythmia risk stratification of patients after myocardial infarction using personalized heart models.* Nat Commun, **2016**. 7: p. 11437.

34. Ashikaga, H., et al., *Feasibility of image-based simulation to estimate ablation target in human ventricular arrhythmia.* Heart Rhythm, **2013**. 10(8): p. 1109-16.

35. Deng, D., et al., *Accuracy of prediction of infarct-related arrhythmic circuits from image-based models reconstructed from low and high resolution MRI.* Front Physiol, **2015**. 6: p. 282.

36. Maguire, C.T., et al., *Implications of ventricular arrhythmia vulnerability during murine electrophysiology studies.* Physiol Genomics, **2003**. 15(1): p. 84-91.

37. Zahid, S., et al., *Feasibility of using patient-specific models and the "minimum cut" algorithm to predict optimal ablation targets for left atrial flutter.* Heart Rhythm, **2016**. 13(8): p. 1687-98.

38. Krummen, D.E., et al., *Mechanisms of human atrial fibrillation initiation: clinical and computational studies of repolarization restitution and activation latency.* Circ Arrhythm Electrophysiol, **2012**. 5(6): p. 1149-59.

39. Vadakkumpadan, F., et al., *Image-based models of cardiac structure in health and disease.* Wiley Interdiscip Rev Syst Biol Med, **2010**. 2(4): p. 489-506.

40. McDowell, K.S., et al., *Methodology for patient-specific modeling of atrial fibrosis as a substrate for atrial fibrillation.* J Electrocardiol, **2012**. 45(6): p. 640-5.

41. McDowell, K.S., et al., *Mechanistic inquiry into the role of tissue remodeling in fibrotic lesions in human atrial fibrillation.* Biophys J, **2013**. 104(12): p. 2764-73.

42. McDowell, K.S., et al., *Virtual electrophysiological study of atrial fibrillation in fibrotic remodeling.* PLoS One, **2015**. 10(2): p. e0117110.

43. Bayer, J.D., et al., *A novel rule-based algorithm for assigning myocardial fiber orientation to computational heart models.* Ann Biomed Eng, **2012**. 40(10): p. 2243-54.

44. Courtemanche, M., R.J. Ramirez, and S. Nattel, *Ionic mechanisms underlying human atrial action potential properties: insights from a mathematical model.* Am J Physiol, **1998**. 275(1): p. H301-21.

45. ten Tusscher, K.H. and A.V. Panfilov, *Alternans and spiral breakup in a human ventricular tissue model.* Am J Physiol Heart Circ Physiol, **2006**. 291(3): p. H1088-100.

46. Plank, G., et al., *From mitochondrial ion channels to arrhythmias in the heart: computational techniques to bridge the spatio-temporal scales.* Philos Trans A Math Phys Eng Sci, **2008**. 366(1879): p. 3381-409.

47. Vigmond, E.J., et al., *Computational tools for modeling electrical activity in cardiac tissue.* J Electrocardiol, **2003**. 36 Suppl: p. 69-74.

48. Vigmond, E.J., et al., *Solvers for the cardiac bidomain equations.* Prog Biophys Mol Biol, **2008**. 96(1-3): p. 3-18.

49. Guo, W., et al., *Changes in action potentials and ion currents in long-term cultured neonatal rat ventricular cells.* Am J Physiol, **1996**. 271(1 Pt 1): p. C93-102.

50. Kopton, R.A., et al., *Cardiac Electrophysiological Effects of Light-Activated Chloride Channels.* Front Physiol, **2018**. 9: p. 1806.

51. Williams, J.C., et al., *Computational optogenetics: empirically-derived voltage- and light-sensitive channelrhodopsin-2 model.* PLoS Comput Biol, **2013**. 9(9): p. e1003220.

52. Karathanos, T.V., P.M. Boyle, and N.A. Trayanova, *Optogenetics-enabled dynamic modulation of action potential duration in atrial tissue: feasibility of a novel therapeutic approach.* Europace, **2014**. 16 Suppl 4(Suppl 4): p. iv69-iv76.

53. Ambrosi, C.M., et al., *Cardiac applications of optogenetics.* Prog Biophys Mol Biol, **2014**. 115(2-3): p. 294-304.

54. Boyle, P.M., et al., *Computational modeling of cardiac optogenetics: Methodology overview & review of findings from simulations.* Comput Biol Med, **2015**. 65: p. 200-8.

55. Boyle, P.M., et al., *A comprehensive multiscale framework for simulating optogenetics in the heart.* Nat Commun, **2013**. 4: p. 2370.

56. Jacques, S.L. and B.W. Pogue, *Tutorial on diffuse light transport.* J Biomed Opt, **2008**. 13(4): p. 041302.

57. Ripoll, J., et al., *Experimental determination of photon propagation in highly absorbing and scattering media.* J Opt Soc Am A Opt Image Sci Vis, **2005**. 22(3): p. 546-51.

58. Bishop, M.J., et al., *Synthesis of voltage-sensitive optical signals: application to panoramic optical mapping.* Biophys J, **2006**. 90(8): p. 2938-45.

59. Boyle, P.M., T.V. Karathanos, and N.A. Trayanova, *Cardiac Optogenetics: 2018.* JACC Clin Electrophysiol, **2018**. 4(2): p. 155-167.

60. Ambrosi, C.M., et al., *Optogenetics-enabled assessment of viral gene and cell therapy for restoration of cardiac excitability.* Sci Rep, **2015**. 5: p. 17350.

61. Bishop, M.J., et al., *The role of photon scattering in optical signal distortion during arrhythmia and defibrillation.* Biophys J, **2007**. 93(10): p. 3714-26.

62. Swartling, J., et al., *Changes in tissue optical properties due to radio-frequency ablation of myocardium.* Med Biol Eng Comput, **2003**. 41(4): p. 403-9.

63. Boyle, P.M., E. Entcheva, and N.A. Trayanova, *See the light: can optogenetics restore healthy heartbeats? And, if it can, is it really worth the effort?* Expert Rev Cardiovasc Ther, **2014**. 12(1): p. 17-20.

64. Boyle, P.M., T.V. Karathanos, and N.A. Trayanova, *"Beauty is a light in the heart": the transformative potential of optogenetics for clinical applications in cardiovascular medicine.* Trends Cardiovasc Med, **2015**. 25(2): p. 73-81.

65. Crocini, C., et al., *Optogenetics gets to the heart: A guiding light beyond defibrillation.* Prog Biophys Mol Biol, **2017**. 130(Pt B): p. 132-139.

66. Entcheva, E., *Cardiac optogenetics.* Am J Physiol Heart Circ Physiol, **2013**. 304(9): p. H1179-91.

67. Bingen, B.O., et al., *Light-induced termination of spiral wave arrhythmias by optogenetic engineering of atrial cardiomyocytes.* Cardiovasc Res, **2014**. 104(1): p. 194-205.

68. Nussinovitch, U. and L. Gepstein, *Optogenetics for suppression of cardiac electrical activity in human and rat cardiomyocyte cultures.* Neurophotonics, **2015**. 2(3): p. 031204.

69. Funken, M., et al., *Optogenetic Hyperpolarization of Cardiomyocytes Terminates Ventricular Arrhythmia.* Front Physiol, **2019**. 10: p. 498.

70. Berndt, A., et al., *Structure-guided transformation of channelrhodopsin into a light-activated chloride channel.* Science, **2014**. 344(6182): p. 420-4.

71. Wietek, J., et al., *Conversion of channelrhodopsin into a light-gated chloride channel.* Science, **2014**. 344(6182): p. 409-12.

72. Guru, A., et al., *Making Sense of Optogenetics.* Int J Neuropsychopharmacol, **2015**. 18(11): p. pyv079.

73. Govorunova, E.G., et al., *RubyACRs, nonalgal anion channelrhodopsins with highly red-shifted absorption.* Proc Natl Acad Sci U S A, **2020**. 117(37): p. 22833-22840.

74. Lin, Y., et al., *Zacopride Exerts an Antiarrhythmic Effect by Specifically Stimulating the Cardiac Inward Rectifier Potassium Current in Rabbits: Exploration of a New Antiarrhythmic Strategy.* Curr Pharm Des, **2020**. 26(44): p. 5746-5754.

75. Zhai, X.W., et al., *The IK1/Kir2.1 channel agonist zacopride prevents and cures acute ischemic arrhythmias in the rat.* PLoS One, **2017**. 12(5): p. e0177600.

76. Elnakish, M.T., et al., *Effects of zacopride, a moderate IK1 channel agonist, on triggered arrhythmia and contractility in human ventricular myocardium.* Pharmacol Res, **2017**. 115: p. 309-318.

77. Liu, Q.H., et al., *A novel discovery of IK1 channel agonist: zacopride selectively enhances IK1 current and suppresses triggered arrhythmias in the rat.* J Cardiovasc Pharmacol, **2012**. 59(1): p. 37-48.

78. Li, J., et al., *Optical capture and defibrillation in rats with monocrotaline-induced myocardial fibrosis 1 year after a single intravenous injection of adeno-associated virus channelrhodopsin-2.* Heart Rhythm, **2021**. 18(1): p. 109-117.

79. Wasala, N.B., J.H. Shin, and D. Duan, *The evolution of heart gene delivery vectors.* J Gene Med, **2011**. 13(10): p. 557-65.

80. Greenberg, B., et al., *Calcium upregulation by percutaneous administration of gene therapy in patients with cardiac disease (CUPID 2): a randomised, multinational, double-blind, placebo-controlled, phase 2b trial.* Lancet, **2016**. 387(10024): p. 1178-86.

81. Quiñonez Uribe, R.A., et al., *Energy-Reduced Arrhythmia Termination Using Global Photostimulation in Optogenetic Murine Hearts.* Front Physiol, **2018**. 9: p. 1651.

82. Kim, R.H., et al., *Waterproof AlInGaP optoelectronics on stretchable substrates with applications in biomedicine and robotics.* Nat Mater, **2010**. 9(11): p. 929-37.

83. Kim, T.I., et al., *Injectable, cellular-scale optoelectronics with applications for wireless optogenetics.* Science, **2013**. 340(6129): p. 211-6.

84. Berry, R.G., Matthew; Lars Gjesteby and Ge Wang *, *X-Optogenetics and U-Optogenetics: Feasibility and Possibilities* Photonics, **2015**.

85. Entcheva, E. and M.W. Kay, *Cardiac optogenetics: a decade of enlightenment.* Nat Rev Cardiol, **2021**. 18(5): p. 349-367.

86. Huang, K., Q. Dou, and X.J. Loh, *Nanomaterial mediated optogenetics: opportunities and challenges.* RSC Advances, **2016**. 6(65): p. 60896-60906.

87. Rao, P., et al., *Near-infrared light driven tissue-penetrating cardiac optogenetics via upconversion nanoparticles in vivo.* Biomed Opt Express, **2020**. 11(3): p. 1401-1416.

88. Xu, L., et al., *3D multifunctional integumentary membranes for spatiotemporal cardiac measurements and stimulation across the entire epicardium.* Nat Commun, **2014**. 5: p. 3329.

Chapter 4 | Optogenetic Modulation of Arrhythmia Triggers: Proof-of-Concept from Computational Modeling

Reproduced in part from Ochs A.R. and Boyle P.M. "Optogenetic Modulation of Arrhythmia Triggers: Proof-of-Concept from Computational Modeling." Cellular and Molecular Bioengineering 2023 (currently in revision).

4.1 Abstract

Introduction: Early afterdepolarizations (EADs) are secondary voltage depolarizations associated with reduced repolarization reserve (RRR) that can trigger lethal arrhythmias. Underlying EAD mechanisms are difficult to study, so the ability to suppress or provoke EADs would be experimentally useful. Here, we use computational simulations to assess the feasibility of subthreshold optogenetic stimulation modulating the propensity for EADs (cell-scale) and EAD-associated ectopic beats (organ-scale).

Methods: We modified a ventricular ionic model by reducing rapid delayed rectifier potassium (0.25–0.1 × baseline) and increasing L-type calcium (1.0–3.5 × baseline) currents to create RRR conditions with varying severity. We used single cardiomyocytes models and left ventricular models derived from late gadolinium enhanced magnetic resonance imaging of post-myocardial infarction patients. We simulated optogenetic stimulation of ChR2 (depolarizing) or GtACR1 (repolarizing).

Results: In cell-scale simulations without illumination, EADs were seen for 164 of 416 RRR conditions. Subthreshold stimulation of GtACR1 reduced EAD incidence by up to 85.4% (25/416 RRR conditions; 0.1 μW/mm^2); in contrast, subthreshold ChR2 excitation increased EAD incidence by up to 136.6% (388/416 RRR conditions; 50 μW/mm^2). At the organ scale, we assumed simultaneous, uniform illumination of the epicardial and endocardial surfaces. GtACR1-mediated suppression (10–50 μW/mm^2) and ChR2-mediated EAD unmasking (50–100 μW/mm^2) were feasible in three distinct ventricular models.

Conclusions: Our findings suggest that optogenetics could be used to silence or provoke both EADs and EAD-associated ectopic beats. Validation in animal models could lead to exciting new experimental regimes, and potentially to novel anti-arrhythmia treatments.

4.2 Introduction

Early afterdepolarizations (EADs) are spontaneous depolarizations during cardiac action potential (AP) repolarization that are strongly associated with arrhythmogenic events like torsade de pointes (TdP) and sudden cardiac death (1, 2). It is understood that EADs occur in the presence of conditions that increase inward ionic currents and decrease outward ionic currents, known as reduced repolarization reserve (RRR) (1-3). RRR can result from either congenital factors, such as ion channelopathy (e.g., long QT syndrome) (4, 5) or acquired arrhythmogenic drivers such as APD-prolonging drugs (3, 6), cardiac ischemia (7), or heart failure (8). However, the link between EADs and TdP is not fully understood. EADs occur stochastically in single cells and RRR alone does not explain EAD genesis (2). Mechanistically linking these cell-scale events to organ-scale phenomena (i.e., propagating ectopic wavefronts that lead to extra heartbeats) is difficult. Consequently, the ability to suppress or provoke EAD-mediated triggered activity in tissue and organ scale environments would be extremely useful to experimentalists. For instance, whole organ preparations like Langendorff-perfused mouse hearts could be a viable and consistent experimental platform for studying EAD-associated ectopic beat propensity. Currently available methods, such as direct current injection or pharmaceutical intervention, lack spatiotemporal specificity and disrupt underlying EAD behavior.

Optogenetic stimulation of cardiac tissue (9) could provide a means of exploring EAD mechanisms. This method incorporates microbial light-sensitive ion channels and pumps into cardiomyocytes to allow light-mediated, spatiotemporally precise stimulation (10). Numerous studies have explored novel applications using this technique, including control of spiral wave chirality (11), neuromodulation of the heart (12-14), arrhythmia termination (15-18), and

modulation of AP properties to correcting for short and long QT syndromes (19, 20). Notably, nearly all of these studies used optogenetic stimulation to elicit sustained depolarizing currents. This is not conducive for studying EADs, since the constant light-mediated stimulation would disrupt the underlying electrical phenomena. More recently, scientists have begun examining the use of *subthreshold* (i.e., non-AP evoking) optogenetic stimulation to alter tissue electrophysiological properties without eliciting a propagating response. Examples include: control of spiral wave drift and termination (21), creating electric turbulence in previously stable environments (22), and modulating electrical alternans dynamics to destabilize reentrant arrhythmias (23). We hypothesized that subthreshold optogenetic stimuli could be used to modulate EAD propensity at the cell scale and EAD-associated ectopic beat emergence at the organ scale.

In the present study, we use computational simulations to evaluate this hypothesis in RRR-afflicted models of ventricular cardiomyocytes and infarcted human ventricles. We incorporate biophysically realistic models of two opsins: an outward current anion channelrhodopsin (GtACR1) (24, 25) and an inward current cation channelrhodopsin-2 (ChR2) (26, 27). Stimulation of both GtACR1 and ChR2 is used to attenuate or exacerbate factors underlying EADs, respectively. First, we conduct simulations in a realistic ventricular cell model to down- or up-regulate EAD occurrence across a parameter space of RRR conditions. Then, we simulate RRR-afflicted patient-derived left ventricular (LV) models to examine down- and up-regulation of EAD-associated ectopic beat propensity. We provide proof-of-concept evidence that subthreshold optogenetic stimulation can be used to suppress or evoke EAD phenomena (i.e., EADs in simulated cardiomyocytes and ectopic beats in LV models) during RRR conditions across multiple biophysical scales.

4.3 Methods

EADs in simulated human ventricular cardiomyocytes

We used the ventricular action potential model developed by O'Hara et al. (ORd) (28) in all cell and organ-scale simulations. The ORd fast sodium current (I_{Na}) was replaced with the ten Tusscher et al. (29) formulation to facilitate compatibility with organ-scale modeling, as advised by the ORd developers (28, 30). To generate EAD-favoring RRR conditions, we varied scaling factors of conductance for two ionic currents in a manner similar to previous publications (31, 32). The rapid delayed rectifier K^+ current (I_{Kr}) was varied from 0.25–0.10 × baseline by steps of 0.01, and the L-type Ca^{2+} current (I_{CaL}) was varied from 1.0–3.5 × baseline by steps of 0.1.

Single cell simulations were conducted using 416 permutations of these two scaling factors. Each virtual cardiomyocyte was paced at 1 Hz frequency (pulse duration: 1 ms; stimulus amplitude: 60 pA/pF). The simulation was conducted twice, with either 290 or 291 stimuli, then evaluated for a final screening window of 9 or 8 s for EAD occurrence using a custom Matlab script (total simulation duration of 300 s). EADs were classified by any positive deflection in the membrane voltage (V_m) time derivative (dV_m/dt) during repolarization after each stimulus (evaluated from 100 to 999 ms within a given 1000 ms interval). An RRR condition was marked with EAD presence if either simulation had EADs detected. It was necessary to conduct and evaluate two simulation protocols (290 or 291 stimuli) because some RRR conditions had EAD fluctuations persisting for >1000 ms that were terminated by the subsequent stimulus, which would lead to an erroneous "no EADs" classification.

Electrophysiological simulation of human post-myocardial infarction ventricles

Simulations were conducted in three finite element LV models (**Fig. 4.1**) reconstructed from late gadolinium enhanced magnetic imaging resonance (LGE-MRI) scans as part of a prior study (33, 34). These models were freely available from a published data set of 24 ischemic cardiomyopathy patients with prior myocardial infarction (MI) (33). In all three cases, the mesh resolution of the publicly available version was increased via a single iteration of tetrahedral subdivision (edge length in publicly available versions ~1 mm; for models used in this study: ~500

μm), which moved the models into the agreed-upon tolerable range for numerical convergence (35). The temporal discretization was 25 μs, as in past studies (36, 37).

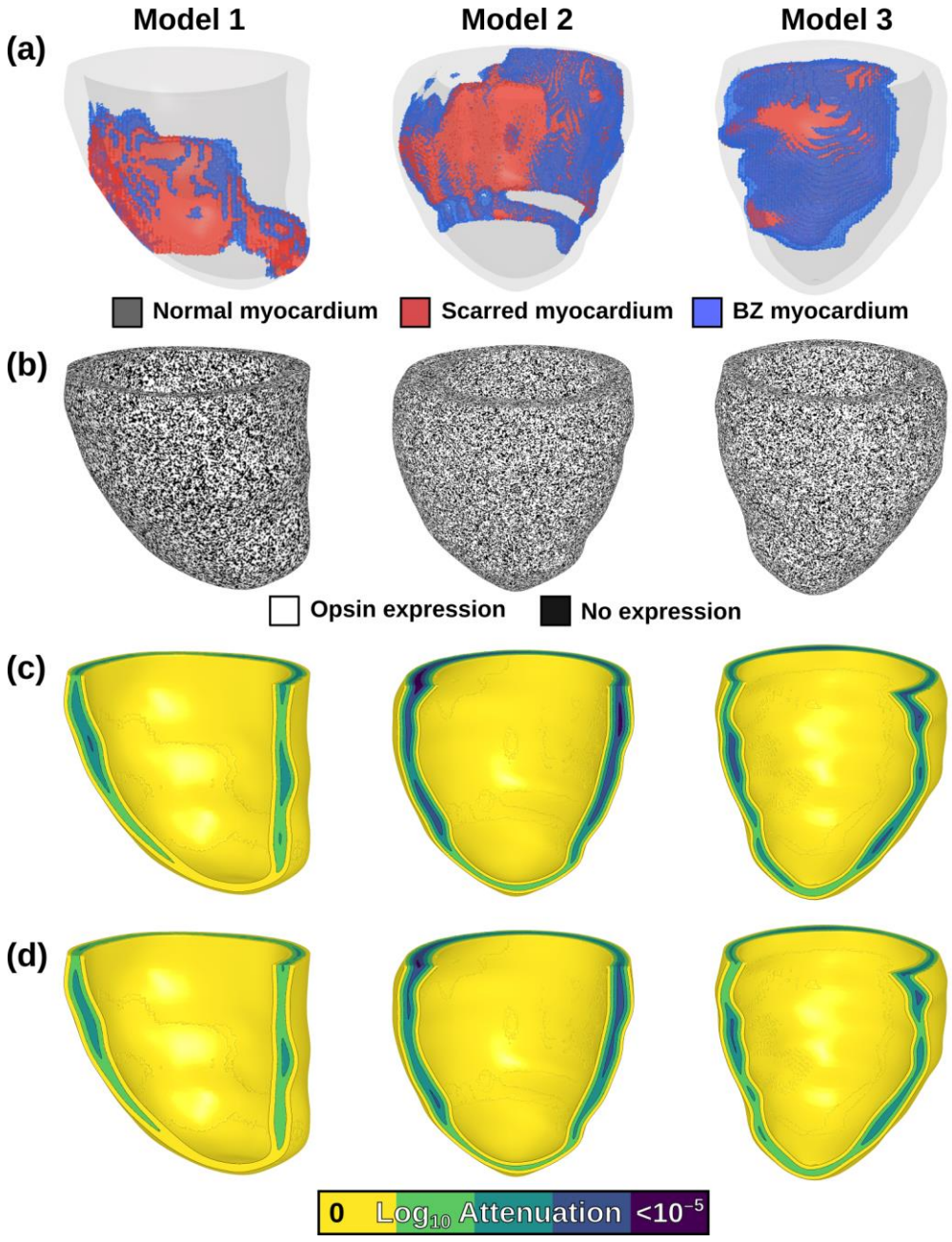

Figure 4.1*: Patient-specific, post-MI LV models reconstructed from LGE-MRI scans.* ***A****: Spatial distribution of tissue is shown; normal myocardium (gray), non-conductive scar (red), and electrically remodeled border zone (BZ; blue).* ***B****: Opsin transfection patterns are shown in each model, where white denotes opsin expression and black denotes lack of expression.* ***C-D****: Light attenuation for green (C) and blue (D) light stimuli applied uniformly and simultaneously to the epicardial and endocardial surfaces.*

When selecting three LV models from the available twenty-four, we analyzed the extent of myocardial scar and the relative location of infarcted tissue within the myocardial wall (e.g.: epicardial dominant, endocardial dominant, or transmural) for all possible candidates (**Fig. 4.2**). The first model (Model 1) was selected for its moderate scar burden (15.4% scar, 2.09% BZ) and balanced transmural scar distribution. Other two models selected had larger scar burden with predominantly sub-endocardial infarcts: Model 2 (19.1% scar, 2.84% BZ) and Model 3 (17.5% scar, 6.61% BZ), contrasted against the average for all 24 possible models (11.4% scar, 2.95% BZ).

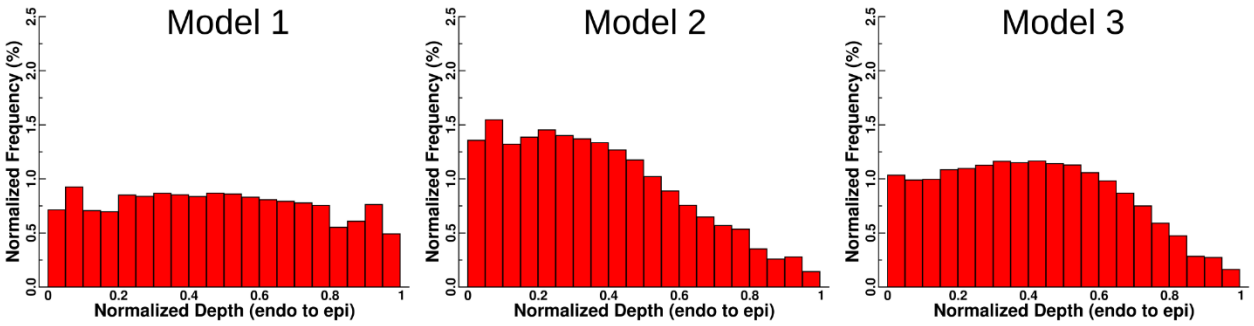

Figure 4.2*: Scar distributions in three patient-derived LV models used in this study, after normalization by model volume. Model numbers correspond to visuals shown in Figure 1.*

These models had representations of normal myocardium, peri-infarct border zone (BZ), and infarct segmented from patient-specific LGE-MRI scans, as described by the authors of the original study (33, 34). Realistic fiber orientations were represented using a rules-based approach, as originally described by Bayer et al. 2012 (38). We modeled scar as non-conductive, as in prior work (16, 33, 34, 36, 37). BZ tissue was modeled with identical ionic properties to normal myocardium (36) to eliminate possible confounding effects from RRR conditions. As in prior studies (37, 39), tissue scale electrical conductivity in the longitudinal direction (i.e., parallel to fibers; σ_L) in normal myocardium and BZ was identical (0.255 S/m). In the transverse direction (i.e., perpendicular to fibers; σ_T) this value was reduced in normal myocardium to reflect anisotropy of conduction (0.0775 S/m), and reduced even further in BZ tissue (7.75 mS/m) to represent effects of electrophysiological remodeling in the infarct periphery (36).

Electrical conduction at tissue scale was simulated using a finite element approximation of the monodomain equation (40, 41); this approach for modeling cardiac electrophysiology has been extensively validated in prior work (16, 36, 42-44). Ordinary differential equations associated with action potential simulations were solved using the Rush-Larsen scheme (45) for ion channel gating variables and forward Euler integration elsewhere. The governing partial differential equation for the monodomain formulation was solved with the full (non-lumped) mass matrix using a Crank-Nicholson scheme to improve model stability (40). All simulations were conducted using freely available software (openCARP) (46).

EAD-associated ectopic beats in organ scale models

For a subset of RRR conditions examined in cell-scale simulations, we ran simulations in LV models as described above. In each case, an initial electrical stimulus (t = 0 ms) was applied to the entire LV endocardial surface to approximate sinus activation via excitation of the His-Purkinje system. Subsequent spatiotemporal evolution of V_m was monitored for the occurrence of a sustained and propagating EAD-associated ectopic excitation (simulation duration: 1500 ms). We classified presence of an ectopic beat for a given RRR condition as any organ-wide depolarization during the repolarization period following the initial endocardial stimulus.

Optogenetic modulation of electrophysiology via light stimulation of GtACR1 or ChR2

The response to light stimulation of two opsins (GtACR1 and ChR2) was simulated using previously published photocurrent models. I_{GtACR1} was represented using a 2-state Markov chain model (37) created from measurements taken from neonatal rat ventricular myocytes (24). I_{ChR2} was represented using a 4-state model generated from ChR2(H134R)-expressing HEK293 cells (27), which agreed well with action potential-clamped guinea pig ventricular myocytes. As in our past study, peak GtACR1 channel conductance was modeled as 1.4 mS/cm^2 (37), assuming a membrane capacitance of 100 pF (within physiological range) (47). ChR2 channel conductance was modeled as 0.17 mS/cm^2, to match the recorded peak ChR2(H134R) photocurrent from an

earlier study (48). Based on different studies examining opsin transfection for 1-12 months following viral injection (48, 49), opsin expression was represented in 58.2% of non-infarct (normal and BZ) tissue in a diffuse pattern (**Fig. 4.1B**) (16). The spatial patterns of expression for the two opsins (i.e., GtACR1 and ChR2) were identical within each patient-derived model. In organ-scale simulations where optogenetic stimulation was applied, global illumination began at the simulation start (t = 0 ms) and was maintained for the entire simulation duration.

Modeling of light attenuation

Realistic light attenuation via scattering and absorption in myocardium was simulated using the exponential decay approximation, as in prior modeling work (19, 37, 50). In brief, we defined parameter a (value between 0 and 1; **Eqn 4.1**) using coefficients for light scattering (μ_s'), light absorption (μ_a), and anisotropy factor (g), which was then used to calculate the diffusion coefficient D (**Eqn 4.2**) (51).

$$a = 1 - \frac{4}{5} \cdot \frac{\mu_s' + \mu_a}{\mu_s' \cdot (1+g) + \mu_a} \tag{4.1}$$

$$D = \frac{1}{3(\mu_s' + \mu_a * a)} \tag{4.2}$$

As in previous work (37), we used μ_a = 0.1, μ_s' = 1.42, g = 0.9 (52) for green light (515 nm) and μ_a = 0.52 and D = 0.183 (53) for blue light (488 nm). These parameters resulted in exponential decay constants ($\delta = \sqrt{D/\mu_a}$) of 519.6 μm and 593.2 μm for green and blue light, respectively.

In all cases of organ-scale optogenetic stimulation, we represented concurrent illumination of the endocardial and epicardial LV surfaces. We modeled the process in this manner because we anticipated the effect of light attenuation would be too large for sub-threshold optogenetic stimuli to affect organ-scale EAD propensity if only one surface was illuminated. Light stimulation was represented by imposing a surface irradiance ($\overline{E_e}$), then modifying that value in the

myocardial volume based on distance (r) from the nearest point on the illuminated surface (**Eqn 4.3**) (19, 50):

$$E_e(r) = \overline{E_e} e^{-r/\delta} \quad (4.3)$$

E_e distributions in each LV model for the endo- and epicardial surfaces were calculated separately, then summed together (i.e., superimposed) to accurately represent the net illumination effect from dual surface illumination (**Fig. 4.1C-D**).

Illumination protocols for optogenetic modulation of EAD and ectopic beat propensity

To assess the feasibility of modulating EAD propensity, we repeated cell-scale simulations for all RRR configurations and pacing protocols described above, but with the addition of either constant GtACR1 or ChR2 stimulation. In all cases, light onset was at simulation initialization (t = 0 ms) and persisted for the entire duration (300 s); each of these simulations was evaluated for the presence of EADs as described above. For EAD suppression, we tested constant GtACR1 illumination strengths of 1 nW/mm^2 to 1 µW/mm^2 (order of magnitude steps); for evoking EADs, we used different amplitudes of 1–500 µW/mm^2 (half-order of magnitude steps), owing to the distinct energy requirements of ChR2.

For organ scale simulations, six RRR conditions were selected from the cell-scale simulations (see highlighted green and blue boxes in **Fig. 4.4A**). Without optogenetic stimulation, three of these conditions had EADs (green), while the other three did not (blue). This allowed a framework suitable for testing the efficacy of EAD suppression or provocation via subthreshold GtACR1 and ChR2 stimulation, respectively. RRR conditions were applied uniformly to all normal myocardium and BZ tissue in organ-scale simulations. Simulated concurrent epi- and endocardial illumination began at t = 0 ms, and continued for the entire simulation duration (1500 ms).

Metrics to predict success or failure of ectopic beat modulation via optogenetic stimulation

To increase the generalizability and translational potential of our findings, we derived quantitative metrics exclusively on quantities that could be measured experimentally. Namely, we for these metrics we took into account exclusively ventricular anatomy (i.e., chamber dimensions, wall thickness), without accounting for scar or border zone, and light stimulus characteristics (i.e., intensity, attenuation rate). The first metric was conceived to approximate the total irradiance absorbed by the entire ventricular myocardium in response to a particular light stimulus (**Eqn 4.4**):

$$Total\ Volumetric\ Irradiance\ (TVI) = \frac{\sum_{i=1}^{N} E_{e,i}}{Vol} \tag{4.4}$$

where *N* is the number of nodes in the finite element grid; $E_{e,i}$ is the irradiance delivered to the i^{th} node in the grid based on **Eqn 4.3**; and *Vol* is the total myocardial tissue volume. The second metric was identical to the first, but with base 10 logarithmic scaling of the node-wise irradiance values (**Eqn 4.5**):

$$Total\ Volumetric\ Log\ Irradiance\ (TV_L I) = \frac{\sum_{i=1}^{N} log_{10}(E_{e,i})}{Vol} \tag{4.5}$$

For each organ-scale simulation conducted in the study, we classified the outcome as success (i.e., if the stimulus suppressed or provoked an ectopic beat for GtACR1- and ChR2-expressing experiments, respectively) or failure. We then calculated *TVI* and $TV_L I$ for the corresponding optogenetic stimuli and applied receiver operating characteristic (ROC) analysis to assess the predictive capacity of both metrics.

4.4 Results

Early afterdepolarizations in simulated ventricular myocytes under reduced repolarization reserve

To establish RRR conditions for EAD testing in simulated single cardiomyocytes, we adapted a previously published approach (32, 54). Maximal channel conductance values for I_{Kr} and I_{CaL} ionic currents were down- and up-regulated, respectively. Specifically, scaling factors tested were 0.25–0.10 × baseline for I_{Kr} (steps of 0.01), and 1.0–3.5 × baseline for I_{CaL} (steps of

0.1). We also determined the minimum single cell irradiance values necessary to elicit action potentials; the purpose here was to define the range of optogenetic stimuli defined as subthreshold (i.e., below that minimum irradiance). These were found to be ≤0.1 μW/mm^2 for GtACR1 and ≤50 μW/mm^2 for ChR2.

Representative voltage traces are highlighted in **Figure 4.3** to demonstrate EAD suppression using GtACR1 (**Fig. 4.3A**) and EAD provocation using ChR2 (**Fig. 4.3B**) across different RRR conditions. When evaluating the entire parameter space, we found that 164 of 416 simulations (39.4%) had EADs develop (**Fig. 4.4A**). When constant optogenetic stimulation was applied to the simulated cardiomocytes, the proportion of EAD-occurring RRR conditions reduced under subthreshold GtACR1 stimulation (**Fig. 4.4B-C**) and increased under subthreshold ChR2 stimulation (**Fig. 4.4D-E**). Specifically, GtACR1 stimulation at very low irradiance (0.05 μW/mm^2) reduced EAD incidence to 79/416 conditions (19.0%; **Fig. 4.4B**), while a stronger stimulus (0.1 μW/mm^2) caused further reduction to 25/416 conditions (6.0%; **Fig. 4.4C**). Inversely, ChR2 stimulation at a low irradiance (10 μW/mm^2) increased EAD incidence to 264/416 conditions (63.5%; **Fig. 4.4D**), while a stronger stimulus (50 μW/mm^2) caused further increase to 388/416 conditions (93.3%; **Fig. 4.4E**).

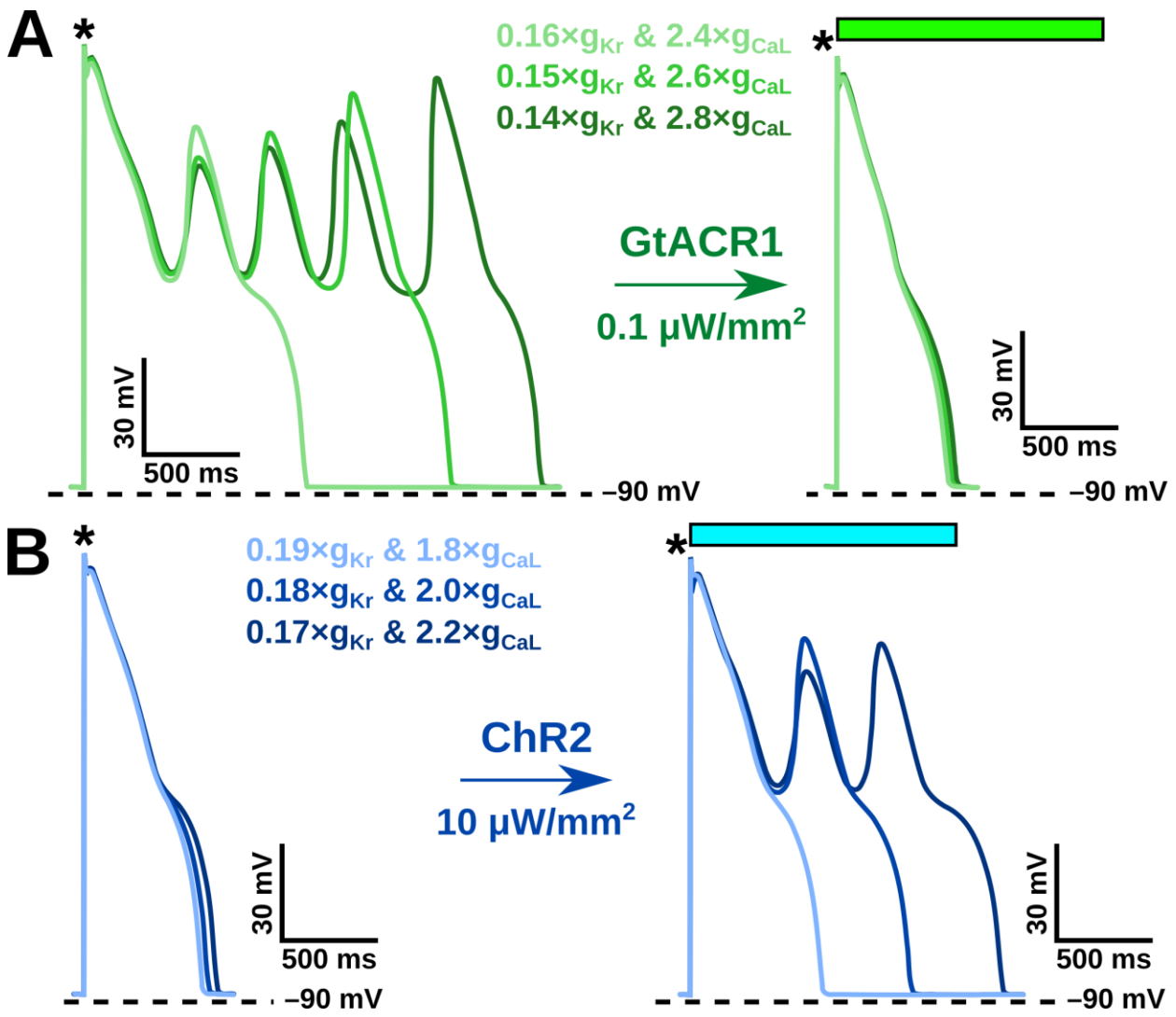

***Figure 4.3**: EAD occurrence can be down- or up-regulated in a simulated cardiomyocyte using subthreshold optogenetic stimulation. **A**: Representative traces of membrane voltage over time [$V_m(t)$] for conditions with EADs that are suppressed by constant GtACR1 stimulation (0.1 μW/mm^2). **B:** Representative $V_m(t)$ for traces without EADs are evoked by constant ChR2 stimulation (10 μW/mm^2). The different shades of blue and green trace colors correspond to the six RRR conditions highlighted in Figure 3A and tested in organ-scale simulations.*

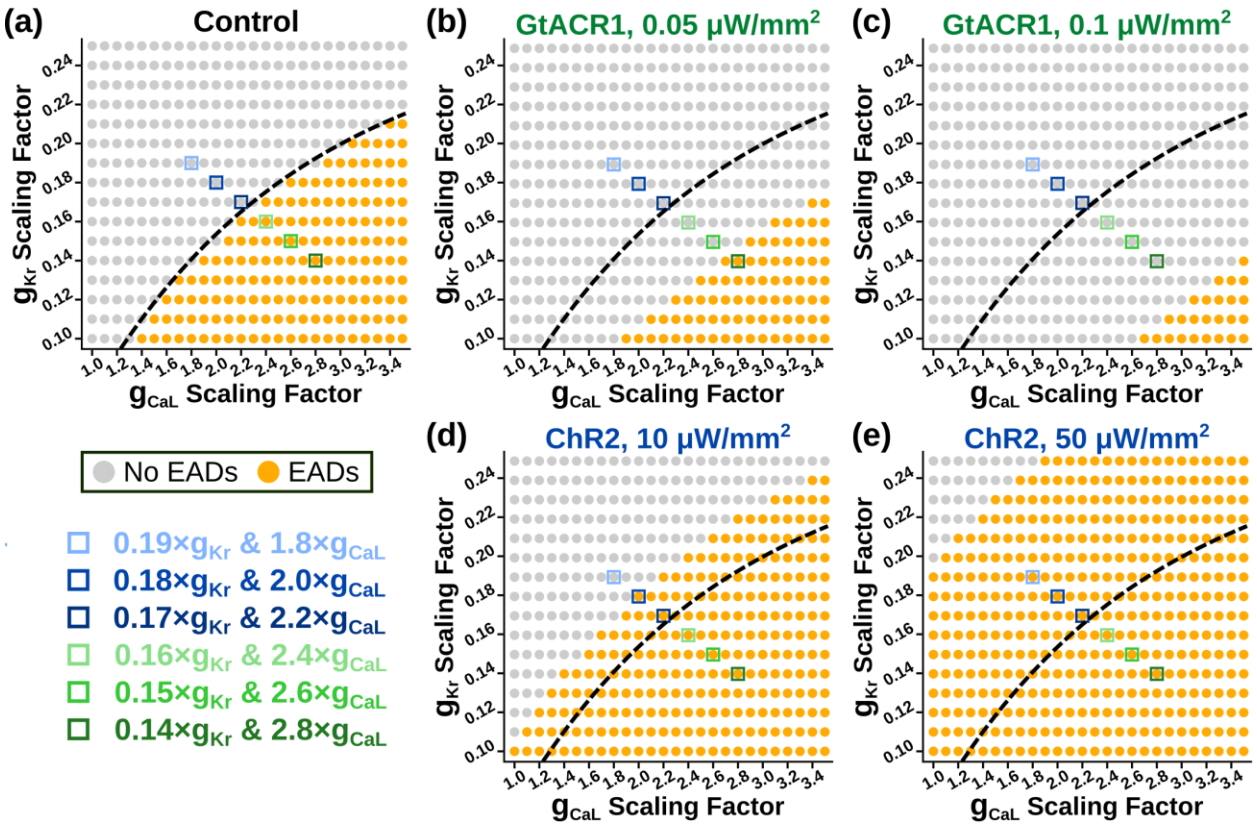

***Figure 4.4**: EAD occurrence at various RRR conditions in a simulated ventricular cardiomyocyte. **A**: Baseline EAD incidence in control condition (no optogenetic stimulation). **B-C**: When GtACR1 stimulation is applied at 0.05 μW/mm² (**B**) or 0.1 μW/mm² (**C**), overall EAD incidence is reduced. **D-E**: When ChR2 stimulation is applied at 10 μW/mm² (**D**) or 50 μW/mm² (**E**), overall EAD incidence is increased. Dashed line denotes the threshold between conditions without and with EADs in (A). Shaded blue and green boxes correspond to the six RRR conditions shown in Figure 2 $V_m(t)$ traces and tested in organ-scale simulations.*

Ectopic beats in organ-scale LV models under reduced repolarization reserve

We conducted organ-scale simulations in three patient-derived LV models (**Fig. 4.1**). Due to differences in electrical source-sink dynamics compared to the cell-scale milieu, first we established the organ-scale subthreshold optogenetic stimulation irradiances for both opsins. The GtACR1- and ChR2-expressing LV models were illuminated simultaneously from the epicardial and endocardial surfaces, then examined at steady state (chosen as t = 2000 ms). Using this method, we found that the subthreshold optogenetic stimulation irradiances were 1–10 μW/mm² for GtACR1 and 10–100 μW/mm² for ChR2 (half order-of-magnitude steps for both; **Fig. 4.5**).

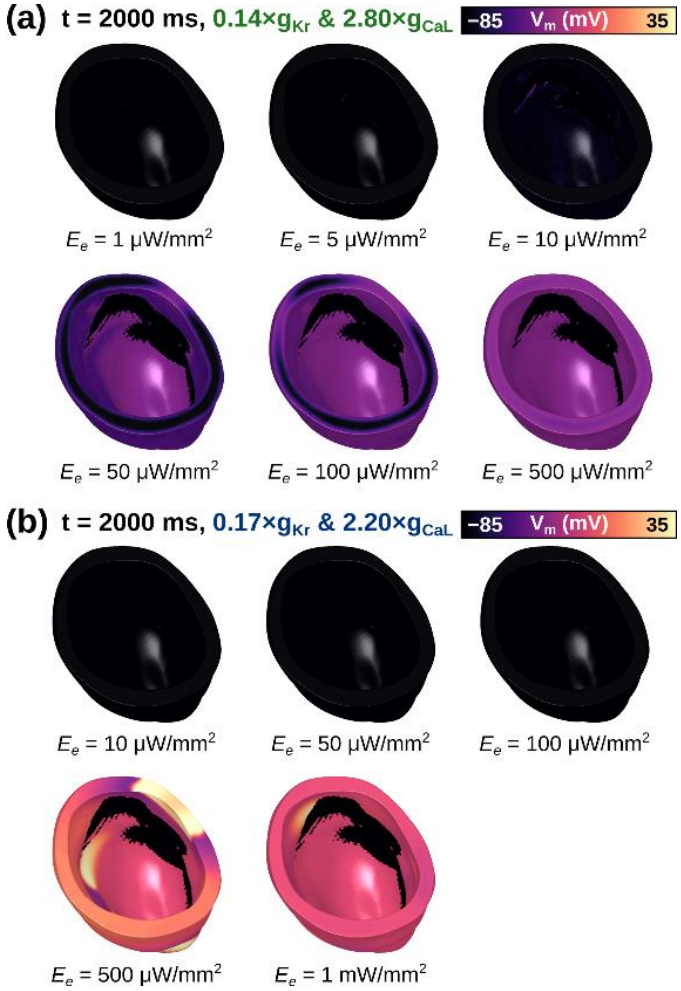

Figure 4.5*: The effects of constant optogenetic stimulation applied to RRR-afflicted LV models (without paced sinus rhythm). Simultaneous epi- and endocardial illumination with* ***A)*** *GtACR1 or* ***B)*** *ChR2 expression is applied at t = 0 for 2000 ms duration. Snapshots of activity at 2000 ms are visualized using a relevant RRR condition for each (GtACR1: 0.14 × I_{Kr}, 2.8 × I_{CaL}; ChR2: 0.17 × I_{Kr}, 2.2 × I_{CaL}). Conditions with elevated resting V_m or arrhythmia occurrence were considered suprathreshold for the purposes of this study.*

From the cell-scale parameter analysis, a subset of six RRR conditions with and without EADs at baseline were selected (see colored boxes superimposed on grid in **Fig. 4.4** for specific combinations of g_{Kr} and g_{CaL} multipliers). Due to source-sink differences at cellular versus organ-scale environments, cellular EAD presence at a specific RRR condition does not necessitate an ectopic beat in the LV model simulations. However, we found that all six RRR conditions matched the projected ectopic beat outcome across the three LV models (i.e., EAD-prone conditions did have ectopic beats at baseline while EAD-lacking conditions did not show ectopy at baseline).

When subthreshold epi- and endocardial green light illumination of GtACR1-expressing LV models was simulated, we found that 5 and 10 μW/mm^2 irradiances suppressed ectopic beats in 17 of 18 cases (2 irradiances × 3 RRR conditions × 3 models; **Fig. 4.6**). A representative example of an optogenetically-suppressed ectopic beat is shown in **Figure 4.7**. When subthreshold epi- and endocardial blue light illumination of ChR2-expressing LV models was simulated, we found that 50 and 100 μW/mm^2 irradiances provoked ectopic beats in 13 of 18 cases (2 irradiances × 3 RRR conditions × 3 models; **Fig. 4.8**). A representative example of an optogenetically-provoked ectopic beat is shown in **Figure 4.9**. In simulations that presented ectopic beats, we consistently observed both EADs and re-excitations occurring in tissue proximal to scar tissue (see $V_m(t)$ insets in **Figs. 4.7A & 4.9B**).

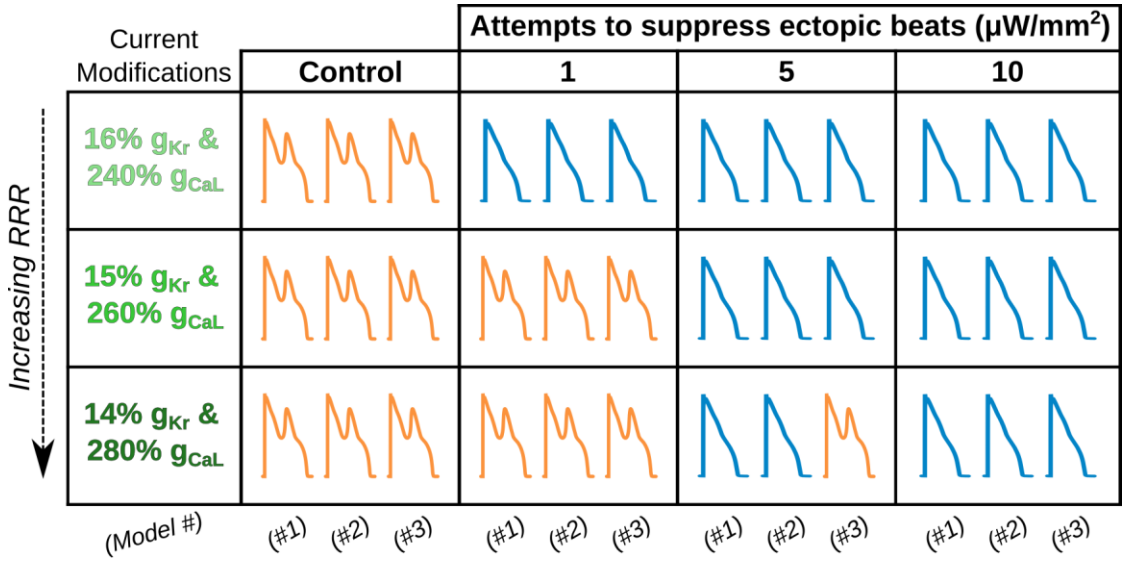

***Figure 4.6**: Suppressed ectopic beats with subthreshold GtACR1 stimulation. Orange $V_m(t)$ trace symbolizes ectopic beat occurrence and blue $V_m(t)$ trace represents no ectopic beat occurrence for a given RRR condition and irradiance. Within a specific column and row, the three traces correspond in order to patient Models 1, 2, and 3.*

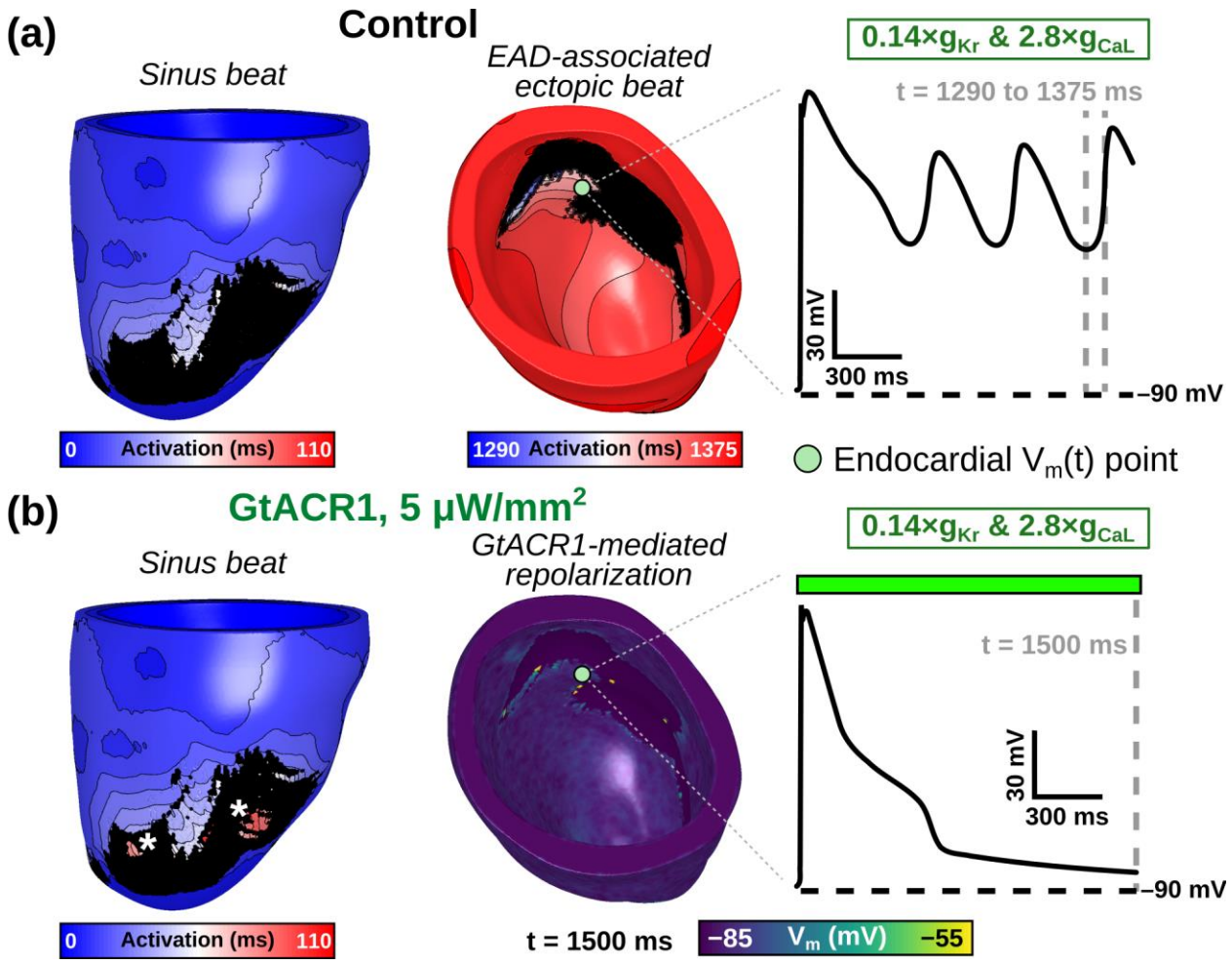

***Figure 4.7**: Representative examples of LV model simulations without (control) and with subthreshold GtACR1 stimulation. **A**: Activation sequence for simulated sinus activation beginning at t = 0 (left) is followed by multiple ectopic re-excitations originating from an endocardial focus (right), which are the consequence of local EADs (inset panel). **B**: When 5 µW/mm^2 illumination is applied to the GtACR1-expressing model from (A), all triggered activity is suppressed. During sinus activation (left) some previously unexcited epicardial regions surrounded by scar (*) are activated via direct optogenetic stimulation. Illumination is applied uniformly and simultaneously to the epicardial and endocardial surfaces at t = 0 ms. V_m(t) location is consistent between (A) and (B).*

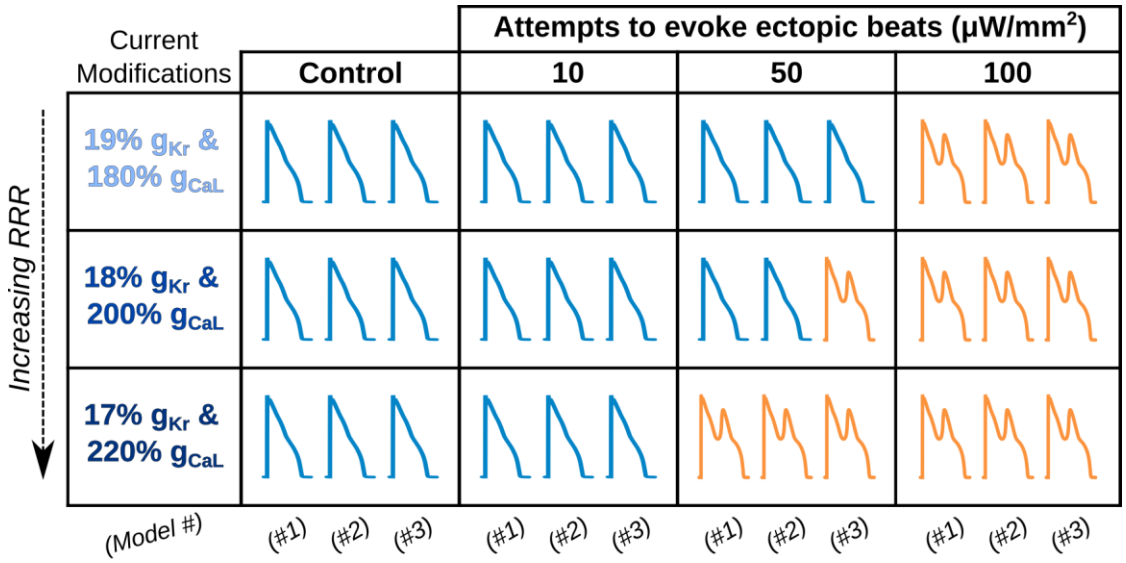

Figure 4.8: *Evoked ectopic beats with subthreshold ChR2 stimulation. Orange $V_m(t)$ trace symbolizes ectopic beat occurrence and blue $V_m(t)$ trace represents no ectopic beat occurrence for a given RRR condition and irradiance. Within a specific column and row, the three traces correspond in order to patient Models 1, 2, and 3.*

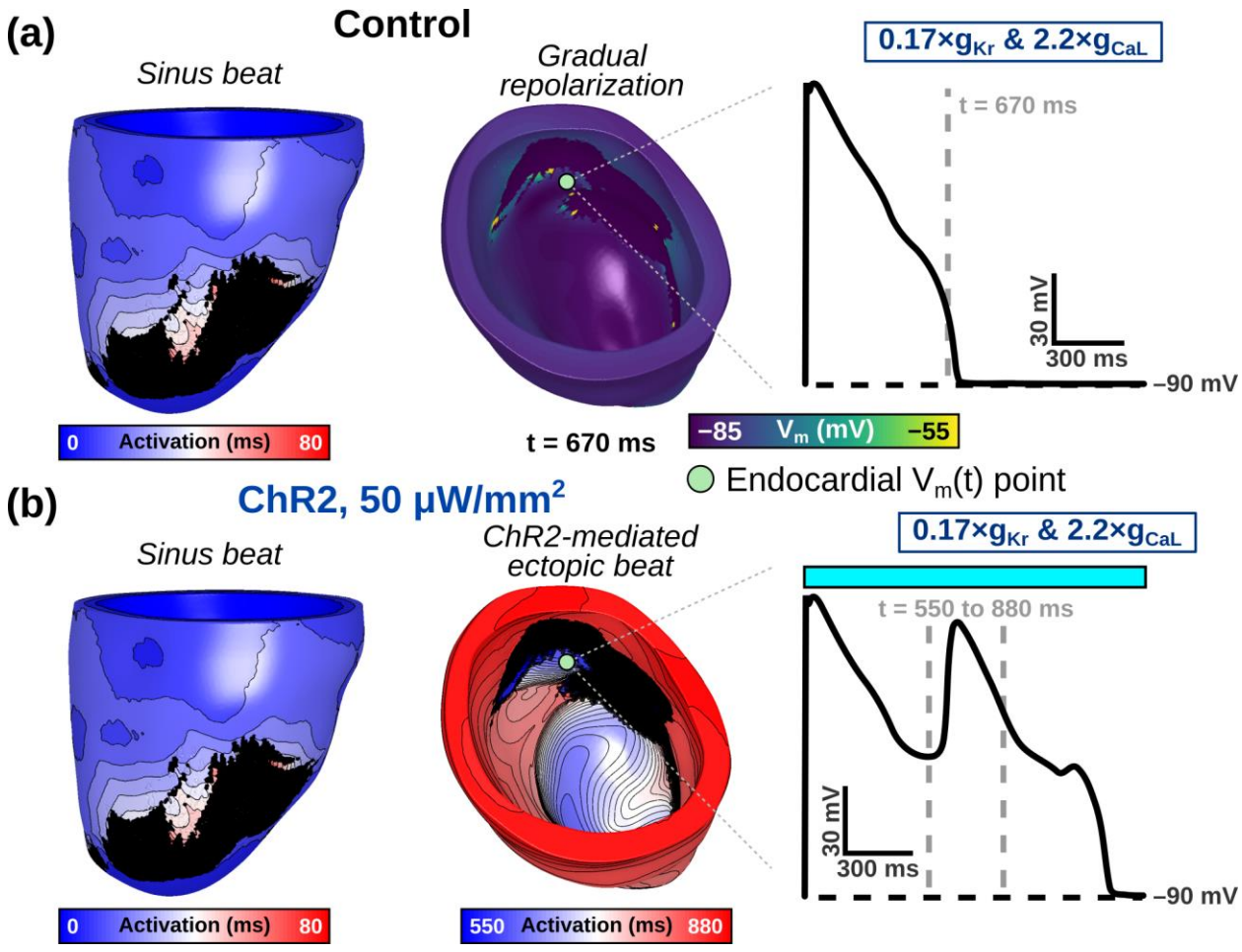

***Figure 4.9**: Representative examples of organ-scale simulations without (control) and with ChR2-mediated subthreshold stimulation. **A**: At baseline, sinus activation beginning at t = 0 (left) leads to gradual repolarization (right) without EADs developing (inset panel). **B**: When 50 μW/mm^2 illumination is added to the ChR2-expressing model from (A), an ectopic beat emerges (right) after a brief delay (inset panel). Illumination is applied uniformly and simultaneously to the epicardial and endocardial surfaces at t = 0 ms. V_m(t) location is consistent between (A) and (B).*

To contrast dual surface illumination against single surface endocardial or epicardial illumination, simulations were conducted using the maximal subthreshold irradiance for both opsins (10 μW/mm^2 for GtACR1 and 100 μW/mm^2 for ChR2). We found that both single surface illumination strategies were completely ineffective in preventing ectopic beats (GtACR1 expression; 0 of 9 cases), regardless of the irradiance or RRR condition tested (**Fig. 4.10**). However, for ChR2-expressing left ventricles, epicardial-only illumination had identical success to dual surface illumination (i.e., 9 of 9 cases promoted ectopic beats); endocardial-only illumination had mixed results (6 of 9 cases promoted ectopic beats; **Fig. 4.11**).

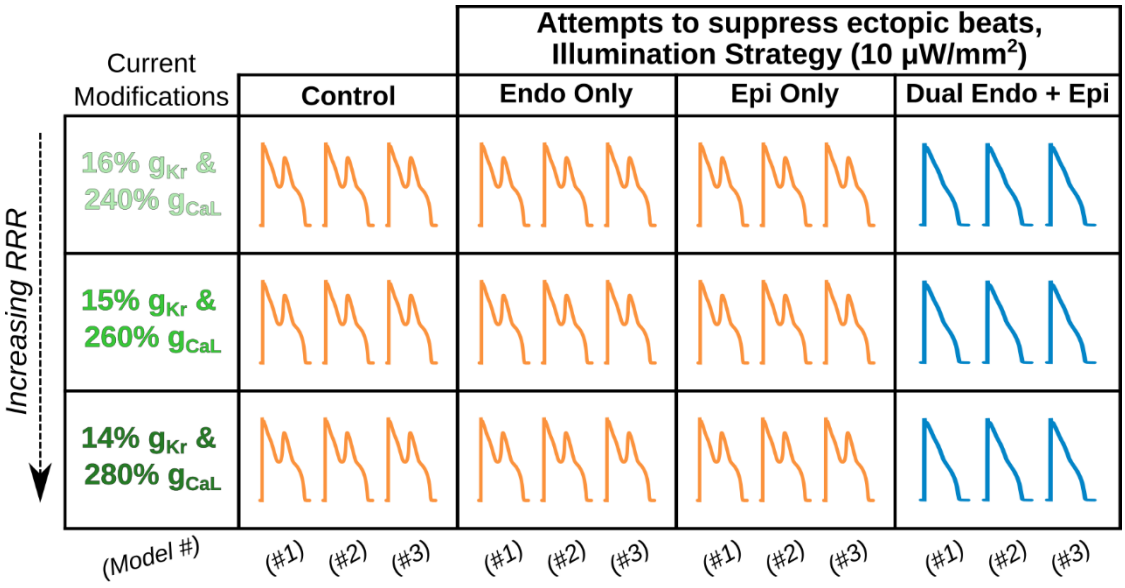

***Figure 4.10**: Comparison of illumination strategies when attempting to suppress ectopic beats with 10 μW/mm^2 GtACR1 stimulation. Orange V_m(t) trace represents an ectopic beat occurrence and blue V_m(t) trace represents no ectopic beat occurrence for a given RRR condition and irradiance. Within a specific column and row, the three traces correspond to patient Models 1, 2, and 3 in order.*

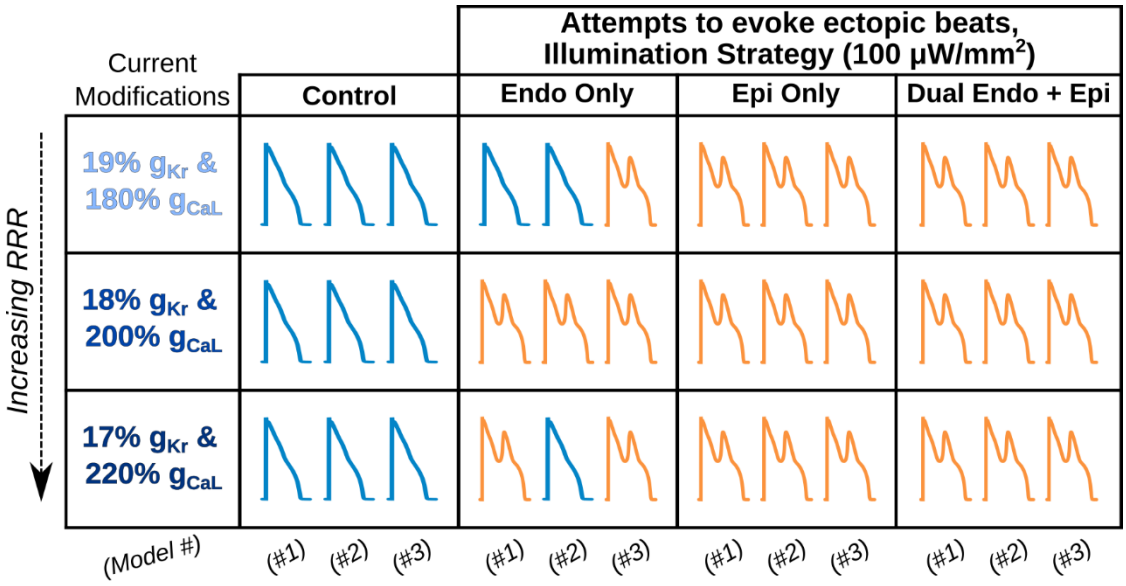

***Figure 4.11**: Comparison of illumination strategies when attempting to evoke ectopic beats with 100 μW/mm² ChR2 stimulation. Orange $V_m(t)$ trace represents an ectopic beat occurrence and blue $V_m(t)$ trace represents no ectopic beat occurrence for a given RRR condition and irradiance. Within a specific column and row, the three traces correspond to patient Models 1, 2, and 3 in order.*

Outcomes of optogenetic modulation of ectopic beat can be predicted

As described in Methods, for each simulated configuration in our study we calculated two metrics (*TVI and* TV_LI) based solely on ventricular anatomy and light stimulus characteristics. We found that TV_LI was an excellent predictor of ectopic beat suppression via GtACR1-based stimulation (ROC area under the curve [AUC] = 0.956; **Figs. 4.12A-B**), but the *TVI* metric had inferior performance (AUC = 0.722; **Figs. 4.13A-B**). In contrast, for attempts to provoke ectopic beats via blue light stimulation of ChR2, the *TVI* metric was superior (AUC = 0.872 vs. 0.538; **Figs. 4.12C-D** and **Figures 4.13C-D**).

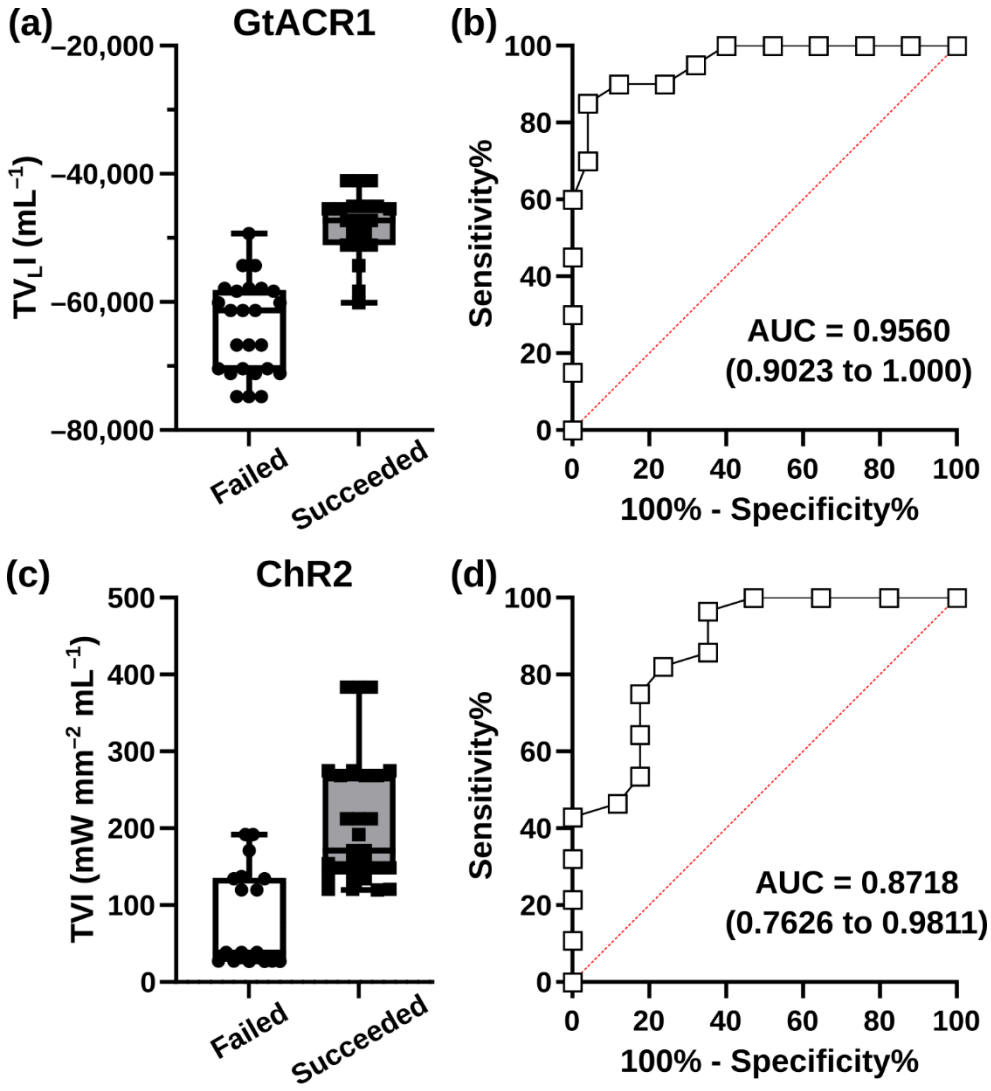

Figure 4.12: *Total volumetric irradiance metrics can predict optogenetic modulation success rates.* ***A****: Raw TV_LI values for all simulations in which GtACR1-based suppression of ectopic beating failed or succeeded.* ***B:*** *ROC analysis of the latter.* ***C-D:*** *Same as* ***A-B*** *but for TVI metric applied in the context of ChR2-based ectopic beat provocation.*

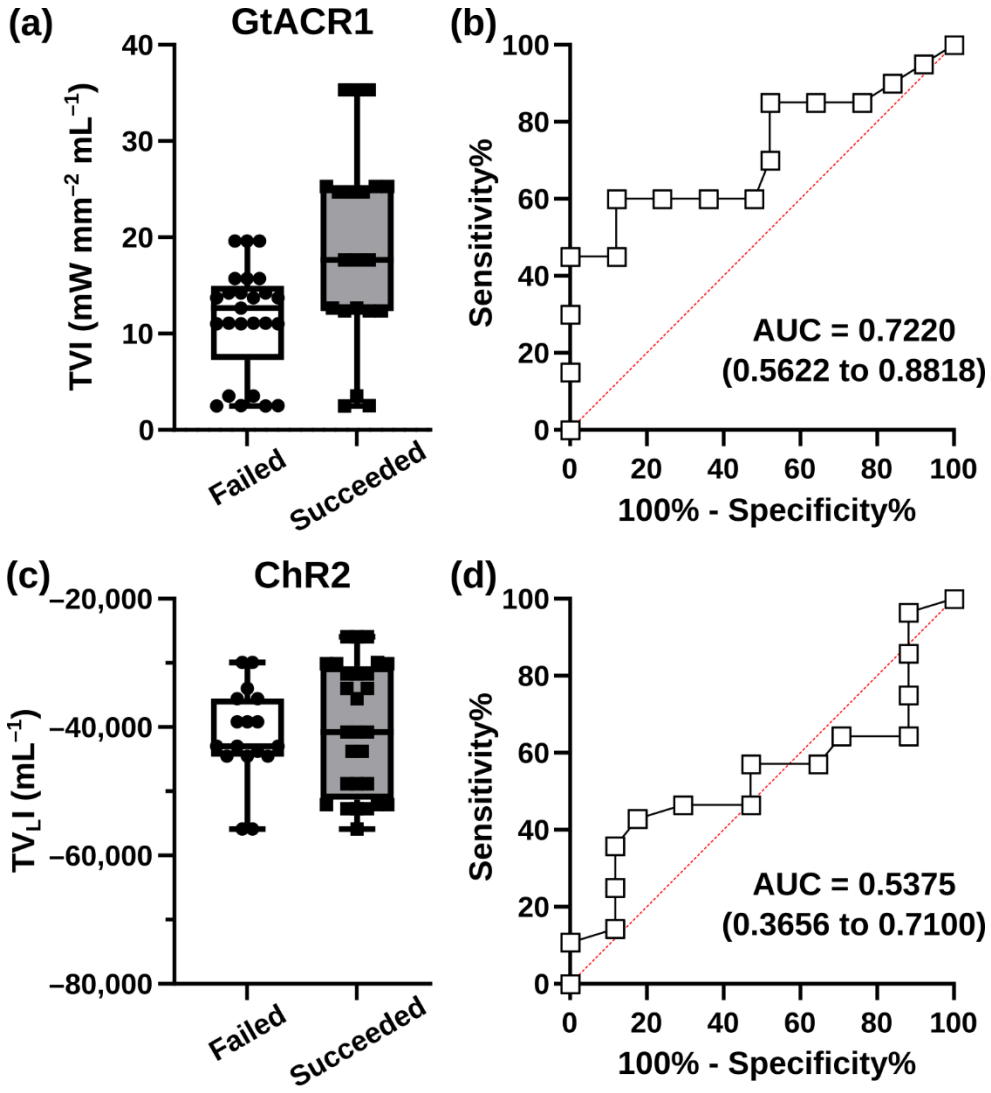

Figure 4.13: *Total volumetric irradiance metrics are not universally predictive of optogenetic modulation success rates.* ***A****: Raw TVI values for all simulations in which GtACR1-based suppression of ectopic beating failed or succeeded.* ***B****: ROC analysis of the latter.* ***C-D****: Same as* ***A-B*** *but for TV_LI metric applied in the context of ChR2-based ectopic beat provocation.*

4.5 Discussion

In this study, we used subthreshold optogenetic stimulation to modulate EADs and EAD-associated ectopic beats in computational models of ventricular myocytes and patient-derived LV models. The main findings are as follows: 1) both EADs and ectopic beats could be suppressed (with GtACR1) or evoked (with ChR2) using very low irradiances (0.01–100 μW/mm^2) under RRR conditions; 2) dual epi- and endocardial illumination was required for ectopic beat

suppression (GtACR1) but both dual and epicardial-only illumination strategies were sufficient to provoke an ectopic beat (ChR2); and 3) total volumetric irradiance calculations demonstrated combining ventricular anatomy and illumination strategy can broadly distinguish between effective and ineffective outcomes. Our study has demonstrated that optogenetic stimulation at very low irradiances can be used to modulate EAD occurrence and ectopic beat propensity under specific RRR conditions.

Early studies in cardiac optogenetics (55, 56) considered the possibility of applying low intensity optogenetic stimuli, too weak to evoke or overtly suppress action potentials, but strong enough to elicit subtle electrophysiological changes in cardiac environments. Our study defines this effect as “subthreshold” optogenetic stimulation and adds to this growing recent trend within cardiac optogenetics. An early group to capitalize upon this phenomenon was Hussaini et al., who demonstrated control of spiral wave dynamics in cardiac tissue (21). The authors found that a low-amplitude ChR2 current caused the spiral core to drift towards illuminated regions *in silico*. This technique was exploited to manipulate the direction and speed of the spiral wave core trajectory using selectively patterned and timed illumination. A different spiral wave study by Majumder et al. used uniform ChR2 stimulation to initiate wave break in simulated cardiac tissue using pulsed light (22). By reducing the excitable gap of repolarizing tissue between waves, this subthreshold perturbation affected membrane voltage enough to cause electrical turbulence in a previously stable state. Finally, Biasci et al. systematically varied and characterized subthreshold ChR2 stimulation in isolated cardiomyocytes and Langendorff-perfused mouse hearts to study cardiac alternans (23). Here, subthreshold illumination increased the incidence of cardiac alternans, generally thought of as pro-arrhythmic; however, in this context, the net effect was deemed cardioprotective, since it prompted an apparent increase in the rate of VT self-termination. Our work differs from the latter studies in that it uses subthreshold optogenetic modulation to affect EAD and ectopic beat propensities under various RRR conditions. Use of

GtACR1 or other inhibitory opsins to suppress or reduce electrical activity may prove consequential in other forthcoming studies.

Premature ventricular complexes (PVCs), which are often synonymous with ectopic (extra) beats, have remained an area of active study (57-59). It has been previously established that increased PVC burden is associated with increased risk of heart failure, reduced left ventricular ejection, and mortality (60). Despite advances in care, it has remained difficult to proactively differentiate between PVC-presenting individuals who experience adverse consequences from those without negative outcomes. Furthermore, not all PVCs are necessarily triggered by EAD events. We argue that, at a minimum, the methodology that we simulate in this study could be used to characterize mechanisms of the EAD-associated PVCs. The ability to either forcibly lower membrane voltage or hasten spontaneous depolarizations could tip the balance away from or towards PVC occurrence, regardless of the underlying initiation mechanism. This would be a potentially helpful experimental tool to enable probing and dissection of mechanisms underlying PVCs, given the fact that ectopic excitations are stochastic in nature and their occurrence can be inconsistent. Although any translational applications to clinical environments would be beneficial, substantial further research into this method would be needed beforehand.

It is generally accepted that EADs and PVCs are interrelated in structurally abnormal tissue (e.g., patients with long QT syndrome [LQTS], previous MI, or AP duration [APD] prolonging pharmaceuticals). It is believed that dispersion of repolarization in these conditions can be arrhythmogenic, due to differences in repolarization time leading to conduction block and reentry. Transmural dispersion of repolarization exists in healthy adult hearts (61) and this effect can be exacerbated APD-prolonging genetic mutations as in LQTS (3, 58, 62). In our study, we empirically observed longer repolarization times occurring at tissue in close proximity to scar regions. Since we used homogeneous light distribution to the entire endocardium and epicardium,

spatially targeted illumination strategies were not attempted to correct these repolarization differences. Experimentalists and modelers alike have previously used spatiotemporally controlled light stimulation to achieve aims such as correcting APD duration in short QT syndrome (19), defibrillate VT using a triple barrier pattern (63), and terminate atrial fibrillation using various optrode densities (64). If future research emerges suggesting that EAD-associated ectopic beats could be mitigated by reducing dispersion of repolarization, then use of spatially delineated optical stimuli could be further explored.

Previous studies have attempted to link EAD mechanisms at cellular scales to triggered activity at tissue and organ scales (7, 31, 32, 54, 65-67). Our findings in simulated ventricular cardiomyocytes suggest that cell-scale optogenetic modulation of these arrhythmic phenomena should be quite feasible via subthreshold stimulation of GtACR1 or ChR2. An important caveat is that both opsins have repolarizing *and* depolarizing effects that depend on action potential phase (during which V_m traverses the range between ≈–85 mV and ≈30 mV). Phase dependency of optogenetic current arises from the intrinsic property of opsin reversal potential (GtACR1: –40 mV; ChR2: 0 mV). This point was emphasized in two recent studies (20, 68), which showed that in some situations GtACR1 can be used to *pace* zebrafish hearts and ChR2 stimulation can *silence* electrical activity. Despite these interesting findings, the cellular configurations evaluated in our study still found that the rate of EAD occurrence was robustly decreased by GtACR1 stimulation or increased by ChR2 stimulation, as compared to non-illuminated virtual myocytes. Since EADs can be challenging to study experimentally, an interesting potential application of our findings would be for use in patch clamp experiments (69, 70). Given the findings from our study, we anticipate that the propensity of EADs in such preparations could be modulated using subthreshold optogenetic stimuli.

Our methodology for modeling EADs is deterministic (i.e., EADs occur consistently on every beat), which is distinct from the stochastic process that underlie the phenomena in nature

(2, 67, 69, 70). This reductionist approach was a necessary simplification for our study, since it allowed us to establish whether optogenetic stimulation could dynamically modulate the occurrence of cell- or organ-scale arrhythmia triggers under tightly controlled conditions. When the identical set of model parameters was incorporated in cell- and LV-scale models, we previously hypothesized that a corresponding outcome was not predetermined (i.e., RRR conditions that produced EADs did not necessarily guarantee PVCs at the organ level), due to the large differences in source-sink relationship between these two contexts. Of note, we found that all six of the RRR conditions highlighted in **Fig. 4.4A** did have corresponding effect in cell- and organ-scale models (i.e., the presence of lack of EADs or ectopy, respectively).

In the organ-scale simulations conducted, all three LV models had combinations of RRR severity and irradiance that resulted in provoked or suppressed ectopic beats compared to the baseline state (**Figs. 4.7 & 4.8**). We found that conditions with more RRR generally required higher irradiances for consistent ectopy suppression and lower irradiances for evoking ectopic beats. This is consistent with the idea that optogenetic ectopy modulation has higher energy demands than evoking ectopic beats under the evaluated RRR conditions. An interesting example was failed ectopic beat suppression simulation in Model 3 (14% I_{Kr} & 280% I_{CaL}, 5 μW/mm^2 GtACR1 stimulation; **Fig. 4.6**). In this simulation, micro reentry occurred via epicardial conduction through a narrow isthmus of BZ and healthy tissue, nestled in a dense mass of scar tissue, leading to re-excitation and ectopic beat propagation on the endocardial surface in BZ tissue held at elevated V_m (≈ –50 mV) by continuous GtACR1 stimulation. This example highlights that optogenetic stimulation at less-than-maximal subthreshold irradiances may occasionally fail due to patient-specific anatomical substrate but does not contradict the evidence that near maximal subthreshold stimuli (10 μW/mm^2 for GtACR1, 100 μW/mm^2 for ChR2; **Figs. 4.6 & 4.8**) consistently suppressed and evoked ectopic beats in this study.

A noteworthy aspect of our modeling is that dual endo- and epicardial illumination was initially simulated in all RRR conditions. When we compared these results to single surface illumination strategies, we found that ectopy suppression via GtACR1 stimulation was no longer possible (0 of 18 successes for both single surface strategies using 10 μW/mm^2; **Fig. 4.10**). This was consistent with our prior expectations, since single surface illumination would not prevent the formation of a larger repolarization gradient between the lit and unlit surfaces, leading to re-excitation and ultimately an ectopic beat. Interestingly, for evoking ectopic beats via ChR2 stimulation we found that epicardial only illumination was as effective as dual surface illumination (9 of 9 in both cases; **Fig. 4.11**). This finding is exciting because it suggests a new experimental technique wherein PVC "hotspots" (i.e., areas where ectopic beats *could* occur but do not necessarily occur *frequently*) could be revealed via constant ChR2 stimulation in Langendorff-perfused mouse hearts, potentially in the context of genetic or pharmacological intervention(s) to prolong AP duration (i.e., RRR). Light attenuation concerns have been previously raised about optogenetic stimulation in human hearts (16, 39), due to their thicker walls compared to those of small animals (15-17). Our success here with epicardial-only illumination in simulated human hearts opens the door for an exciting new approach that could be applied in large heart, providing a more spatiotemporally controllable complement to existing methods for eliciting arrhythmia triggers to study arrhythmia mechanisms (e.g., subepicardial injection of norepinephrine) (71).

An ongoing difficulty with research examining EADs and ectopic beats is establishing firm mechanistic links between cell, tissue, and organ-scale phenomena. In our study, we observed that ectopic beat triggers tended to localize near regions of scar tissue. We believe that this was due to spatial heterogeneity in source-sink mismatch (72), as proximity to non-conductive scar reduces the electrotonic sink and consequently the necessary threshold for the initiation of a propagating response. Previous research has highlighted that the minimum number of synchronized cells presenting EADs decreases as source-sink mismatch increases (67). EADs

have also been observed in isolated BZ cardiomyocytes, albeit during isoproterenol infusion (73). However, it is also worth noting that our BZ tissue modeling differs from the methodology used in previous studies (36, 37). Whereas these studies incorporated reductions to the I_{Kr}, I_{CaL}, slow delayed outward potassium rectifier current I_{Ks}, and inward sodium (Na^+) current I_{Na}, our study did not implement any ionic current changes in BZ regions. Here, our intent was to avoid interference with the already model-wide changes to I_{Kr} and I_{CaL} as a part of RRR conditions. Consequently, the only difference between healthy myocardium and BZ tissue was 90% reduction of conductivity in BZ as compared to myocardium, consistent with experimental conduction velocity measurements (74). These tradeoffs were necessary to keep consistency between the RRR conditions applied to the patient LV models, as otherwise differences observed in the BZ tissue would be difficult to attribute to prolonged APDs alone.

Another potential limitation of our study is the potential extrapolation of very low amplitude irradiances. For instance, evaluated irradiances in the experimental data underlying the GtACR1 model was 8 $\mu W/mm^2$ to 7.7 mW/mm^2 (24). A different study using ChR2 evaluated irradiances in the range of 2 to 11 $\mu W/mm^2$ (23) could observe <1 mV voltage changes in an isolated cardiomyocyte. In our study, the range of evaluated GtACR1 irradiances spanned 0.05 to 500 $\mu W/mm^2$ across both cell- and organ-scale modeling. There must be physiological limits of detection below a certain irradiance for each opsin variant, but there is a lack of published experimental data to corroborate this threshold. Consequently, caution should be exercised when considering irradiances below 1 $\mu W/mm^2$.

A key finding of our study is that the outcome of organ-scale optogenetic trigger modulation can be predicted using metrics based exclusively on cardiac anatomy, optical stimulus parameters, and myocardial light attenuation properties. These metrics did not include information about opsin distribution or expression level, nor did they consider the extent or spatial distribution of infarct or border zone. Interestingly, while there was a relatively straightforward association

between *TVI* and optogenetic PVC provocation success, the predictive metric for GtACR1-based PVC suppression was the version involving summation of $\log_{10}$ scaled E_e values (TV_LI). This recalls prior work assessing the feasibility of defibrillation via low-energy pulsed electrical stimuli, which showed a power law relationship between field strength and elicited activations (75).

Future work in this area will benefit from a rich environment of new optogenetic constructs and light delivery techniques. Recent advances in optogenetics established a new class of naturally occurring, K^+-conducting channelrhodopsins, including kalium rhodopsins (HcKCR1 and HcKCR2) (76, 77) and *Wobblia* inhibitory channelrhodopsin (WiChR) (77). These discoveries may prompt a departure from the use of chloride (Cl^-)-conducting anion channelrhodopsins (e.g., GtACR1), in part because of ongoing concerns about sufficient intracellular Cl^- recovery in cardiomyocytes following continuous illumination. K^+-conducting channelrhodopsins have high ratios of K^+ to Na^+ conduction, but further characterization in mammalian cardiomyocytes will be needed to progress the field. Although WiChR was expressed in atrial-like human induced pluripotent stem cell-derived cardiomyocytes (77), it is still unclear if non-negligible Na^+ conduction could trigger action potentials upon illumination and how continuous stimulation might disrupt K^+ homeostasis.

Advances in light delivery technology have continued to help reduce barriers to the feasibility of attempting cardiac optogenetics solutions in larger mammals. For instance, a recent proof-of-concept study successfully implanted a wireless, battery-free optoelectrode in a conscious rat and could successfully optogenetically stimulate the entire heart (78). Previously, *in vivo* optogenetic stimulation in small animals had occurred while the animal was unconscious with battery leads exiting the chest cavity (17, 18, 79). Another exciting advance is the emergence of wireless implantable cardiac devices that are bioresorbable without leads or batteries (80, 81). These studies showed that energy harvesting may eliminate the need for a battery, paving the way for devices that can safely dissolve within several weeks post-implantation. It may be possible

to modify this class of devices to provide illumination using micro-LEDs instead (82). Another possible alternative to implantable devices for illumination are up-converting nanoparticles, which release photons in response to absorption of ultrasound or X-rays (83). This has been successfully achieved by pacing rat hearts using near-infrared illumination and up-converting nanoparticle films (84). Further characterization is needed to validate this method across a larger variety of experimental circumstances.

4.6 Conclusions

We used computational modeling to present a proof-of-concept approach for using subthreshold optogenetic stimulation to suppress (GtACR1) or provoke (ChR2) EADs across a range of RRR conditions. Ectopic beats could be consistently suppressed or provoked using subthreshold light stimuli in all three post-MI, patient-derived LV models tested. Our findings using epicardial-only illumination in ChR2-sensitized left ventricles suggest that Langendorff-perfused hearts could be used to study ectopic beat development under RRR conditions. Our characterized range of RRR conditions and irradiances in simulated single myocytes provides a novel technique for future potential experimental work.

4.7 References

1. Weiss, J.N., et al., *Early afterdepolarizations and cardiac arrhythmias.* Heart Rhythm, **2010**. 7(12): p. 1891-9.

2. Qu, Z., et al., *Early afterdepolarizations in cardiac myocytes: beyond reduced repolarization reserve.* Cardiovasc Res, **2013**. 99(1): p. 6-15.

3. Varró, A. and I. Baczkó, *Cardiac ventricular repolarization reserve: a principle for understanding drug-related proarrhythmic risk.* Br J Pharmacol, **2011**. 164(1): p. 14-36.

4. El-Sherif, N., G. Turitto, and M. Boutjdir, *Acquired long QT syndrome and torsade de pointes.* Pacing Clin Electrophysiol, **2018**. 41(4): p. 414-421.

5. Modell, S.M. and M.H. Lehmann, *The long QT syndrome family of cardiac ion channelopathies: a HuGE review.* Genet Med, **2006**. 8(3): p. 143-55.

6. Myles, R.C., et al., *Decreased inward rectifying K+ current and increased ryanodine receptor sensitivity synergistically contribute to sustained focal arrhythmia in the intact rabbit heart.* J Physiol, **2015**. 593(6): p. 1479-93.

7. Dutta, S., et al., *Early afterdepolarizations promote transmural reentry in ischemic human ventricles with reduced repolarization reserve.* Prog Biophys Mol Biol, **2016**. 120(1-3): p. 236-48.

8. Johnson, D.M. and G. Antoons, *Arrhythmogenic Mechanisms in Heart Failure: Linking beta-Adrenergic Stimulation, Stretch, and Calcium.* Front Physiol, **2018**. 9: p. 1453.

9. Boyle, P.M., T.V. Karathanos, and N.A. Trayanova, *Cardiac Optogenetics: 2018.* JACC Clin Electrophysiol, **2018**. 4(2): p. 155-167.

10. Entcheva, E. and M.W. Kay, *Cardiac optogenetics: a decade of enlightenment.* Nat Rev Cardiol, **2021**. 18(5): p. 349-367.

11. Burton, R.A., et al., *Optical control of excitation waves in cardiac tissue.* Nat Photonics, **2015**. 9(12): p. 813-816.

12. Cokic, M., et al., *Optogenetic Stimulation of G(i) Signaling Enables Instantaneous Modulation of Cardiomyocyte Pacemaking.* Front Physiol, **2021**. 12: p. 768495.

13. Makowka, P., et al., *Optogenetic stimulation of G(s)-signaling in the heart with high spatio-temporal precision.* Nat Commun, **2019**. 10(1): p. 1281.

14. Yu, L., et al., *Optogenetic Modulation of Cardiac Sympathetic Nerve Activity to Prevent Ventricular Arrhythmias.* J Am Coll Cardiol, **2017**. 70(22): p. 2778-2790.

15. Bruegmann, T., et al., *Optogenetic termination of atrial fibrillation in mice.* Cardiovasc Res, **2018**. 114(5): p. 713-723.

16. Bruegmann, T., et al., *Optogenetic defibrillation terminates ventricular arrhythmia in mouse hearts and human simulations.* J Clin Invest, **2016**. 126(10): p. 3894-3904.

17. Nyns, E.C.A., et al., *Optogenetic termination of ventricular arrhythmias in the whole heart: towards biological cardiac rhythm management.* Eur Heart J, **2017**. 38(27): p. 2132-2136.

18. Nyns, E.C.A., et al., *An automated hybrid bioelectronic system for autogenous restoration of sinus rhythm in atrial fibrillation.* Sci Transl Med, **2019**. 11(481): p. eaau6447.

19. Karathanos, T.V., P.M. Boyle, and N.A. Trayanova, *Optogenetics-enabled dynamic modulation of action potential duration in atrial tissue: feasibility of a novel therapeutic approach.* Europace, **2014**. 16 Suppl 4(Suppl 4): p. iv69-iv76.

20. Gruber, A., et al., *Optogenetic modulation of cardiac action potential properties may prevent arrhythmogenesis in short and long QT syndromes.* JCI Insight, **2021**. 6(11).

21. Hussaini, S., et al., *Drift and termination of spiral waves in optogenetically modified cardiac tissue at sub-threshold illumination.* Elife, **2021**. 10.

22. Majumder, R., et al., *Pulsed low-energy stimulation initiates electric turbulence in cardiac tissue.* PLoS Comput Biol, **2021**. 17(10): p. e1009476.

23. Biasci, V., et al., *Optogenetic manipulation of cardiac electrical dynamics using sub-threshold illumination: dissecting the role of cardiac alternans in terminating rapid rhythms.* Basic Res Cardiol, **2022**. 117(1): p. 25.

24. Govorunova, E.G., et al., *Anion channelrhodopsins for inhibitory cardiac optogenetics.* Sci Rep, **2016**. 6: p. 33530.

25. Govorunova, E.G., et al., *Natural light-gated anion channels: A family of microbial rhodopsins for advanced optogenetics.* Science, **2015**. 349(6248): p. 647-50.

26. Boyden, E.S., et al., *Millisecond-timescale, genetically targeted optical control of neural activity.* Nat Neurosci, **2005**. 8(9): p. 1263-8.

27. Williams, J.C., et al., *Computational optogenetics: empirically-derived voltage- and light-sensitive channelrhodopsin-2 model.* PLoS Comput Biol, **2013**. 9(9): p. e1003220.

28. O'Hara, T., et al., *Simulation of the undiseased human cardiac ventricular action potential: model formulation and experimental validation.* PLoS Comput Biol, **2011**. 7(5): p. e1002061.

29. ten Tusscher, K.H. and A.V. Panfilov, *Alternans and spiral breakup in a human ventricular tissue model.* Am J Physiol Heart Circ Physiol, **2006**. 291(3): p. H1088-100.

30. Sanchez-Alonso, J.L., et al., *Microdomain-Specific Modulation of L-Type Calcium Channels Leads to Triggered Ventricular Arrhythmia in Heart Failure.* Circ Res, **2016**. 119(8): p. 944-55.

31. Vandersickel, N., et al., *Spatial Patterns of Excitation at Tissue and Whole Organ Level Due to Early Afterdepolarizations.* Front Physiol, **2017**. 8: p. 404.

32. Zimik, S., et al., *A Comparative Study of Early Afterdepolarization-Mediated Fibrillation in Two Mathematical Models for Human Ventricular Cells.* PLoS One, **2015**. 10(6): p. e0130632.

33. Mendonca Costa, C., et al., *Pacing in proximity to scar during cardiac resynchronization therapy increases local dispersion of repolarization and susceptibility to ventricular arrhythmogenesis.* Heart Rhythm, **2019**. 16(10): p. 1475-1483.

34. Mendonca Costa, C., et al., *Left ventricular endocardial pacing is less arrhythmogenic than conventional epicardial pacing when pacing in proximity to scar.* Heart Rhythm, **2020**. 17(8): p. 1262-1270.

35. Niederer, S.A., et al., *Verification of cardiac tissue electrophysiology simulators using an N-version benchmark.* Philos Trans A Math Phys Eng Sci, **2011**. 369(1954): p. 4331-51.

36. Arevalo, H.J., et al., *Arrhythmia risk stratification of patients after myocardial infarction using personalized heart models.* Nat Commun, **2016**. 7: p. 11437.

37. Ochs, A.R., et al., *Optogenetic Stimulation Using Anion Channelrhodopsin (GtACR1) Facilitates Termination of Reentrant Arrhythmias With Low Light Energy Requirements: A Computational Study.* Front Physiol, **2021**. 12: p. 718622.

38. Bayer, J.D., et al., *A novel rule-based algorithm for assigning myocardial fiber orientation to computational heart models.* Ann Biomed Eng, **2012**. 40(10): p. 2243-54.

39. Karathanos, T.V., et al., *Opsin spectral sensitivity determines the effectiveness of optogenetic termination of ventricular fibrillation in the human heart: a simulation study.* J Physiol, **2016**. 594(23): p. 6879-6891.

40. Vigmond, E.J., et al., *Computational tools for modeling electrical activity in cardiac tissue.* J Electrocardiol, **2003**. 36 Suppl: p. 69-74.

41. Plank, G., et al., *From mitochondrial ion channels to arrhythmias in the heart: computational techniques to bridge the spatio-temporal scales.* Philos Trans A Math Phys Eng Sci, **2008**. 366(1879): p. 3381-409.

42. Maguire, C.T., et al., *Implications of ventricular arrhythmia vulnerability during murine electrophysiology studies.* Physiol Genomics, **2003**. 15(1): p. 84-91.

43. Ashikaga, H., et al., *Feasibility of image-based simulation to estimate ablation target in human ventricular arrhythmia.* Heart Rhythm, **2013**. 10(8): p. 1109-16.

44. Deng, D., et al., *Accuracy of prediction of infarct-related arrhythmic circuits from image-based models reconstructed from low and high resolution MRI.* Front Physiol, **2015**. 6: p. 282.

45. Rush, S. and H. Larsen, *A practical algorithm for solving dynamic membrane equations.* IEEE Trans Biomed Eng, **1978**. 25(4): p. 389-92.

46. Plank, G., et al., *The openCARP simulation environment for cardiac electrophysiology.* Comput Methods Programs Biomed, **2021**. 208: p. 106223.

47. Guo, W., et al., *Changes in action potentials and ion currents in long-term cultured neonatal rat ventricular cells.* Am J Physiol, **1996**. 271(1 Pt 1): p. C93-102.

48. Vogt, C.C., et al., *Systemic gene transfer enables optogenetic pacing of mouse hearts.* Cardiovasc Res, **2015**. 106(2): p. 338-43.

49. Li, J., et al., *Optical capture and defibrillation in rats with monocrotaline-induced myocardial fibrosis 1 year after a single intravenous injection of adeno-associated virus channelrhodopsin-2.* Heart Rhythm, **2021**. 18(1): p. 109-117.

50. Boyle, P.M., et al., *A comprehensive multiscale framework for simulating optogenetics in the heart.* Nat Commun, **2013**. 4: p. 2370.

51. Ripoll, J., et al., *Experimental determination of photon propagation in highly absorbing and scattering media.* J Opt Soc Am A Opt Image Sci Vis, **2005**. 22(3): p. 546-51.

52. Swartling, J., et al., *Changes in tissue optical properties due to radio-frequency ablation of myocardium.* Med Biol Eng Comput, **2003**. 41(4): p. 403-9.

53. Bishop, M.J., et al., *Synthesis of voltage-sensitive optical signals: application to panoramic optical mapping.* Biophys J, **2006**. 90(8): p. 2938-45.

54. Vandersickel, N., et al., *A study of early afterdepolarizations in a model for human ventricular tissue.* PLoS One, **2014**. 9(1): p. e84595.

55. Entcheva, E., *Cardiac optogenetics.* Am J Physiol Heart Circ Physiol, **2013**. 304(9): p. H1179-91.

56. Williams, J.C. and E. Entcheva, *Optogenetic versus Electrical Stimulation of Human Cardiomyocytes: Modeling Insights.* Biophys J, **2015**. 108(8): p. 1934-45.

57. Amoni, M., et al., *Discrete sites of frequent premature ventricular complexes cluster within the infarct border zone and coincide with high frequency of delayed afterdepolarizations under adrenergic stimulation.* Heart Rhythm, **2021**. 18(11): p. 1976-1987.

58. Huang, X., et al., *Spontaneous initiation of premature ventricular complexes and arrhythmias in type 2 long QT syndrome.* Am J Physiol Heart Circ Physiol, **2016**. 311(6): p. H1470-H1484.

59. Zhang, Z., et al., *Mechanisms of Premature Ventricular Complexes Caused by QT Prolongation.* Biophys J, **2021**. 120(2): p. 352-369.

60. Marcus, G.M., *Evaluation and Management of Premature Ventricular Complexes.* Circulation, **2020**. 141(17): p. 1404-1418.

61. Glukhov, A.V., et al., *Transmural dispersion of repolarization in failing and nonfailing human ventricle.* Circ Res, **2010**. 106(5): p. 981-91.

62. Shah, S.R., K. Park, and R. Alweis, *Long QT Syndrome: A Comprehensive Review of the Literature and Current Evidence.* Curr Probl Cardiol, **2019**. 44(3): p. 92-106.

63. Crocini, C., et al., *Optogenetics design of mechanistically-based stimulation patterns for cardiac defibrillation.* Sci Rep, **2016**. 6: p. 35628.

64. Boyle, P.M., et al., *Termination of re-entrant atrial tachycardia via optogenetic stimulation with optimized spatial targeting: insights from computational models.* J Physiol, **2018**. 596(2): p. 181-196.

65. Chang, M.G., et al., *Dynamics of early afterdepolarization-mediated triggered activity in cardiac monolayers.* Biophys J, **2012**. 102(12): p. 2706-14.

66. Chang, M.G., et al., *Bi-stable wave propagation and early afterdepolarization-mediated cardiac arrhythmias.* Heart Rhythm, **2012**. 9(1): p. 115-22.

67. Xie, Y., et al., *So little source, so much sink: requirements for afterdepolarizations to propagate in tissue.* Biophys J, **2010**. 99(5): p. 1408-15.

68. Kopton, R.A., et al., *Cardiac Electrophysiological Effects of Light-Activated Chloride Channels.* Front Physiol, **2018**. 9: p. 1806.

69. Sato, D., et al., *Synchronization of chaotic early afterdepolarizations in the genesis of cardiac arrhythmias.* Proc Natl Acad Sci U S A, **2009**. 106(9): p. 2983-8.

70. Sato, D., et al., *Irregularly appearing early afterdepolarizations in cardiac myocytes: random fluctuations or dynamical chaos?* Biophys J, **2010**. 99(3): p. 765-73.

71. Myles, R.C., et al., *Local beta-adrenergic stimulation overcomes source-sink mismatch to generate focal arrhythmia.* Circ Res, **2012**. 110(11): p. 1454-64.

72. Spector, P., *Principles of cardiac electric propagation and their implications for re-entrant arrhythmias.* Circ Arrhythm Electrophysiol, **2013**. 6(3): p. 655-61.

73. Dries, E., et al., *Altered adrenergic response in myocytes bordering a chronic myocardial infarction underlies in vivo triggered activity and repolarization instability.* J Physiol, **2020**. 598(14): p. 2875-2895.

74. Yao, J.A., et al., *Remodeling of gap junctional channel function in epicardial border zone of healing canine infarcts.* Circ Res, **2003**. 92(4): p. 437-43.
75. Luther, S., et al., *Low-energy control of electrical turbulence in the heart.* Nature, **2011**. 475(7355): p. 235-9.
76. Govorunova, E.G., et al., *Kalium channelrhodopsins are natural light-gated potassium channels that mediate optogenetic inhibition.* Nat Neurosci, **2022**. 25(7): p. 967-974.
77. Vierock, J., et al., *WiChR, a highly potassium-selective channelrhodopsin for low-light one- and two-photon inhibition of excitable cells.* Sci Adv, **2022**. 8(49): p. eadd7729.
78. Ausra, J., et al., *Wireless, fully implantable cardiac stimulation and recording with on-device computation for closed-loop pacing and defibrillation.* Sci Adv, **2022**. 8(43): p. eabq7469.
79. Nyns, E.C.A., et al., *Optical ventricular cardioversion by local optogenetic targeting and LED implantation in a cardiomyopathic rat model.* Cardiovasc Res, **2022**. 118(10): p. 2293-2303.
80. Choi, Y.S., et al., *A transient, closed-loop network of wireless, body-integrated devices for autonomous electrotherapy.* Science, **2022**. 376(6596): p. 1006-1012.
81. Choi, Y.S., et al., *Fully implantable and bioresorbable cardiac pacemakers without leads or batteries.* Nat Biotechnol, **2021**. 39(10): p. 1228-1238.
82. Yang, Y., et al., *Wireless multilateral devices for optogenetic studies of individual and social behaviors.* Nat Neurosci, **2021**. 24(7): p. 1035-1045.
83. Berry, R.G., Matthew; Lars Gjesteby and Ge Wang *, *X-Optogenetics and U-Optogenetics: Feasibility and Possibilities* Photonics, **2015**.
84. Rao, P., et al., *Near-infrared light driven tissue-penetrating cardiac optogenetics via upconversion nanoparticles in vivo.* Biomed Opt Express, **2020**. 11(3): p. 1401-1416.

Chapter 5 | Optogenetic Modulation of Induced Pluripotent Stem Cell-derived Cardiomyocytes in silico Can Increase or Suppress Spontaneous Beating Rate

5.1 Abstract

Myocardial infarctions (MIs) contribute to significant morbidity and mortality worldwide. A promising potential treatment is engraftment of pluripotent stem cell-derived cardiomyocytes (PSC-CMs), but dangerous ventricular engraftment arrhythmias (EAs) have prevented potential clinical trials. Optogenetics is the use of light-sensitive ion channels and pumps (opsins) to elicit currents in response to light, and could prove beneficial for controlling and suppressing EAs. In this study, we evaluated the stimulation of three different opsins (ChR2, GtACR1, and hypothetical "WiChR-like") in computational models of PSC-CMs and 2D post-MI tissue models. We found that ChR2 and GtACR1 both accelerated the spontaneous beating rate of PSC-CMs and the occurrence of EAs. Stimulation with WiChR-like opsin could suppress PSC-CM spontaneous beating and EA propensity. Preliminary analysis indicates that maintaining cellular excitability during PSC-CM beating suppression is possible under a narrow range of irradiances. Further study is needed to identify EA can be suppressed while maintaining PSC-CM graft excitability.

5.2 Introduction

Myocardial infarction is the cessation of blood flow to part of the heart because of a clot, leading to tissue necrosis and possible sudden cardiac death (SCD). Because the heart has very limited regenerative capability (1), there are significant morbidity and mortality risks associated with previous MI (2). For those who survive the first months following MI, progression into heart failure is common; the reduction of mechanical force resulted in compensatory increased contraction, which creates a negative feedback loop. Existing HF treatments (such as beta blockers) do not prevent further decline into HF but instead merely slow the decline (3). Consequently, there is a strong need to help reverse or mitigate the damage to cardiac contractility that leads to HF (1).

Cell-based therapeutic treatment of post-MI cardiac decline and prevention of HF have been previously attempted using non-myocyte paracrine exposure (4), indirect muscularization (5), and direct muscularization (6-8). Of these, direct muscularization treatments have established improved contractile function in post-MI hearts (6-8). This involves the implantation of pluripotent stem-cell derived cardiomyocytes (PSC-CMs) into the post-MI heart, typically either using an engrafted tissue patch (cultured *in vitro*) or injections of PSC-CMs (1). However, dangerous ventricular arrhythmias (coined "engraftment arrhythmias", EAs) have also been observed occurring from 1 to 2-6 weeks (6, 8) after PSC-CM engraftment in large animal models. The emergence of EAs has hobbled progress in this research, preventing advancement into clinical trials. While the precise mechanism of EA remains unknown, electroanatomical mapping and interrogation by electric pacing suggest EA originate from the engrafted PSC-CMs as a focal source (i.e., emerging from within) (6, 9). This is supported by the well-known fact that PSC-CMs beat spontaneously and are typically far more immature relative to adult cardiomyocytes (10). Previous modeling studies have examined the occurrence of EA (11-14), but fail to provide experimental tools to directly modulate EA propensity.

One hypothetical avenue for controlling PSC-CM electrical activity could be optogenetic stimulation. Optogenetics is the genetic expression of light-sensitive, ion-trafficking proteins into mammalian cell membranes (15-17). Optogenetics has been previously used to terminate VT in small animals (18, 19). However, these studies stimulated channelrhodopsins with positive reversal potentials ($E_{rev} \approx 0$ to 10 mV) to defibrillate VT through depolarizing currents that fill the excitable gap and reduce tissue excitability. A lesser explored area has been optogenetic *suppression* of arrhythmias. Recent studies have begun examining the use of "subthreshold" optogenetic stimulation to finely modulate electrophysiological conditions enough to change experimental conditions (20, 21). Together, these advances suggest that optogenetic stimulation could be precisely controlled to affect PSC-CM spontaneous beating. A previous study examined

the application of optogenetic stimulation to PSC-CMs (22) but focused on pacing and spiral waves in small engineered heart tissues rather than preventing PSC-CM spontaneous beating or examining engraftment arrhythmias in post-MI environments. Given the expensive nature and lack of experimental clarity from large animal studies, there is a strong need for precise control of EA in order to study mechanisms and develop therapeutic measures.

In this study, we examine whether low-amplitude optogenetic stimulation could potentially be used to both up and down-regulate spontaneous beating in simulated PSC-CMs. We also examine whether optogenetic stimulation could possibly be used to control the emergence of EA in histology-derived tissue models (14). Specifically, we will evaluate three opsins with different intended effects: channelrhodopsin-2 (ChR2) for depolarizing currents, anion channelrhodopsin-1 (GtACR1) for both depolarizing and repolarizing currents, and a hypothetical hyperpolarizing opsin. This hypothetical opsin is based on recent data characterizing the naturally-occurring, potassium-conducting dominant ion channel Wobblia inhibitory ChannelRhodopsin (WiChR) (23). We modified the GtACR1 photocurrent model's reversal potential, half-decay rate after illumination cessation, and maximum absorption wavelength to create a "WiChR-like" opsin. If successful, our work will lay the crucial groundwork to better understand and address EA, in addition to evaluating possible therapeutic avenues.

5.3 Methods

We conducted simulations using experimentally-validated, biophysically-detailed ionic models for human induced PSC-CMs (24) and human ventricular cardiomyocytes (25), respectively. Before all simulations, both ionic models were run to steady state conditions. Specifically, the PSC-CM model was permitted to spontaneously beat for 60 cycle lengths. The V_m state was saved at maximum diastolic potential (MDP; i.e., the first instance where the dV_m/dt derivative changed from negative to positive). Since the ventricular CM model does not

spontaneously beat, it was electrically paced at a similar frequency to the PSC-CM model (basic cycle length, BCL = 910 ms) to reach steady state.

Optogenetic stimulation was modeled using three hypothetical opsins: Channelrhodopsin-2, *Guillardia theta* anion channelrhodopsin-1, and *Wobblia* inhibitory channelrhodopsin. The published 4-state ChR2 (26) and 2-state GtACR1 (27) photocurrent models were derived from available experimental data. The hypothetical WiChR opsin is based off a recent publication by Vierock et al. (23). Due to a lack of irradiance ranges published in that publication, we modified the GtACR1 photocurrent model with key parameter changes to create hyperpolarizing stimulation. Because the photocurrent model is not directly sourced from WiChR characterization data, we refer to this model as the "WiChR-like" photocurrent model. We believed that this was an appropriate comparison due to both the lack of a notable peak current and low photocurrent desensitization in both opsins.

Specifically, we modified the reversal potential (E_{rev}), half-decay constant (τ_{off}), and applied wavelength from the GtACR1 photocurrent model (27) to reflect WiChR characteristics. E_{rev} was set as –90 mV (vs. GtACR1 E_{rev}: –40 mV), τ_{off} was changed from 350 ms (from GtACR1 τ_{off}: 119 ms), and its responsive wavelength was change to blue light. Single channel conductance (g_{WiChR}) was unaltered because there was insufficient data at multiple irradiances to support the change, but comparison to GtACR1 photocurrent data in cardiomyocytes (28) suggest that WiChR has at least an equivalent conductance, if not higher. WiChR was irradiated with 488 nm wavelength light, rather than its maximum responsive wavelength of 460 nm (23), due to how close 460 nm was to the wavelength used with ChR2 (488 nm).

To evaluate the effects of optogenetic stimulation, we applied constant optogenetic stimulation to a simulated PSC-CM cell (i.e., at t = 0 ms) for the full simulation duration (4000 ms). The primary outcome was whether optogenetic stimulation using the three opsins either increased or decreased PSC-CM spontaneous beating rate. Increasing irradiances were evaluated until PSC-CM spontaneous beating ceased.

Next, we sought to evaluate whether certain opsin and irradiance combinations altered cellular excitability in a simulated PSC-CM. Constant optogenetic stimulation for each opsin was applied for the simulation duration (from t = 0 ms to 3000 ms), with electrical stimulation applied twice at 1000 and 2000 ms. Following each electrical stimulation, the primary outcome was whether an action potential was elicited, and the secondary outcome was evaluating whether an AP morphology typical of adult cardiomyocytes occurred.

In this study, we also used three histology-derived models of left ventricle slices recently published by our group (14). Two non-human primates (macaque monkeys) sourced these three tissue models: Model 1 came from one non-human primate, and Models 2 and 3 came from the other non-human primate. These corresponded (in order) to Model 1, Model 3, and Model 4 used our previous study (14). Detailed methods for the histology images and model reconstruction are described in Liu et al. (6) and Gibbs et al. (14), respectively. In brief, the slice models were constructed using triangles with an average edge length of ~50 μm. Each region (normal "host" myocardium, engrafted "graft" PSC-CM tissue, or post-MI scar) were assigned within the finite element model (**Fig. 5.1**). The host tissue was assigned a human ventricular AP model (25), graft tissue was assigned a human PSC-CM model (24), and scar tissue was assigned to the passive (non-conductive) model. Cardiac fiber orientations were approximated in a manner appropriate of their circular helix organization in human ventricles (14).

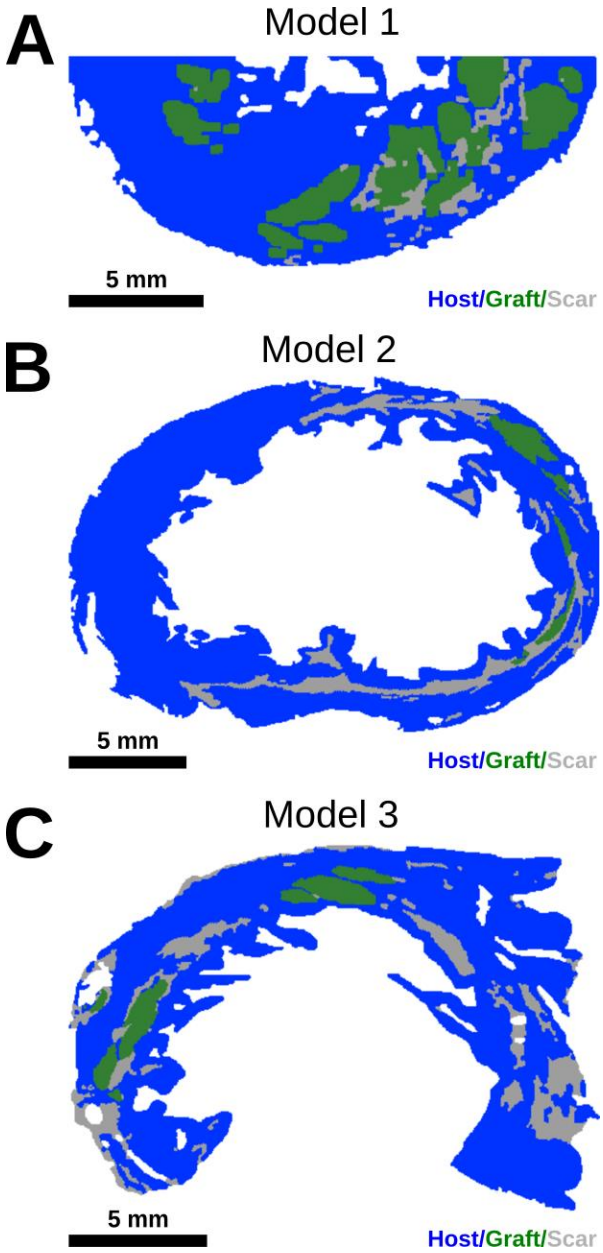

Figure 5.1*: Histology-derived 2D slice models are delineated by host, graft, and scar regions.* ***A-C****: Three models are used in this study: Model 1 (A), Model 2 (B), and Model 3 (C). Blue denotes healthy myocardium (Host), green denotes PSC-CM tissue (Graft), and gray denotes post-MI infarct scar (Scar). Figure reproduced with permission from Gibbs CE et al. J Physiol 2023.*

We modelled coupling between graft and host tissue using a method recently published by our group (14). Briefly, the boundary of all graft regions was broken up into finite element connections and assigned as uncoupled (no electrical current flow) or coupled (current flow possible). Since the distribution of graft-host coupling is not well understood, we stochastically assigned uncoupled vs. coupled conditions randomly across a given boundary such that the

overall proportion of connectiveness was constant (i.e., 10% coupling would result in 90% of edges being uncoupled and 10% being coupled to host tissue) and conducted simulations across 10 permutations for each each coupling value, model, opsin, and irradiance value. The coupling proportion was imposed on a graft-by-graft basis (i.e., each distinct region of graft tissue resulted in the same coupling proportion).

Epicardial illumination was applied uniformly in each model using an exponential decay approximation (27). In previous studies (18, 27), opsin expression was modeled at a reduced proportion of ≈58.2% due to a past study evaluating long-term transfection (29). However, in this study we considered that PSC-CM cells would be cultured *in vitro* and would have short timescales until action after engraftment. Therefore, in this study the PSC-CM graft regions of the tissue models were modeled with 100% opsin transfection. The monodomain formulation was used in all simulations.

5.4 Preliminary Results and Discussion

Single cell simulations using an iPSC-CM ionic model

At baseline, without any optogenetic stimulation, the simulated PSC-CM cell beats spontaneously (24). When constant optogenetic stimulation was applied to the PSC-CM from t = 0 ms to 4000 ms (the full evaluated interval), ChR2 and GtACR1 stimulation upregulated spontaneous beating (**Fig. 5.2A-B**) and WiChR-like stimulation downregulated spontaneous beating (**Fig. 5.2C**). All three opsins had irradiances that eventually suppressed spontaneous beating: 500 μW/mm^2 for ChR2 (**Fig. 5.2A**), 1 μW/mm^2 for GtACR1 (**Fig. 5.2B**), and 0.1 μW/mm^2 (**Fig. 5.2C**) for WiChR-like. However, those irradiances for ChR2 and GtACR1 stimulation were also characterized by repolarization failure at V_m above MDP (≈–20 mV and ≈–33 mV, respectively; **Figs. 5.2A-B**). Only WiChR-like stimulation could suppress spontaneous beating without repolarization failure (100 nW/mm^2 and 1 μW/mm^2; **Fig. 5.2C**).

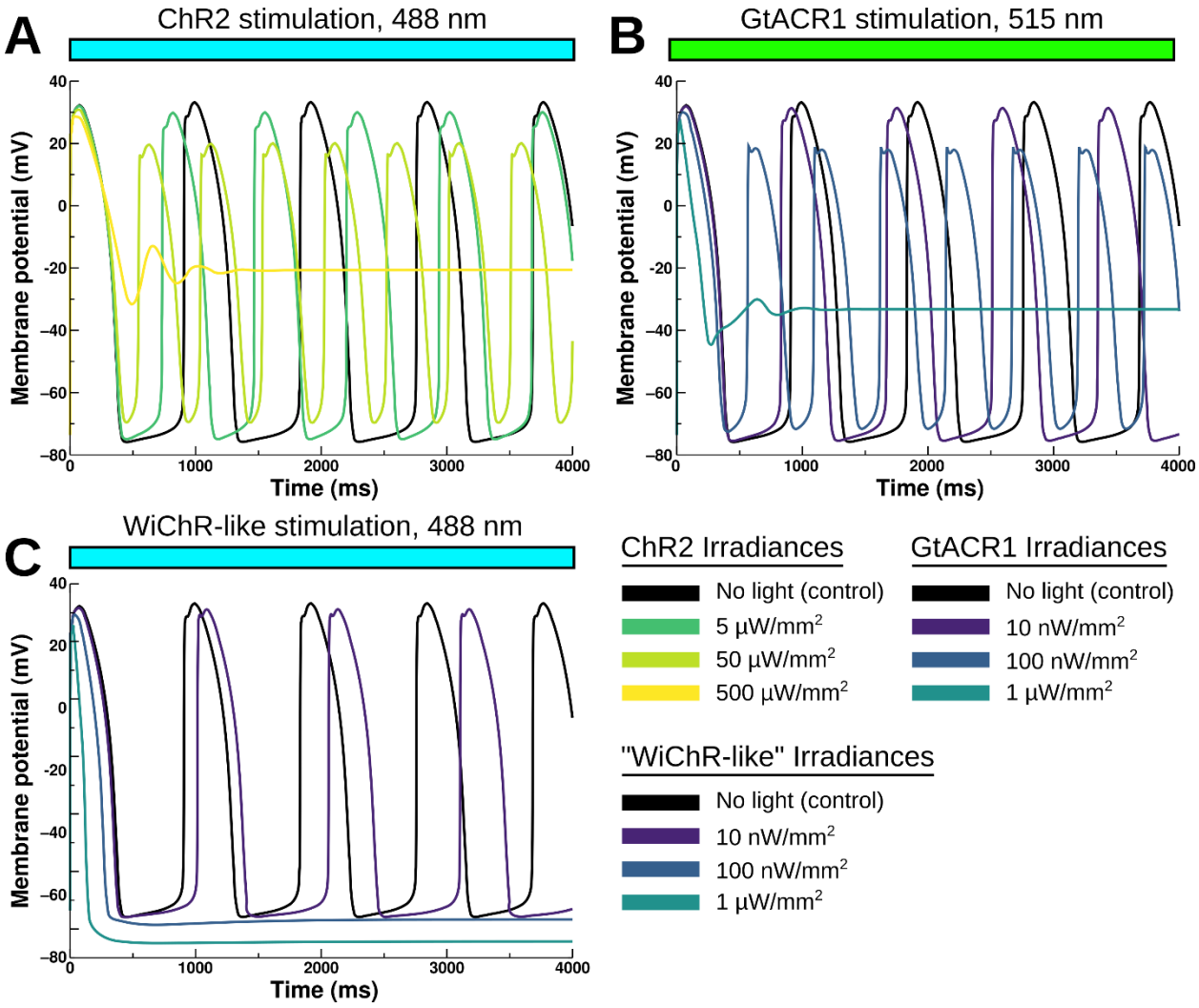

Figure 5.2*: PSC-CM spontaneous beating can be silenced using constant optogenetic stimulation. Optogenetic stimulation used either (A) ChR2, (B) GtACR1, or (C) WiChR-like stimulation. Constant illumination began at t = 0 ms and persisted for the full simulation duration.*

These findings indicate that the reversal potential of each of the evaluated opsins was a strong determinant of the suppression of PSC-CM spontaneous activity. Although it was unsurprising that ChR2 accelerated the spontaneous electrical activity, it *was* initially surprising that GtACR1 resulted in hastened beating. Previous studies have noted the opsin's both depolarizing and repolarizing effects (27, 30). These depolarizing currents appeared to raise the MDP and reduce repolarization time (i.e., increase spontaneous beating frequency) as irradiance increased. Between ChR2 and GtACR1, there are nuanced differences in changes to the AP notch and gradual V_m rise during diastole, but both ultimately had the same outcome (increased

spontaneous beating rate and eventual repolarization failure). However, WiChR-like stimulation mildly prolonged the diastolic interval at 10 nW/mm^2, and completely suppressed spontaneous beating at higher irradiances. These results reinforce the hypothesis that only opsin E_{rev} below the MDP value could suppress PSC-CM spontaneous beating without repolarization failure.

Next, we sought to evaluate whether the evaluated irradiances for each opsin would prevent cellular excitability under electrical stimulation. We simulated constant optogenetic stimulation and applied electrical stimulation twice at 1000 ms intervals. At baseline, the two electrical stimuli did not disrupt the PSC-CM spontaneous beating (**Fig. 5.3**). However, under constant ChR2 stimulation the electrical stimuli failed to recapitulate a typical action potential and maintain cellular excitability at the tested irradiances (**Fig. 5.3A**). Similarly, GtACR1 also failed to remain cell excitability during constant illumination (**Fig. 5.3B**). In comparison, WiChR-like stimulation had a single irradiance which demonstrated relatively unimpaired cellular excitability via a recognizable action potential morphology (100 nW/mm^2; **Fig. 5.3C**). However, at higher irradiances (0.5 and 1 µW/mm^2), the action potentials formed but were extremely abbreviated. This suggests that there is a very narrow irradiance band for WiChR-like stimulation that both suppresses spontaneous APs while also retaining cellular excitability.

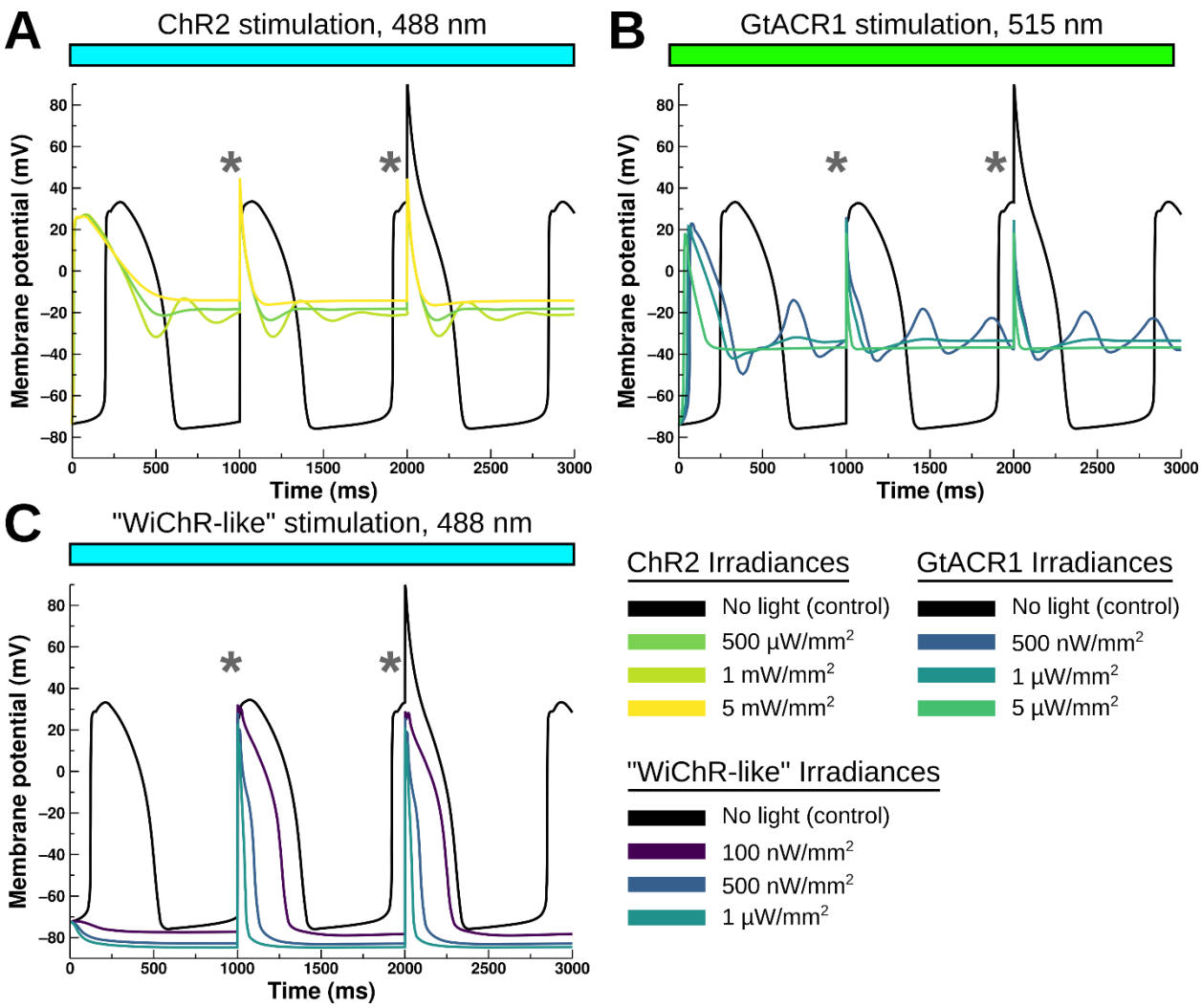

Figure 5.3*: Cell excitability is hindered during constant optogenetic stimulation.* ***A-C****: Optogenetic stimulation begins at t = 0 ms for either ChR2 (A), GtACR1 (B), or WiChR-like (C) and persists for the full simulation duration (3000 ms). Electrical stimulation is applied at t = 1000 and 2000 ms in all conditions (gray* ******* *marks). The high No light (control) V_m value seen at t = 2000 ms is due to electrical stimulation during action potential peak.*

To test the efficacy of optogenetic stimulation on graft-to-host excitations, we simulated three slice models at varied graft-to-host coupling values (2.5%, 10%, and 20%) for ten permutations per condition. The occurrence of tissue-scale complete graft-to-host excitation was used here as a proxy for EA occurrence. In control stimulations without optogenetic stimulation, graft-to-host excitation peaks at 10% graft boundary coupling (**Fig. 5.4**). There was also notable intra-model variability, with Model 1 having significantly higher EA propensity than either Models 2 or 3 (which were nearly non-responsive to EA). Both the “low” and “high” coupling values (2.5%

and 20%) had relatively low EA. This agrees with the findings established in a recent publication by our group (14), which instead used a faster beating, more immature modified version of the same PSC-CM model (24).

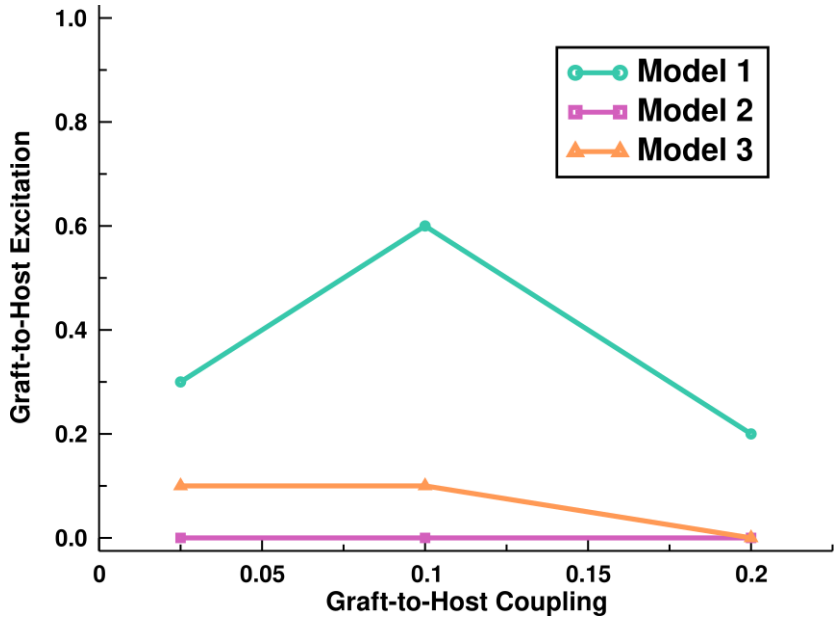

Figure 5.4*: Control condition outcomes in 2D slice models. EA occurrence (Y-axis) is compared against graft-to-host boundary coupling proportion (X-axis) across three slice models. Coupling proportions are evaluated at 2.5, 10, and 20% amounts, across 10 permutations each.*

When optogenetic stimulation was applied to each model using epicardial illumination, ChR2 (**Fig. 5.5**) and GtACR1 (**Fig 5.6**) stimulation ultimately increased graft-to-host propensity while WiChR-like (**Fig. 5.7**) stimulation ultimately prevented any graft-to-host excitations at the highest irradiances . At lower graft-to-host coupling (2.5%), ChR2 and GtACR1 stimulation had a more modest effect on graft-to-host propensity (**Figs. 5.5A & 5.6A**). At 10% coupling, increasing irradiances had dramatically stronger rises in EA propensity with ChR2 (**Fig. 5.5B**) and similar rises with GtACR1 (**Fig. 5.6B**). However, there was also small but marked decrease in graft-to-host propensity using GtACR1 stimulation in Models 2 and 3 (from 5-10 $\mu W/mm^2$ to 50 $\mu W/mm^2$), suggesting that GtACR1 may have a more complicated effect on graft-to-host propensity. At 20% coupling, ChR2- and GtACR1-mediated increases of EA propensity were very similar: sudden rises from zero to complete EA propensity across one irradiance order of magnitude

(**Figs. 5.5C & 5.6C**). Interestingly, although Model 2 had nonexistent (0 of 10) and Model 3 had low (0-1 of 10) EA propensity at baseline across all couplings, but both ChR2 and GtACR1 stimulation at high irradiances resulted in high EA propensity at higher coupling values (10 & 20%; **Figs. 5.5B-C, 5.6B-C**). In comparison, WiChR-like stimulation did not increase EA propensity in any evaluated condition (as compared to baseline) and started to consistently reduce EA occurrence at 0.1 to 1 µW/mm^2 in all coupling conditions (**Figs. 5.7**). Complete abolishment of EA was achieved by 0.5 1 µW/mm^2 in Models 2 & 3, and by 5 to 50 µW/mm^2 in Model 1 across all coupling conditions.

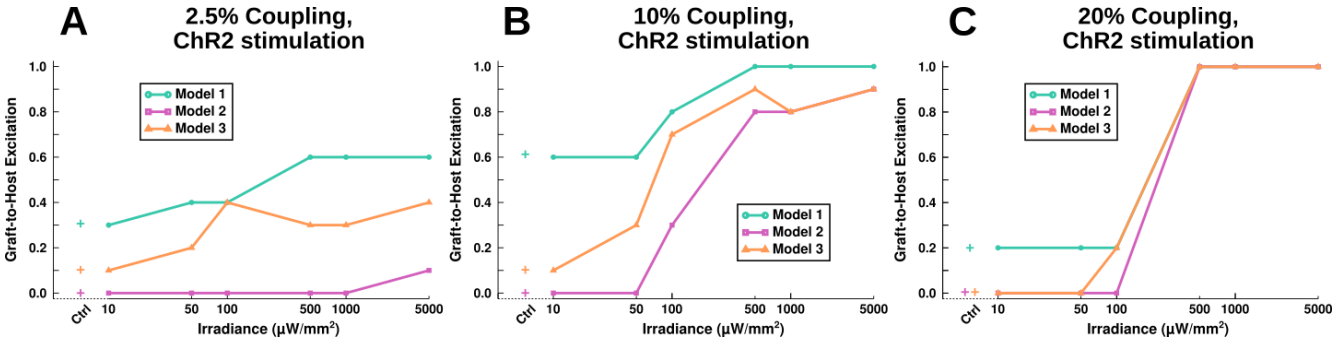

***Figure 5.5**: Constant ChR2 stimulation increases graft-to-host excitation in 2D models. A-C: Outcome was measured as a proportion of graft-to-host excitation (EA; Y-axis) occurring across 10 randomized boundary permutations for a given coupling proportion of either 2.5% (A), 10% (B), or 20% (C). Plus markers denote control data.*

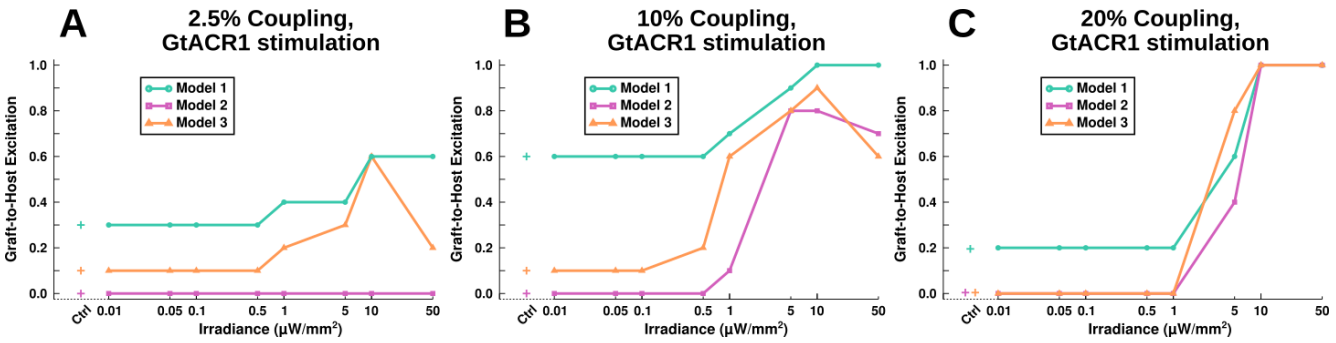

***Figure 5.6**: Constant GtACR1 stimulation increases graft-to-host excitation in 2D models. A-C: Outcome was measured as a proportion of graft-to-host excitation (EA; Y-axis) occurring across 10 randomized boundary permutations for a given coupling proportion of either 2.5% (A), 10% (B), or 20% (C). Plus markers denote control data, identical to as shown in Figure 5.5.*

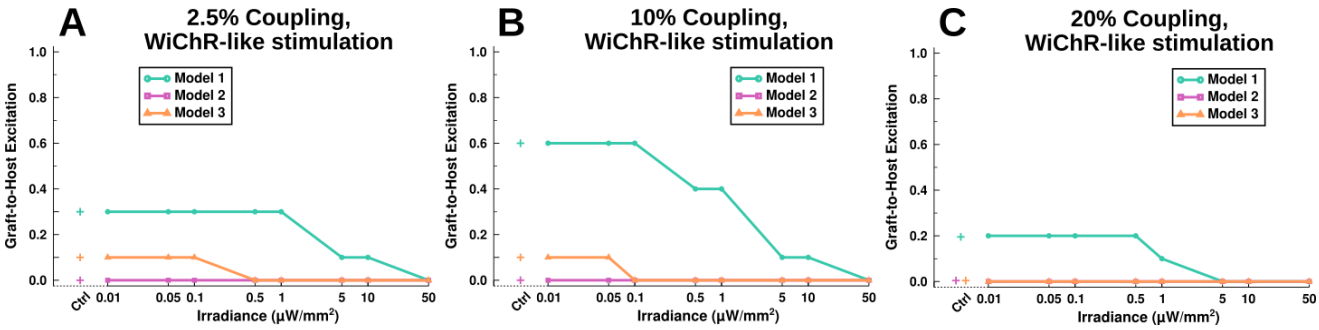

Figure 5.7*: Constant WiChR-like stimulation decreases graft-to-host excitation in 2D models. A-C: Outcome was measured as a proportion of graft-to-host excitation (EA; Y-axis) occurring across 10 randomized boundary permutations for a given coupling proportion of either 2.5% (A), 10% (B), or 20% (C). Plus markers denote control data, identical to as shown in Figure 5.5.*

The change in graft-to-host propensity across three slice models and three coupling values broadly agree with the cell-scale findings: ChR2 and GtACR1 stimulation broadly increased graft-to-host propensity while WiChR-like stimulation decreased graft-to-host excitations. Strikingly, EA occurrence did not increase at weaker WiChR-like stimulation (i.e., 1 to 50 μW/mm^2) although single cell simulations had established that spontaneous beating *could* still happen at those irradiances. This suggests that use of a hyperpolarizing opsin with a relatively high photocurrent could be effective tool in suppressing PSC-CM ectopic activation. For ChR2 and GtACR1 stimulation at higher irradiances, the increase of graft-to-host excitation was likely because the optogenetic stimulation was sufficiently strong enough to cause a graft-to-host excitation soon after illumination. In other words, a simulation with initial tissue-wide excitation followed by indefinitely voltage clamped PSC-CM graft regions would still be classified as graft-to-host excitation, especially since both optogenetic currents (applied at t = 0 ms) would have been depolarizing relative to the resting V_m within the PSC-CM grafts.

Finally, we wished to evaluate whether the constant optogenetic stimulation would impair electrical conduction into the optogenetically-modulated PSC-CM graft regions. When considering a representative example lacking optogenetic stimulation, graft-to-host excitation propagated throughout the model (**Fig. 5.8A**). When 1 μW/mm^2 WiChR-like stimulation was applied using epicardial illumination, the spontaneous activity was suppressed (data not shown).

When the same optogenetic stimulation was applied, but with additional epicardial electrical stimulation, we observed that host-to-graft excitation successfully conducted into the same graft islands as in the control simulation (**Fig. 5.8B**). This suggests that optogenetic stimulation sufficient to prevent spontaneous activity can still allow host-to-graft excitation wavefronts to propagate throughout a given model.

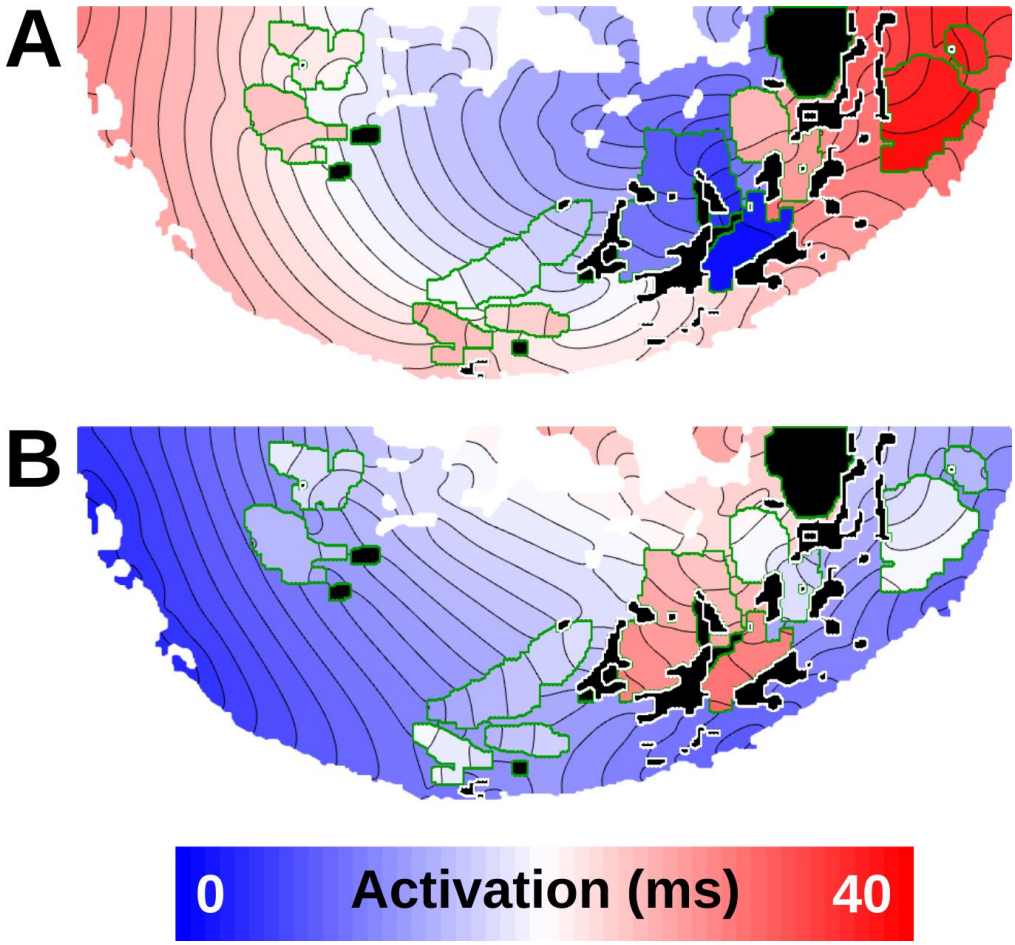

Figure 5.8*: Representative examples of excitation conducting into PSC-CM graft tissue. (**A**) Spontaneous activity results in graft-to-host stimulation that conducts across the entire model. When epicardial illumination with 1 µW/mm^2 WiChR stimulation was added, spontaneous activity was prevented (not shown). (**B**) When epicardial electrical stimulation was added in addition to the optogenetic stimulation, the excitation wavefront achieved host-to-graft excitation in nearly all graft tissue. Green outlines denote PSC-CM graft tissue, and white outlines denote non-conductive scar. All conditions shown at 10% coupling in Model 1.*

5.5 Preliminary Conclusions

In conclusion, we demonstrated that the use of optogenetic stimulation can be used as an experimental tool to affect ectopy in simulated PSC-CM cells and 2D tissue models. We found that ChR2 and GtACR1 stimulation both upregulated spontaneous beating, prevented cellular excitability at irradiances that prevented spontaneous beating, and increased the proportion of graft-to-host excitations in tissue models. In comparison, we found that the hypothetical hyperpolarizing "WiChR-like" opsin could downregulate spontaneous beating, maintain cellular excitability while preventing spontaneous beating, and decreased the proportion of graft-to-host excitations in tissue models.

5.6 References

1. Laflamme, M.A. and C.E. Murry, *Heart regeneration.* Nature, **2011**. 473(7347): p. 326-35.

2. Boateng, S. and T. Sanborn, *Acute myocardial infarction.* Dis Mon, **2013**. 59(3): p. 83-96.

3. Chatterjee, N.A. and J.P. Singh, *Novel Interventional Therapies to Modulate the Autonomic Tone in Heart Failure.* JACC Heart Fail, **2015**. 3(10): p. 786-802.

4. Tachibana, A., et al., *Paracrine Effects of the Pluripotent Stem Cell-Derived Cardiac Myocytes Salvage the Injured Myocardium.* Circ Res, **2017**. 121(6): p. e22-e36.

5. Wang, L.L., et al., *Local and sustained miRNA delivery from an injectable hydrogel promotes cardiomyocyte proliferation and functional regeneration after ischemic injury.* Nat Biomed Eng, **2017**. 1: p. 983-992.

6. Liu, Y.W., et al., *Human embryonic stem cell-derived cardiomyocytes restore function in infarcted hearts of non-human primates.* Nat Biotechnol, **2018**. 36(7): p. 597-605.

7. Shiba, Y., et al., *Human ES-cell-derived cardiomyocytes electrically couple and suppress arrhythmias in injured hearts.* Nature, **2012**. 489(7415): p. 322-5.

8. Chong, J.J., et al., *Human embryonic-stem-cell-derived cardiomyocytes regenerate non-human primate hearts.* Nature, **2014**. 510(7504): p. 273-7.

9. Romagnuolo, R., et al., *Human Embryonic Stem Cell-Derived Cardiomyocytes Regenerate the Infarcted Pig Heart but Induce Ventricular Tachyarrhythmias.* Stem Cell Reports, **2019**. 12(5): p. 967-981.

10. Morad, M. and X.H. Zhang, *Mechanisms of spontaneous pacing: sinoatrial nodal cells, neonatal cardiomyocytes, and human stem cell derived cardiomyocytes.* Can J Physiol Pharmacol, **2017**. 95(10): p. 1100-1107.

11. Yu, J.K., et al., *A comprehensive, multiscale framework for evaluation of arrhythmias arising from cell therapy in the whole post-myocardial infarcted heart.* Sci Rep, **2019**. 9(1): p. 9238.

12. Yu, J.K., et al., *Assessment of arrhythmia mechanism and burden of the infarcted ventricles following remuscularization with pluripotent stem cell-derived cardiomyocyte patches using patient-derived models.* Cardiovasc Res, **2021**.

13. Yu, J.K., et al., *Computational modeling of aberrant electrical activity following remuscularization with intramyocardially injected pluripotent stem cell-derived cardiomyocytes.* J Mol Cell Cardiol, **2022**. 162: p. 97-109.

14. Gibbs, C.E., et al., *Graft-host coupling changes can lead to engraftment arrhythmia: a computational study.* J Physiol, **2023**.

15. Ambrosi, C.M., et al., *Cardiac applications of optogenetics.* Progress in biophysics and molecular biology, **2014**. 115(2-3): p. 294-304.

16. Boyle, P.M., E. Entcheva, and N.A. Trayanova, *See the light: can optogenetics restore healthy heartbeats? And, if it can, is it really worth the effort?* Expert review of cardiovascular therapy, **2014**. 12(1): p. 17-20.

17. Deisseroth, K., *Optogenetics: 10 years of microbial opsins in neuroscience.* Nat Neurosci, **2015**. 18(9): p. 1213-25.

18. Bruegmann, T., et al., *Optogenetic defibrillation terminates ventricular arrhythmia in mouse hearts and human simulations.* J Clin Invest, **2016**. 126(10): p. 3894-3904.

19. Nyns, E.C.A., et al., *Optogenetic termination of ventricular arrhythmias in the whole heart: towards biological cardiac rhythm management.* Eur Heart J, **2017**. 38(27): p. 2132-2136.

20. Hussaini, S., et al., *Drift and termination of spiral waves in optogenetically modified cardiac tissue at sub-threshold illumination.* Elife, **2021**. 10.

21. Majumder, R., et al., *Pulsed low-energy stimulation initiates electric turbulence in cardiac tissue.* PLoS Comput Biol, **2021**. 17(10): p. e1009476.

22. Gruber, A., et al., *Optogenetic Control of Human Induced Pluripotent Stem Cell-Derived Cardiac Tissue Models.* J Am Heart Assoc, **2022**. 11(4): p. e021615.

23. Vierock, J., et al., *WiChR, a highly potassium selective channelrhodopsin for low-light one- and two-photon inhibition of excitable cells.* Sci Adv, **2022**: p. eadd7729.

24. Kernik, D.C., et al., *A computational model of induced pluripotent stem-cell derived cardiomyocytes incorporating experimental variability from multiple data sources.* J Physiol, **2019**. 597(17): p. 4533-4564.

25. O'Hara, T., et al., *Simulation of the undiseased human cardiac ventricular action potential: model formulation and experimental validation.* PLoS Comput Biol, **2011**. 7(5): p. e1002061.

26. Williams, J.C., et al., *Computational optogenetics: empirically-derived voltage- and light-sensitive channelrhodopsin-2 model.* PLoS Comput Biol, **2013**. 9(9): p. e1003220.

27. Ochs, A.R., et al., *Optogenetic Stimulation Using Anion Channelrhodopsin (GtACR1) Facilitates Termination of Reentrant Arrhythmias With Low Light Energy Requirements: A Computational Study.* Front Physiol, **2021**. 12: p. 718622.

28. Govorunova, E.G., et al., *Anion channelrhodopsins for inhibitory cardiac optogenetics.* Sci Rep, **2016**. 6: p. 33530.

29. Vogt, C.C., et al., *Systemic gene transfer enables optogenetic pacing of mouse hearts.* Cardiovasc Res, **2015**. 106(2): p. 338-43.

30. Kopton, R.A., et al., *Cardiac Electrophysiological Effects of Light-Activated Chloride Channels.* Front Physiol, **2018**. 9: p. 1806.

Chapter 6 | Dissertation Summary and Future Directions

Better understanding the electrophysiological basis of arrhythmias is an important endeavor for addressing the large morbidity and mortality burden in the population. Although rhythm control can often be achieved through various therapies (i.e., anti-arrhythmic drugs, catheter ablation procedures, and implantable devices), not all individuals remain arrhythmia free or instead suffer from significant therapeutic side effects. The above work has established novel *in silico* tools for controlling the initiation and suppression of arrhythmias occurring primarily in post-myocardial infarction settings. In Chapter 3, optogenetic arrhythmia termination was improved in biatrial and biventricular computational models using an anion channelrhodopsin (GtACR1) as compared to previous methods (ChR2). Additionally, we created a biophysically realistic 2-state model for GtACR1 photocurrent for other researchers to utilize. In Chapter 4, we demonstrated that subthreshold optogenetic stimulation could selectively up- or down-regulate early afterdepolarization (cell-scale) and premature ventricular complex (organ-scale) occurrence. In Chapter 5, optogenetic stimulation established preliminary proof-of-concept regulation of spontaneous beating rate in pluripotent stem cell derived cardiomyocytes and engraftment arrhythmia development in 2D slice models. Together, this collection of work advances tools and concepts that the cardiac optogenetics field can utilize to further prove the boundaries of arrhythmia research.

Although considerable proof-of-concept has been established for optogenetic termination of arrhythmias *ex vivo*, *in vivo*, and *in silico*, further advances could be made into both characterizing cardiac optogenetic stimulation and overcoming difficulties of light attenuation. First, studies attempting optogenetic arrhythmia termination have not combined advances in red-shifted opsins (such as Chrimson or RubyACRs) with recent advances in wireless, battery-free light diodes. Second, few to no studies have examined opsin transfection and cardiac optogenetic stimulation in larger animals, which have notably thicker myocardial walls than murine models.

Third, significant recent discoveries of naturally occurring potassium-conducting opsins have not been expressed and characterized in cardiomyocytes yet, which may prove consequential for arrhythmia suppression attempts. All of these considerations should be strongly considered in future works.

When considering the next experiments for Chapter 5, higher quantitative detail of the effects of each opsins' stimulation are needed on the spontaneous beating rate (rather than an inherently qualitative assessment of either increased or decreased spontaneous beating rates). In the histology-derived 2D tissue models, the excitability of PSC-CMs tissue during WiChR-like stimulation needs to be more closely examined. In other words: does the hyperpolarizing WiChR-like stimulation prevent an electrically paced activation from the host entering into the PSC-CM graft? This is an extension of the cellular excitability evaluation conducted in simulated single cells, and necessary to ensure that optogenetic stimulation is not so strong that excitation-contraction coupling is impaired. If tissue excitability was not maintained (i.e., the voltage did not rise significantly), this would presumably affect the long-term maturity and contractile benefit that the PSC-CM engraftment is intended to provide.

A further extension of the 2D tissue models is an expansion of hypothetical PSC-CM engraftment regions into a post-MI, LGE-MRI patient ventricular model. However, significant care must be exercised when considering how to model the engraftment patterns, since PSC-CM engrafted tissue cannot be distinguished from other cardiac tissues via current imaging methods. Furthermore, therapeutic benefit in the tissue models may fail to provide significant results in organ-scale models, given a greater attenuation of light relative to the illuminated (epicardial) surface in 3D as compared to 2D, even after higher applied irradiances.